1-1-2010

The Design And Synthesis Of A Stereotactic Radiosurgical Phantom

Robert Tkaczyk
ryerson

THE DESIGN AND SYNTHESIS OF A STEREOTACTIC RADIOSURGICAL PHANTOM

By

Robert Tkaczyk

A thesis

presented to Ryerson University

in partial fulfillment of the

requirements for the degree of

Master of Science

in the Program of Biomedical Physics

Toronto, Ontario, Canada, 2010

I hereby declare that I am the sole author of this thesis or dissertation.

I authorize Ryerson University to lend this thesis or dissertation to other institutions or individuals for the purpose of scholarly research.

I further authorize Ryerson University to reproduce this thesis or dissertation by photocopying or by other means, in total or in part, at the request of other institutions or individuals for the purpose of scholarly research.

THE DESIGN AND SYNTHESIS OF A STEREOTACTIC RADIOSURGICAL PHANTOM

Robert Tkaczyk

Master of Science, 2010

Biomedical Physics

Ryerson University

Abstract

Stereotactic Radiosurgery involves the use of highly focused ionizing radiation beams to treat localized cancer tumours and lesions. Due to the damaging effects of radiation on healthy tissue, quality assurance checks must take place before treatment to ensure accurate delivery. This is of critical importance in cases like brain tumours, in which the healthy tissue at risk is in close proximity to the target volume. A dodecahedral radiosurgical phantom was designed and fabricated to measure the isocentre variation of a linear accelerator at an isocentric irradiation facility. It was shown that the phantom can localize individual treatment beams to within an uncertainty of 0.2mm. Due to the intrinsic accuracy of the phantom, it was found that careful phantom design and manufacturing as well as an accurate and complex characterization, in terms of measurements, positioning and computer modeling, must take place. This accurate characterization of the phantom is crucial to ensure the accurate treatment of stereotactic radiosurgery. This research is part of a larger project to further develop the phantom we have introduced in order to exploit a wider set of functions pertaining to maintaining accurate treatment delivery.

Acknowledgements

I would like to acknowledge my co-supervisors Dr. Pedro Goldman and Dr. David Beachey for their supervision and help throughout this research. I would also like to acknowledge my supervisor at the German Cancer Research Centre (DKFZ) in Heidelberg, Germany, Dr. Günther Hartmann for his extensive knowledge of Stereotactic Radiosurgery during my student exchange. Finally, I would like to acknowledge Mr. Harry Easton, Head of the machine shop at O.C.C. in Toronto, Canada, and Prof. Gernot Echner, Chief Engineer at DKFZ in Heidelberg, Germany. Without their expertise and experience, this research could not have taken place.

Table of Contents

List of Figures

List of Appendices

Introduction

The use of ionizing radiation to treat cancer has been used successfully for over 100 years. A technique which uses highly focused radiation beams called stereotactic radiosurgery is used to treat intra and extra-cranial tumours. Due to damaging effects of radiation on healthy tissue, strict quality assurance methods must take place to ensure accurate treatment.

Many quality assurance phantoms exist to ensure the devices used during treatments operate properly. A quality assurance device was developed and partially calibrated in this research to localize the radiation beams used in Stereotactic Radiosurgery. Although the research is an ongoing project, it was proven that localization of treatment beams used for radiosurgery can be measured with very high accuracy and precision.

Once a complete phantom has been finished, it can be used at a quality assurance tool for medical physicists to improve their stereotactic radiosurgery treatments.

Stereotactic Radiosurgery

External Beam Radiotherapy (EBRT) is the treatment of cancer using doses of ionizing radiation divided into multiple treatments or fractions delivered from outside the human body. A known amount of radiation is delivered from a linear accelerator to the cancer while minimizing the radiation dose to surrounding healthy tissue. This form of treatment has proven to be very successful and its benefit to society incalculable. EBRT can be divided into several different treatment types depending on the type of lesion and it's location in the patient. One such type of EBRT is called Stereotactic Radiosurgery (SRS).

Stereotactic Radiosurgery is the treatment of cancer and other lesions using a single dose of high energy photons highly focused at an immobilized known point. Typically, SRS is used to treat small intracranial lesions ($<4cm^3$) in a single session, however other similar special techniques including extra-cranial treatments and fractioned regimens also use highly focused radiation beams. The word 'Stereotactic' come from the Latin words Stereo which means "three dimensional or solid" and Tactic which means to "touch". This refers to the stereotactic frame which is fixated to the patient and is used to immobilize the patient during treatment. Typical abnormalities that are treated with SRS are single metastasis, solitary primary brain tumours, arteriovenous malformations and benign conditions or tumours, such as pituitary adenoma and acoustic neuromos (Schell, 1995). SRS is essentially a two step process involving 1) definition of the lesion including it's shape and location, and 2) creation and delivery of the treatment plan. Dosimetric advantages of SRS over conventional radiotherapy are the steep dose drop off outside the treated area (sparing healthy tissue) and the ability to escalate the dose within the lesion. This dose distribution is achieved by focusing multiple non-coplanar collimated radiation beams at a common central point. Although there are dedicated machines that can only treat SRS, such as the Gamma-Knife and the Cyber-Knife (explained below), it is common in cancer centres to use a modified Linear Accelerator (Linac) which has the ability to meet the tight tolerances used in SRS.

Stereotactic Radiosurgery History

The treatment of cancerous tumours using prescribed doses of ionizing radiation has been in use for over 100 years. Treatments in the early 1900's involved directing a collimated beam of ionizing radiation from a radioactive isotope to a predefined area around the tumour. The use of a radioactive isotope for treatment however had serious implications with radiation safety and also with the lengthening of treatment times due to isotope decay. However, technical developments at Universities in high energy physics led to the development of particle accelerators in the 1950's.

Figure 1: Radiosurgery Treatment Units: the Gamma Knife, Cyber Knife, and Linear Accelerator. Adapted from: http://www.siddiqimd.com/technology/cyberknife.htm with slight modification.

The development of Stereotactic Radiosurgery is seen as a combination of efforts by Neurosurgeons, medical physicists, and engineers over the past 50 years (Schell, 1995). Figure 1 shows three treatment units currently in use today which were developed over this time period. The Two units from the left, the Gamma Knife Unit and the Cyber Knife Unit will be described briefly below while the Linear Accelerator on the right will be described in detail.

Stereotactic Radiosurgery was first proposed by the Swedish neurosurgeon named Lars Leksell. Although the stereotactic head frame had already been developed, Lars Leksell was the first to use a stereotactic head frame to immobilize the patient for radiation treatment. He first used 250 kV ortho-voltage x-rays but soon realized that much higher energies were needed to get the necessary doses for deeper lesions. Ortho-voltage x-rays are x-rays that are produced with energies in the 200-500 keV range. Due to this energy, the x-rays are produced preferentially at 90 degrees to the incoming electron beam. Along with collaborators at the University of Uppsala in Sweden, Lars Leksell considered better treatment modalities including proton therapy but ultimately decided that a Co-60 source would be best for these treatments. Similar early efforts were directed at such diverse indications as chronic pain, epilepsy, movement disorders, and psychiatric disorders (Solberg, 1998). Linear accelerators at the time did not have the required precision or accuracy needed for radiosurgery (Benedict, 2008), therefore his group went on to develop the Gamma Unit. Developed in 1967, this treatment unit consisted of 179 cobalt sources, distributed over a hemispheric pattern inside a shielded helmet (Podgorsak, 1998). To get a desired dose distribution, individual cobalt sources had the ability to be plugged or unplugged.

Figure 1 (left image) and Figure 2 show a photograph of a Gamma Knife Unit from Elekta, Inc. (Gamma Knife is the commercial name of the Gamma Unit) and a close up view of the helmet area respectively. From these two figures it can be seen how the patient is placed in the unit as well as how the patients head is fixated with respect to the shielded helmet. Figure 3 depicts a cross sectional view of the Unit showing a simplified schematic of how the Gamma Unit works. The Gamma Knife Unit has proved to be very effective and continues to be used in cancer centres today. However, their high costs and inability to allow imaging before treatment led physicians and physicists to the development of alternative techniques in order to promote a wider application of SRS in other cancer centres (Pike, 1989). Linear Accelerators were therefore looked at as a viable

option and over the next ten years papers were published by multiple researchers on the use of linear accelerators for radiosurgery (Benedict, 2008).

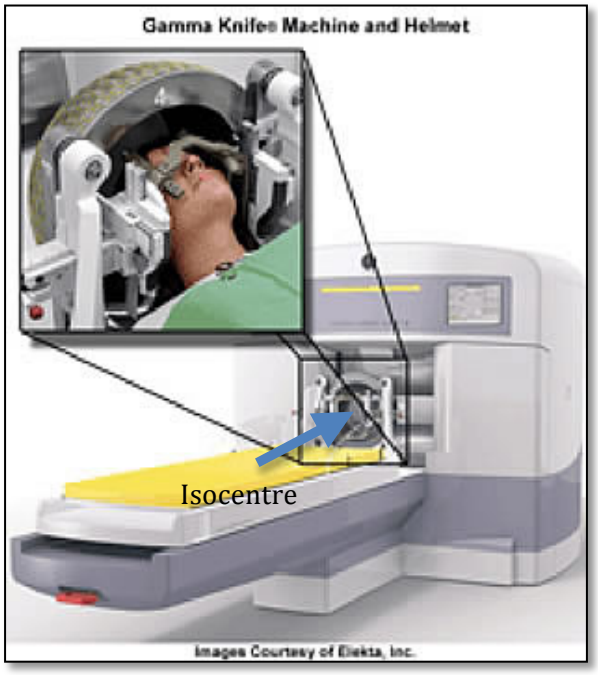

Figure 2: Close up view of the treatment head of a Gamma Knife Treatment Unit. Adapted from http://www.elekta.com/healthcare_international_gamma_knife_surgery.php with slight modification.

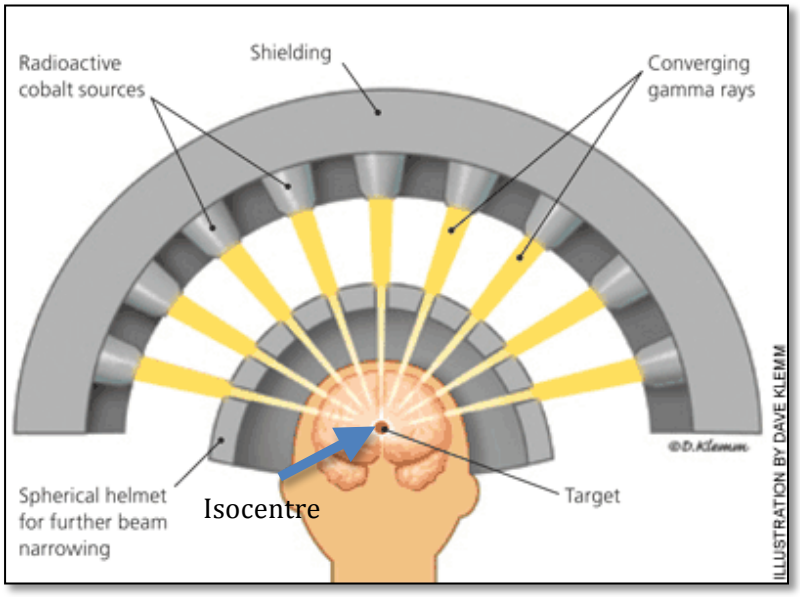

Figure 3: Cross section view of the Gamma Knife Treatment Unit. Adapted from http://www.aafp.org/afp/2008/1201/p1254.html with slight modification.

The development of the first isocentric Cobalt machine at Princess Margaret Hospital in Toronto, Canada was followed by the development of the first isocentric linac in 1960 by Varian. By the time the pioneering works above were published, linear accelerators as radiosurgery tools were commonly perceived as technologically inferior compared to the Gamma Knife in their ability to deliver highly focused precision therapy by the neurosurgery community (Benedict, 2008). The mechanical stability of isocentric Linacs in regards to their gantry and patient rotation mechanisms were and continue to be an issue for SRS. The Gamma Unit on the other hand had no moving parts, and therefore could deliver dose accuracy to the patient within a fraction of a millimetre (Podgorsak, 1989). Work began by Medical Physicists to assess the treatment delivery accuracies of Linacs treating SRS. Medical physicist Wendell Lutz and his physician colleagues at the Joint Center for Radiation Therapy, Boston went on to develop the Winston-Lutz test to check gantry rotation stability and a floor stand to rigidly support the patient's head. Figure 4 shows a depiction of the first Linac stereotactic radiosurgical system. Further improvements to the floor stand at the University of Florida by neurosurgeon William Friedman and physicist Frank Bova led to improved mechanical alignment of linac system to within 0.3 mm, similar to those reported for Gamma Knife systems (Benedict, 2008). This, coupled with advances in imaging modalities, including CT and MRI, and greater computing speeds in the 1980's let SRS gain widespread use in radiosurgical programs.

Early SRS treatment units used circular collimators of different diameters located at a specific distance from the machine's target to shape the radiation beam. However, with the expanding role of SRS in cancer treatment, it became evident that small circular fields would not suffice for larger

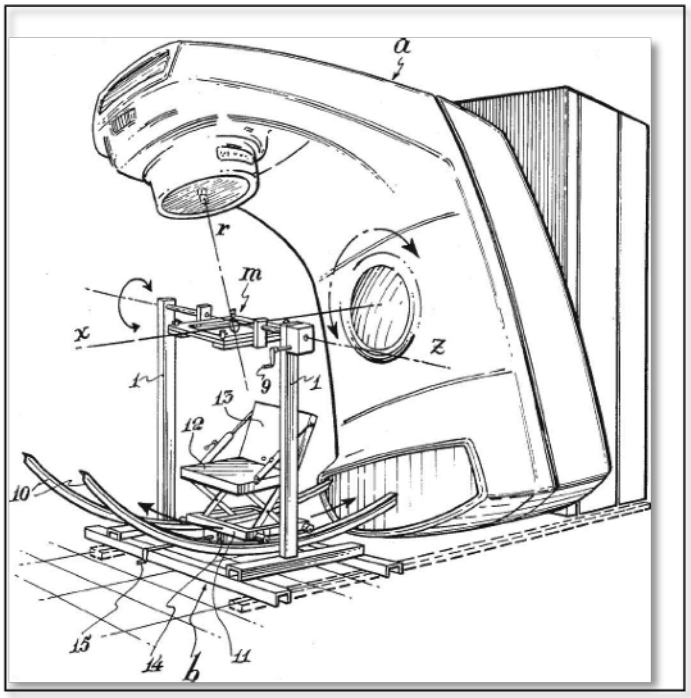

Figure 4: Diagram of the first linac radiosurgery system of Betti and Derechinsky. Adapted from ref. Benedict, 2008.

tumours and tumours located next to radiosensitive organs. This led to the development of conformal stereotactic radiosurgery (CSRS) by means of dynamic field shaping. First developed by Leavitt in 1989, this dynamic collimation system consisted of a series of circular collimators of increasing diameter chosen to circumscribe the maximum projection of the target volume during the arc, supplemented by four independent rectangular vanes having both translational and rotational motion to "trim" the circular radiation field to a trapezoidal shape more closely following the shape of the target projection (Benedict, 2008).

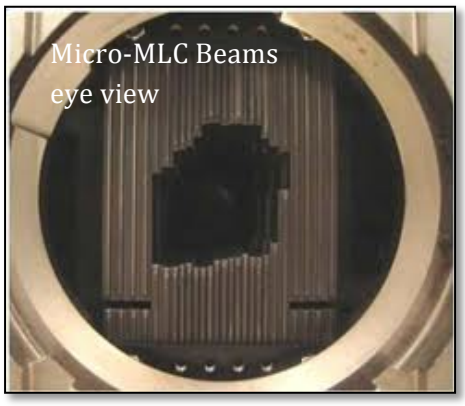

Figure 5: Beams eye view of a micro-leaf collimator. Adapted from http://www.jacmp.org/index.php/jacmp/article/viewArticle/2802/1438 with slight modification.

Following this, the companies BrainLAB and Varian partnered together to create a micro-multi leaf collimator (MLC) collimator with shaping leaves half the thickness of standard leaves. The micro MLC, shown in Figure 5 uses a leaf thickness of 5mm as opposed to the 1cm standard used for conventional radiotherapy giving the leaves the ability to conform to a higher degree to the tumour. Papers have shown that Conformal SRS would improve the dose delivery in approximately 40-70% of the SRS caseload and reduce the treatment time over non-conformal SRS treating at two different locations for irregularly shaped lesions (Schell, 1995).

It is known that fractionation (dividing the full treatment into partial treatments or fractions) during radiotherapy enhances the tumouricidal effects while minimizing normal tissue damage. Although Lars Leksell had intended for radiosurgery to be treated in a single session, research had been done by multiple scientists using fractionation during stereotactic radiosurgical treatments. With the introduction of fractionation to SRS, also called Stereotactic Radiotherapy (SRT), came issues with accurate patient placement with respect to the radiation source on a day to day basis. Early head frames were fixated to the patients skull with pins under locate anaesthesia. These "hard docking frames" frames evolved into "soft docking" frames that could reproduce the patient setup using bite blocks, ear plugs, and nasal supports. Other frames that were developed include a hybrid between the hard and soft docking frames that used implanted titanium screws to attach a removable frame and thermoplastic custom-fitted face masks which were placed over the patient's face and attached to the frame. Current research investigating frame-less radiotherapy uses real time monitoring of optically guided system detecting infrared light emitting diodes (IRLEDs) attached to a custom bite plate (Tome, 2000). For SRT, investigations of the overall treatment accuracy have been published by a number of authors and continue to be published. SRT, while not commonly used in cancer centres, continues to be researched for future development.

The future of SRS will involve attaining better accuracy with development going into image guided radiosurgery for frameless radiosurgery, and improvements with patient positioning using motion tracking. Furthermore, more research is needed in areas such as small field dosimetry, monte-carlo calculations, and new energy sources to keep SRS at the cutting edge of technology.

Medical Linear Accelerators

Medical Linear Accelerators or Linacs are cyclic accelerators isocentrically mounted which accelerate electrons to high energies in the 4MeV to 25MeV range. The Linacs use a gantry system which rotates about a common axis thus aiming the radiation at a point called the isocentre. Electrons are produced from an electron gun are then accelerated across an evacuated waveguide by RF fields. An accelerating waveguide is an evacuated or gas-filled metallic structures of rectangular or circular cross-sections used in transmission of microwaves. The simplest kind of accelerating waveguide is obtained from a cylindrical uniform waveguide by adding a series of disks (irises) with circular holes at the center, placed at equal distances along the tube. These disks divide the waveguide into a series of cylindrical cavities that form the basic structure of the accelerating waveguide in a linac (Podgorsak, 2003). Figure 6 shows a diagram of an accelerating waveguide.

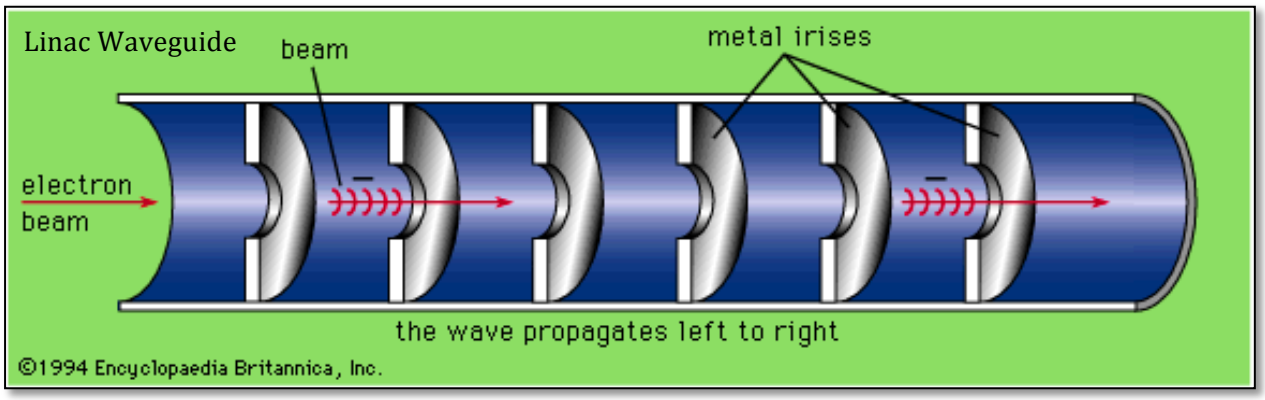

Figure 6: Accelerating waveguide. Adapted from http://www.britannica.com with slight modification.

Although the electrons are accelerated in a straight line, these accelerators are called cyclic due to the electrons movement across the waveguide using alternating potential differences (Podgorsak, 2003). Therapeutic photon beams are created when the accelerated electrons collide with a high Z material target, called the X-ray source, creating forward peaked bremsstrahlung radiation.

The progression of Linacs over the past 40 years can be divided in to 5 distinct generations and has been characterized by the increase in energies of photons and electrons produced by the machines and also by the increase in capability. Early accelerators provided 4-6MV photons while used a fixed flattening filter, external wedges, and symmetric jaws for radiation dose control; and a single transmission ionisation chamber for dose monitoring. The next generation of Linacs in the 10-15MV range also had the capability to produce electron beams using scattering foils and moveable flattening filter. These Linacs also used independent dual ionisation chambers for more reliable dose monitoring. The third generation of Linacs allowed for multiple energies by use of an achromatic bending magnet and added features such as asymmetric jaws and motorized wedges.

Fourth generation Linacs saw great improvements as computing power had increased. Further dose shaping features, including multi leaf collimators and dynamic wedges, were added as well as the introduction of portal imaging. The final generation of Linacs again saw developments in dose shaping with the use of intensity modulation with multi-leaf collimator and full dynamic conformal dose delivery with intensity modulated beams produced with a multi-leaf collimator (Podgorsak, 2003).

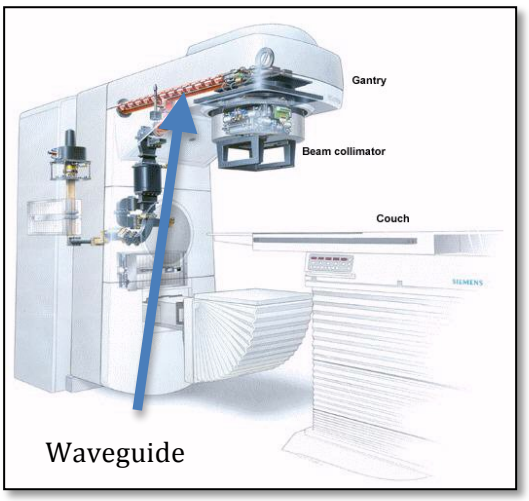

Figure 7: Linac components. Adapted from http://www.cerebromente.org.br/n02/tecnologia/radiocirurg_i.htm with slight modification.

The main components of a Linac are as follows:

- **gantry**
- **gantry stand or support**
- modulator cabinet
- **patient support assembly, i.e., treatment couch**
- control console

The components in bold will be described below as they pertain to the outcome of this research. Figure 7, Figure 8, and Figure 9 respectively show a typical Linac design configuration and design schematic.

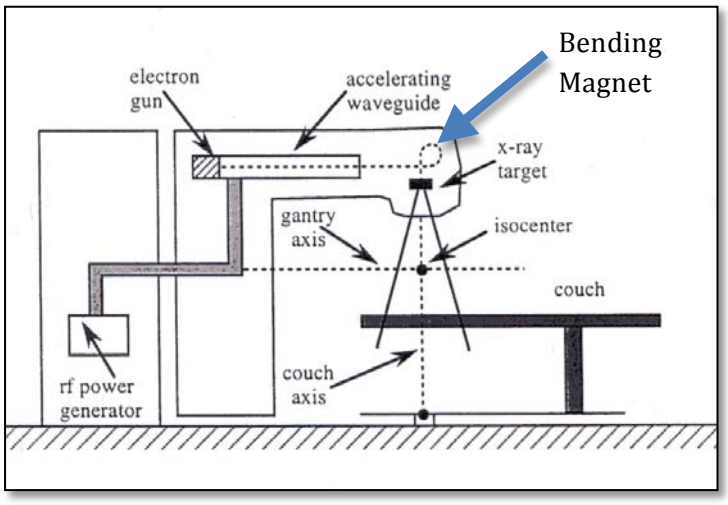

Figure 8: Typical Linac design configuration. Adapted from http://www.adelaideradiotherapycentre.com.au/physics_of_rt.html with slight modification.

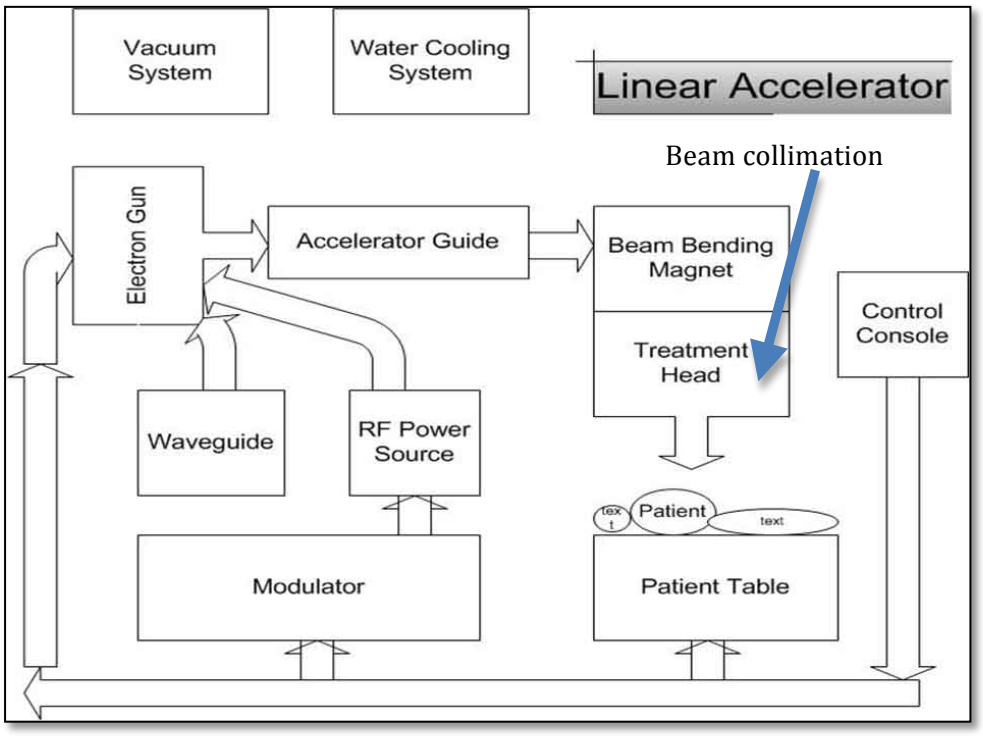

Figure 9: Linac schematic. Adapted from http://its.uvm.edu/medtech/module.html with slight modification.

The gantry contains all the components seen in Figure 9, however, it is the gantry head which produces and shapes the radiation beam. The Linac head or gantry head is composed of several components that allow the shaping and monitoring of electron and photon beams. Photon beams are created using a target and flattening filter combination while electron beams use a scattering foil and special applicator for beam collimation. This assembly is usually mounted on a pair of

sliding rails and can have multiple targets and scattering foils. The collimation system that is used to shape the radiation beam to a maximum of 40x40cm^2 at the Linac isocentre contains a primary collimator, secondary moveable collimator, and in addition to this a multi-leaf collimator (MLC). It must also be noted here that there are actually two isocentres—the mechanical and the x-ray isocentres. The mechanical isocentre of a 'perfect' linac is defined as the point in space where the gantry rotation axis and the beam collimator axis intersect. The x-ray isocentre is the point in space where the gantry rotation axis and the central x-ray of the beam intersect (Arjomandy, 2000). The MLC's are now commonly used to further shape the radiation beam to allow for a higher degree of dose conformality allowing newer techniques such as intensity modulated radiation therapy (IMRT) to be used in cancer centres. IMRT is the use of small beams or 'beamlets' which can be varied in intensity to change the radiation field many times during a treatment. In addition to the collimation, the head of the Linac also holds dual independent ionization chambers to monitor the radiation emitted from the machine. The ionization chambers are also used to monitor the axial and transverse off-axis ionizations to ensure beam uniformity. The Linac can also produce a visible light field projected from the direction of the source which matches the radiation field.

The patient support assembly or treatment couch is used to position the patient at the desired location for treatment. Figures 7 and 10 show the orientation of the couch relative to the gantry and its range of motion. The couch is able to rotate and shift in all the directions indicated in Figure 10.

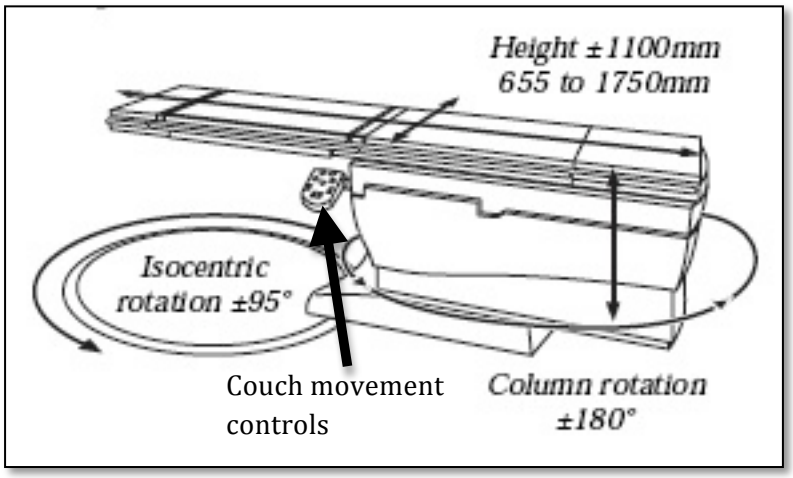

Figure 10: Treatment couch movements. Adapted from http://blog.elekta.com/tag/hexapod/ with slight modification.

Modified Linear Accelerator for Stereotactic Radiosurgery

A modified Linear accelerator for SRS must have accurate and stable mechanical alignment, excellent beam stability during gantry rotation, and suitable energy range. It is modified for stereotactic radiosurgery by mounting an auxiliary collimator to the collimator face plate. This auxiliary collimator minimizes radiation penumbra and allows collimator inserts to produce circular radiation beams (Tsai, 1991).

Linear accelerators must meet more stringent standards due to the high precision required of SRS. The basic requirements for SRS are: (1) accurate localization, (2) mechanical precision, (3) accurate and optimal dose distribution, and (4) patient safety (Schell, 1995).

For accurate localization, the stereotactic localization techniques shall be able to determine the coordinates of a well-defined object (pointer or a bail bearing in a phantom) in the frame coordinate system to within 1 mm for angiography, and 2 mm for CT and MRI. A localization test is described in the System Verification Test section (Schell, 1995).

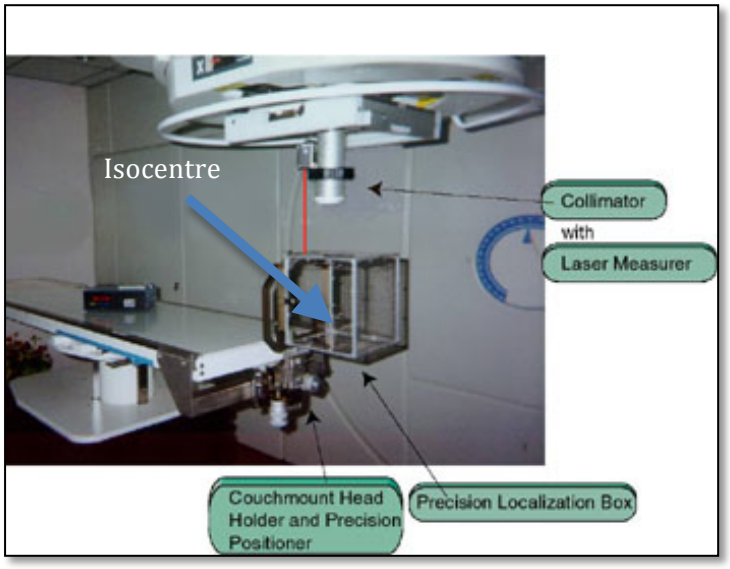

Figure 11: Patient-Frame alignment. Adapted from http://www.stereotaxybymidco.com/photon.html with slight modification.

The Mechanical precision of a Linac must be achievable and maintained in order to allow SRS. The coordinates of the patient-frame system must be aligned with the Linac coordinate system. This allows the treatment target, which is aligned to the patient frame to be located at the isocentre of the machine, Figure 11.

The overall stability of the Linac is measured by examining the rotation axis of the gantry, couch, and collimator and how well they coincide. It is recommended they must coincide to within a 1mm radius sphere (Schell, 1995).

Figure 12: Integra Radionics, Inc. CRW Stereotactic System. Adapted from www.radionics.com with slight modification.

In order to immobilize the patient, a frame system must be used and this frame system must be rigidly coupled to the Linac. Stereotactic frames are most commonly used to immobilize the patients head for intra-cranial treatment, although they also can be used to immobilize other treatment areas. The frames have metal pins which are fixated to known positions in the patients skull. In addition to this, a localization frame (with fiducial rods) is used at CT to correlate frame coordinate position with anatomy. Most SRS applications use one of five stereotactic frames: Brown-Roberts-Wells, Tipal, Leksell, Gill-Thomas-Cosman, or Riechert/ Mundinger (Schell, 1995). Although each frame has a different shape and characteristics, all frames serve the same function: to accurately guide ionizing radiation beams to a target in the brain. Figure 12 shows the CRW stereotactic frame made by Integra Radionics, Inc.

The collimation used for SRS treatments must shape the radiation to provide the high dose conformality required by SRS and must be aligned properly as the precision of the treatment depends heavily on it (Schell, 1995). The alignment of the beam collimation used for SRS typically uses prefabricated circular lead cones stacked on top of each other. These circular cones of different diameters ranging from 5.0mm to 40.0mm are fitted into a linear accelerator for stereotactic radiosurgery treatment. Ideally, cones give the best dose uniformity for small spherical lesions however this can also be achieved using multiple isocentres for irregularly shaped lesions. Figures 13a and 13b show the treatment cones used at the Odette Cancer Centre and the Linac which was investigated in this thesis.

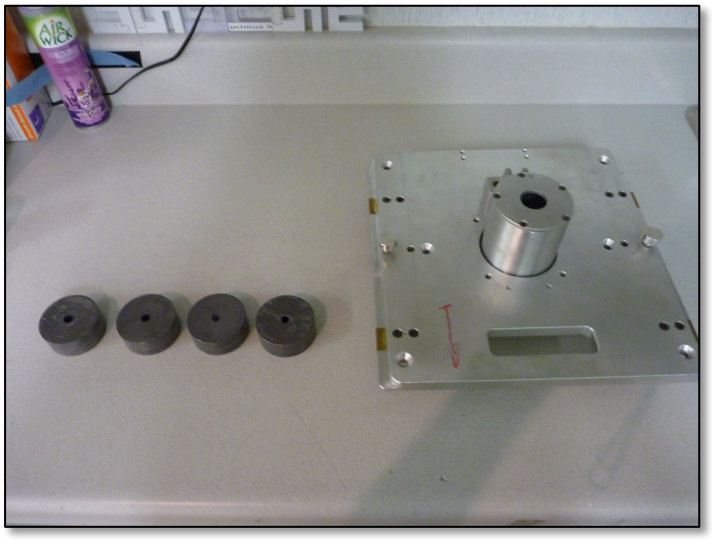

Figure 13a: SRS lead cones used to collimate the radiation and the Tray which houses the stacked cones.

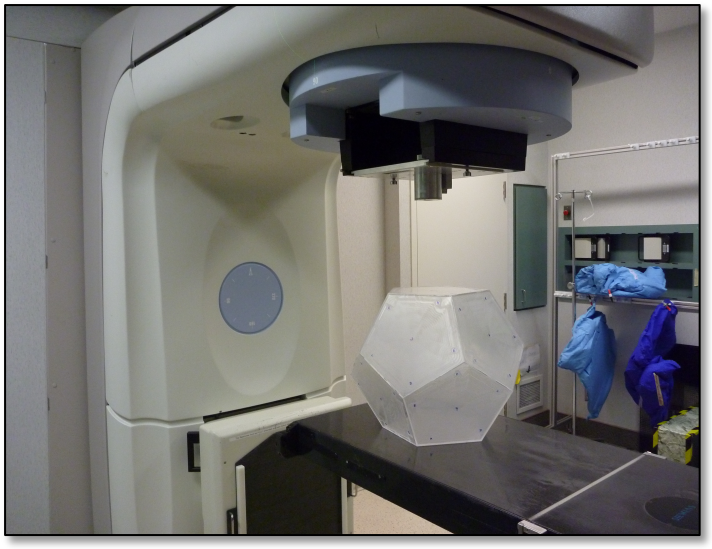

Figure 13b: Siemens dual energy Linac measured for isocentric variation at O.C.C.

In order to properly position the frame and thus the patient at the intended treatment position, a fixed frame of reference is necessary. This is achieved through fixed lasers projected at the isocentre located on the treatment room walls. These are calibrated to within a specific tolerance using a mechanical isocentre pointer fixed to either the couch base plate or to the Linac accessory holder. The lasers project a line across all three principle planes originating at the isocentre.

Stereotactic Radiosurgery Techniques

Stereotactic Radiosurgical techniques can be delivered from modified medical linear accelerators or Co-60 sources (such as the gamma knife unit). While the Gamma-Knife Unit uses the intersection of individual collimated Co-60 sources, a Linac uses a combination of gantry and treatment couch rotations to produce the desired dose distribution. There are many different techniques employed at various cancer centres, each having advantages and disadvantages, however the resulting dose distribution should meet the dosimetric requirements for each treatment.

Narrowly collimated radiation beams are delivered from multiple entry locations focused at the machine isocentre. Parallel and opposing beams are avoided to limit the dose to surrounding healthy tissue.

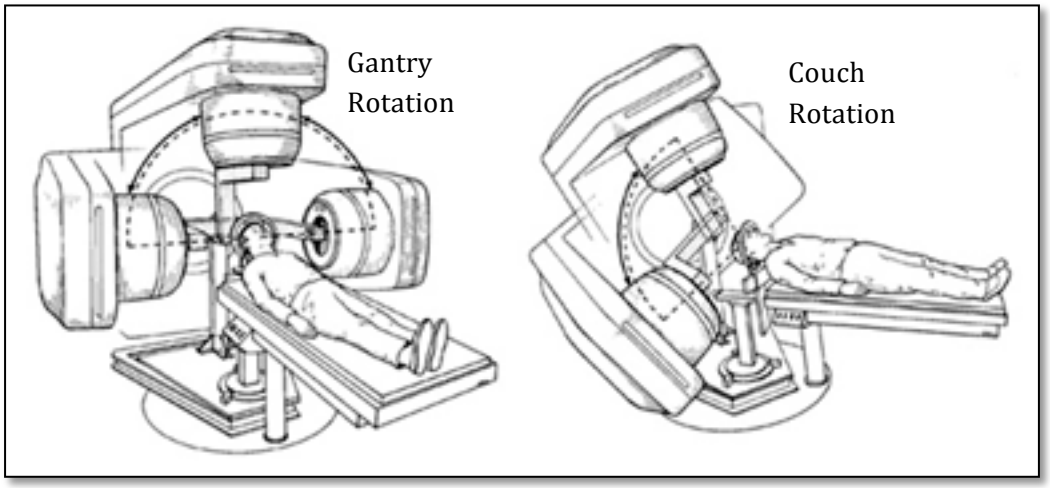

Figure 14: Stereotactic treatment: Linac and couch motions. Adapted from http://www.gammaknifeminnesota.com/stereotacticradiosurgery.html with slight modification.

This allows for a lethal dose of radiation to the target while maintaining a sub-lethal dose for surrounding healthy tissue. For linear accelerator based radiosurgery this is accomplished by rotation of the gantry and treatment couch (turntable) as seen in Figure 14.

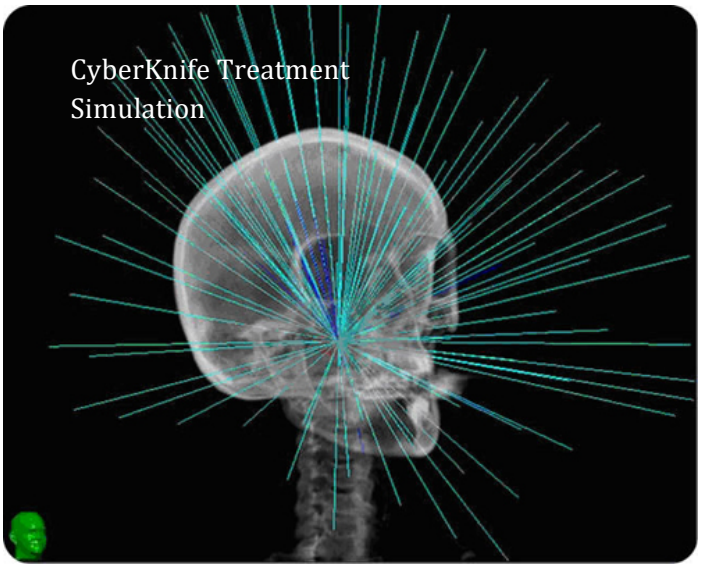

Figure 15: Radiation entry and exit beams used by the CyberKnife Stereotactic Radiosurgery Unit. Adapted from http://www.chscyberknife.com/FRP03.shtml with slight modification.

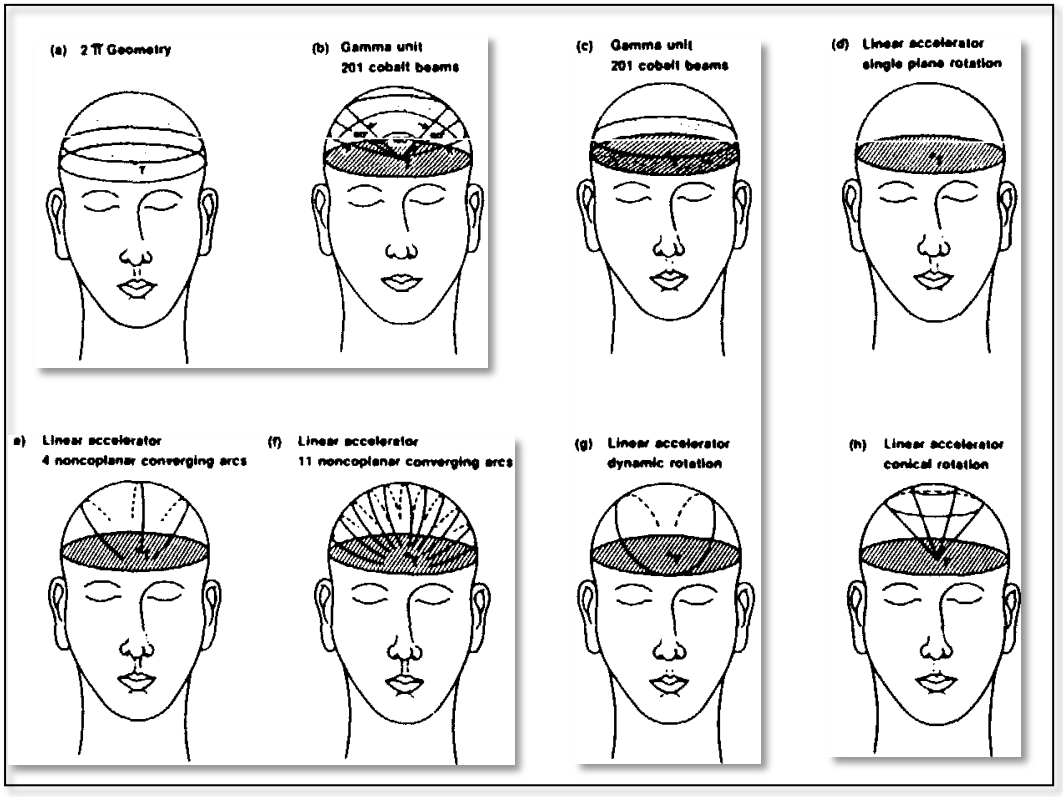

Figure 16: Various Stereotactic Radiosurgery treatment technique patterns. Adapted from Ref. Schell, 1995.

Each arc the gantry completes is repeated at multiple treatment couch angles creating multiple entry and exit points to the target. Figure 15 shows the entry and exit beams for the Cyber-knife Unit. Figures 16b and 16c show the gamma knife unit pattern; Figure 16a shows a single 360° arc in the transverse plane of the patient; Figure 16e shows a four non-coplanar arc geometry; and Figure 16g depicts the dynamic radiosurgery approach. These four approaches produce isodose surfaces with shapes that are unique to the SRS. The dose-volume histograms have been found to be approximately equivalent among the four approaches (Schell, 1995). Previous to advancements in treatment planning systems in the 1980's, standard gantry arc angles and couch angles were used. However, now it is common practice in cancer centres to tailor the dose distribution such that critical structures can be avoided and the prescribed dose is properly delivered to the target. The gamma unit accomplishes this by plugging or unplugging individual radiation sources while arc geometries can be changed with a linear accelerator. It is also common for both accelerators and gamma-units to use multiple isocentres to alter the dose distribution and allow for treatments of irregularly shaped lesions. Circular collimators are used as the dose distribution produced over a hemisphere experiences a much sharper drop off when compared to standard rectangular shaped accelerator collimators (Schell, 1995). The 10 cm. thick cones are placed 23 cm. from the isocentre and must coincide with the radiation source and isocentre.

Two different treatment techniques are used at the Odette Cancer Centre (O.C.C.) in Toronto, Canada. These techniques are accomplished using a couch mounted frame and a Siemens dual energy Primus linear accelerator (6MV and 10MV). The patient is placed on the treatment couch in the supine position (face up) where the frame is rigidly attached on the end of the couch such that the patient's head is held in the frame over the end of the couch. Once the patient in aligned using treatment room wall mounted lasers, the couch lateral and longitudinal movements are restricted and the gantry and couch are moved to their starting position. Treatments using cone sizes smaller than 3cm diameter employ 5 couch angles and gantry arcs of 60 degrees. Treatments using cone sizes larger than 3cm diameter uses 4 couch angles and 75 degree gantry arcs.

Small Cone Size Technique		**Large Cone Size Technique**	
Couch: 60°	Gantry:-150° to -90°	Couch: -56°	Gantry:-150° to -75°
Couch: 30°	Gantry: -90° to -30°	Couch: -22°	Gantry: -75° to -0°
Couch: 0°	Gantry: -30° to -30°	Couch: 22°	Gantry: 0° to 75°
Couch: -30°	Gantry: 30° to 90°	Couch: 56°	Gantry: 75 to 150°
Couch: -60°	Gantry: 90° to -150°		

The collimator settings used for treatment employs a square field size of 4cm x 4cm to allow for different cone sizes to be used while attenuating the beam around the cone field as much as possible. The collimator angle is rotated to 90 degrees and is kept stationary during treatment. The collimator is rotated to 90 degrees as this is the angle at which the cone (firmly attached to the

gantry head in a locked accessory tray) would not fall out due to gravity and any unforeseen mechanical failures in the locked accessory tray.

The rotation coordinate system used for the gantry and treatment couch at O.C.C. can be found in Figures 17 and 18 respectively. For all the data presented here which shows gantry and couch treatment angles, these figures define the angle convention to be used.

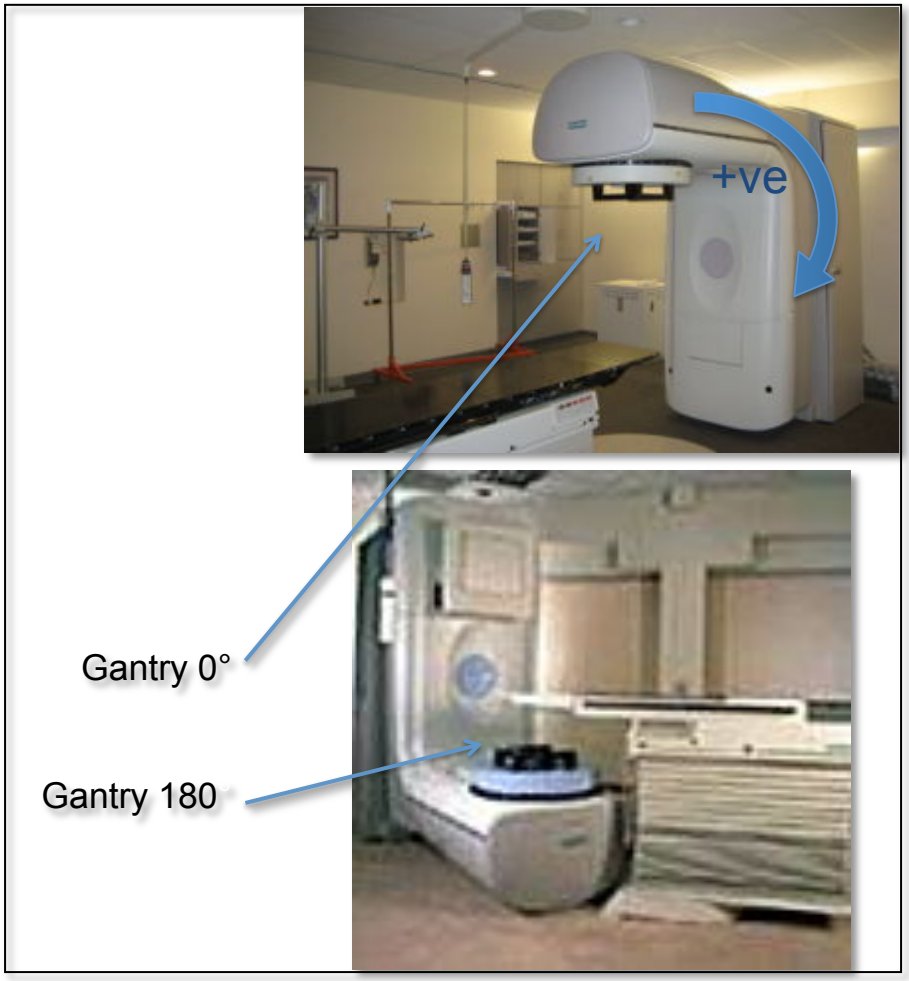

Figure 17: Odette Cancer Centre gantry rotation convention. Adapted from (top) http://www.medwow.com/used-linear-accelerator/siemens/mevatron-primus/124178192.item

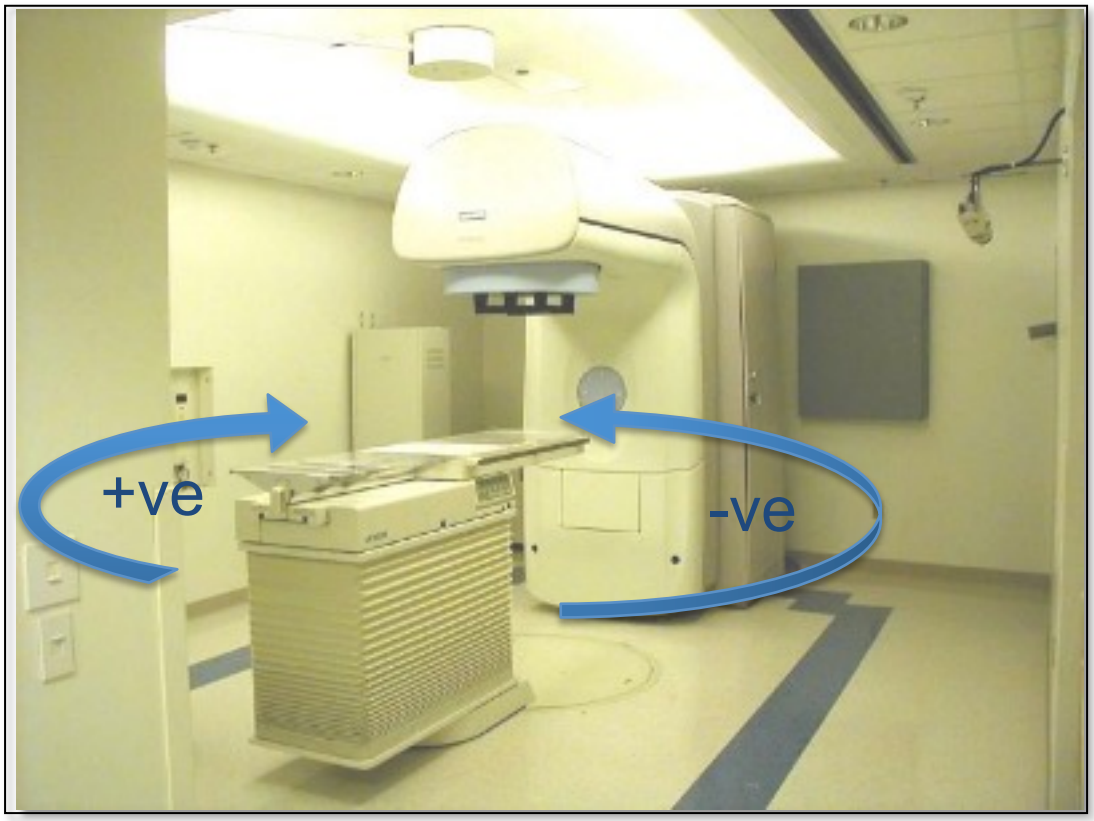

Figure 18: Odette Cancer Centre treatment couch rotation convention. Adapted from http://neevon.com/ with slight modification.

Accuracy of Stereotactic Radiosurgery

The accuracy of a stereotactic radiosurgery treatment depends ultimately on the technological limitations of the treatment unit itself and the stereotactic frame. It also depends on the knowledge of the treatment target and it's radiological response to ionizing radiation. The uncertainty in dose delivery is a result of two processes: (1) target definition and (2) the machine tolerances of the dose delivery apparatus (including the frame). A reasonable perspective on accuracy requirements for SRS should include (1) the current accuracy in external beam therapy; (2) the net result of uncertainties in SRS; (3) the resolution of the target image; and (4) the relationship of the image to the treatment target. Friedman and Bova's (1989) study, (as cited in Schell, 1995) reported uncertainties used in two SRS techniques in target alignment with the beam focus of 0.2-0.4 mm in patient position, whereas the linac setup uncertainty was 1.0 mm.

The definition of a tumour through imaging depends on the resolution of the image and the relationship of the macroscopic image with the microscopic extent of the disease (Schell, 1995). CT image pixel dimensions are typically 0.7mm by 0.7mm, and the separation between slices is not less than 1.0mm. The mechanical position uncertainty of the stereotactic frame is 0.6mm. The gantry rotation axis, collimator rotation axis, and couch rotation axis should coincide within a sphere of

1mm radius (Schell, 1995). The net uncertainty in target localization and treatment delivery is less than 2.0mm for an AVM and 2.4mm for a tumour (Schell, 1995). The uncertainty in dose delivery by any SRS treatment system are significantly less than the clinical knowledge of the location and extent of the tumour as determined by CT or MRI (Schell, 1995). Although the uncertainties associated with treatment delivery are less than those associated with the imaging, the positional accuracy of the treatment should be known during the planning process.

Quality Assurance

Stereotactic Radiosurgery allows a highly accurate radiation dose to be delivered to the target with a high dose gradient drop off to surrounding healthy tissue. There are two main requirements while using stereotactic radiosurgery or radiotherapy: (1) precise stereotactic localization and geometrical definition of the target and (2) precise delivery of the treatment absorbed dose that is tailored to the target (Schell, 1995). In order to assess these requirements, a radiation dosimetry device must be used. Dosimetry of the radiation fields delivered by stereotactic radiosurgical systems has three requirements. 1) Sub-millimetre spatial accuracy of the radiation dosimeter. This ensures volume averaging near the field edges will not occur and rapid dose gradients can be measured. 2) Should provide a map of the dose distribution. 3) Must be able to integrate dose over time. This is necessary to accumulate the dose delivered during each gantry and couch rotation.

Due to the damaging effects of ionizing radiation on healthy tissue, quality assurance (QA) methods must take place to ensure accurate treatment delivery. However, it is not the radiosensitive structures located at a distance from the isocentre that is the greatest risk, rather it is the tissue located adjacent to the lesion that is included in the high dose isocentre region (Greenberg, 2010).

The quality assurance associated with stereotactic radiosurgical treatments involves multiple disciplines including radiation oncology, radiology, neurosurgery, and medical physics. The research presented here is associated with the medical physics discipline and has practicality for medical linear accelerators, therefore the QA information here will only pertain to this.

For a stereotactic radiosurgery program, the Quality Assurance design applies to three stages: (1) the SRS procedure design methodology, which is based on probable risk analysis; (2) the QA for each treatment; and (3) the routine QA tests, which occur at fixed time intervals (Schell, 1995). SRS QA programs differ from institute to institute as there is no universal protocol. This is due to the various constraints at cancer centres including resources, plant layouts, etc. Technical aspects of SRS include accuracy in target localization and in target position during dose delivery, dosimetry, quality assurance, and patient safety (Schell, 1995).

The principal features of the QA programs are (1) verification of the mechanical tolerances. (2) x-ray/light field/laser alignment with isocentre, and (3) verification of the target/tumour with the isocentre prior to treatment (Schell, 1995).

A common test used in SRS QA to check the overall positional accuracy of the radiation delivery is the Winston-Lutz test (Lutz, 1988). These measurements involve projecting a radio-opaque ball from various gantry angles onto a film and looking at variation of the ball's movement with respect to the field edges. Lutz (1998) found that the smallest sphere circumventing nine beam's central axis on each film ranged from 1.2 – 1.8mm and that the distance between the center of this sphere and the center of the steel ball was calculated to be 1.33±0.64mm. based on coordinates determined through CT localizations. Lutz (1998) found that this effective movement of isocentre had the effect of spatially widening the penumbra (region of dose fall- off between target and surrounding tissue) by an amount less than half the diameter of this 'smallest' sphere.

Research

Hypothesis and Specific Aims

The hypothesis of this research is that the radiation isocentre variation from a SRS treatment can be mapped out with sub-millimetre precision using a quality assurance phantom containing film at large enough distances from the isocentre such that individual radiation beam offsets from treatment machine mechanical instabilities are sufficiently magnified. This will be measured by designing and fabricating a SRS quality assurance phantom with specific characteristics and properties. The phantom will be extensively tested and software will be developed to provide isocentre variability results. The isocentre variability map can then be used to correct the aim of the convergent radiation beams bringing them closer to a common isocentre point using either the variation in isocentre due to collimator rotations and/or small field shifts.

The aim this research is to provide a stereotactic radiosurgical phantom that will allow cancer centres to know the isocentre variability of their SRS treatment machines providing them with the information needed to improve the accuracy and precision of the dose distributions delivered.

The dodecahedral phantom we proposed in this thesis offers several advantages when compared to the Winston-Lutz test and cubical phantoms. The larger distance between parallel faces, the larger number of parallel faces and the resulting lack of eccentricity of the entry and exit beam spots on the films allow one to obtain a higher level of accuracy for beam measurements. With a successful implementation, this phantom has the potential to become a standard for radiosurgery quality assurance.

The anticipated significance of the work here is to provide medical physicists with a method to reduce the impact of the radiation isocentre variability of the linear accelerators thus reducing the error in dose received to the target while minimizing the dose to healthy tissue. This in turn will lead to fewer side effects and a better quality of life for the patient.

Phantom Design and Fabrication

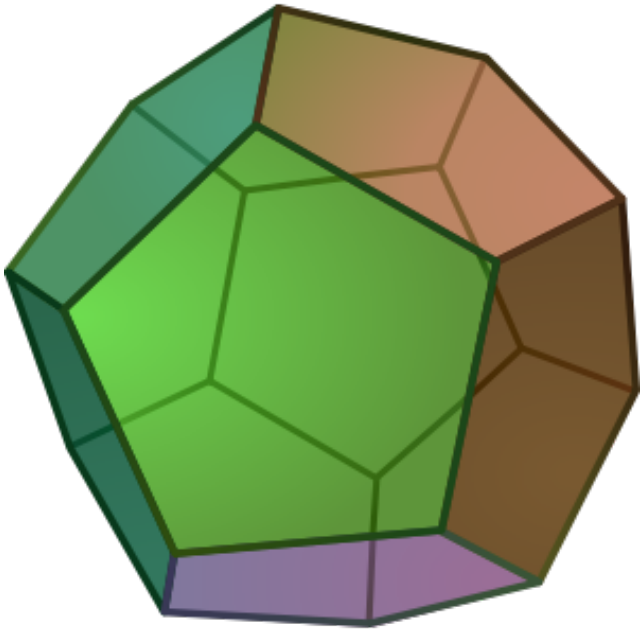

Figure 19: The dodecahedron

Phantom Design

Initial design considerations were first discussed at O.C.C. with the intention to use the machine shop there for phantom construction. O.C.C. is equipped with 12 linear accelerators with one currently being used for SRS treatments (Siemens Primus dual energy unit (6MV and 10MV)) and one Elekta unit for future SRS treatments. The machine shop at O.C.C. is lead by Machinist Mr. Harry Easton, and is fully equipped to accommodate the phantom construction and materials. Before any fabrication was completed in Canada, the research was continued for four months at the DKFZ (German Cancer Research Centre) in Heidelberg, Germany, as part of a new graduate student exchange program and research collaboration between the DKFZ and the Department of Physics at Ryerson University. This presented an excellent opportunity to further the research presented here as the DKFZ is world renowned for cancer research and has excellent resources for the phantom development. The DKFZ has three Siemens Primus treatment units, two of which are used for patient treatment (including stereotactic radiosurgery) and one solely for research. The machine used for initial measurements was essentially identical in all aspects related to the research to the treatment machine characterized at the O.C.C. The thesis work was supervised in Germany by Prof. Dr. Guenther Hartmann while maintaining contacts to supervisors in Canada for guidance. Phantom design and fabrication considerations were discussed with and supervised by the Head Medical Physics Engineer at the DKFZ, Dipl.-Ing Gernot Echner.

The QA phantom that was developed here utilizes Gafchromic EBT film (a radiochromic film manufactured by ISP) at known distances and orientations relative to the isocentre to reconstruct the individual paths created by the converging radiation beams.

Radiochromic film contains a special dye that is polymerized upon exposure to radiation. Radiochromic film is self-developing, requiring neither developer nor fixer. Since radiochromic film is grain less, it has a very high resolution and can be used in high dose gradient regions for dosimetry and thus is ideal for this research (Devic, 2005). Gafchromic EBT film is sensitive in the 1cGy - 800cGy Dose range, it is Energy independent from the keV range into the MeV range, and has uniformity better than 1.5% (International Specialty Products, Inc., 2007). Furthermore, the film can easily be cut to any shape and marked for reference.

Although it has been shown that Linac isocentre variability can be measured using electronic portal imaging devices (Winkler, 2003), the use of the imaging device as a comparison for this research was not investigated due to time constraints.

Two films are located on opposing sides of the phantom such that any radiation beam through the isocentre will be exposed on both films. At O.C.C., an initial design for the phantom was developed taking into consideration all design constrains listed below:

Note: these design constraints and data taken to determine phantom characteristics are described in more detail in the next section.

Phantom Shape – The three dimensional shape must allow for film to be fixed to its outer surface, therefore flat surfaces must be used. The phantom must also exhibit opposing faces to allow beam cross sections to be caught on an entry and exit film. The phantom is to be hollow to minimize the weight and to allow for future quality assurance devices to be inserted internally at the centre of the phantom.

Phantom Size – The phantom must be large enough to significantly reduce the error when measuring individual beam offsets while not allowing collisions between the cone and phantom when there is rotation of the treatment couch and gantry. Weight considerations must also be looked at as the phantom is to be placed at the end of the treatment couch creating strain on the device which holds the phantom in its location. The device will also need to be transported from a storage location to the treatment unit on a push cart.

Phantom Material – The material used must be strong enough to support the weight of the phantom, maintain structural stability, and must have radiation build-up properties to allow for sufficient exposure of the Gafchromic film.

Phantom Shape

The phantom shape was first visualized to be cubical in shape. This shape would have allowed for parallel and opposing planes, easy construction, and simplified computer modelling. However, discussions with Profs. Hartmann and Echner at the DKFZ led to reviews of other shapes concluding that a more unique shape than a cube, the Dodecahedron, would be the best design alternative. This shape, which is closer geometrically to a sphere than a cube allowed for greater opposing film plane distances than the cube, which suffers from collisions near its edges. It must be noted here

that other shapes were investigated, but the face shapes most exhibited would have required cutting the film to a great extent. Furthermore, given the larger number of faces of the dodecahedron shape, it exhibits a superior ability to minimize the angle of incidence of the incoming beams. This benefit is explained later in the Contour Data section.

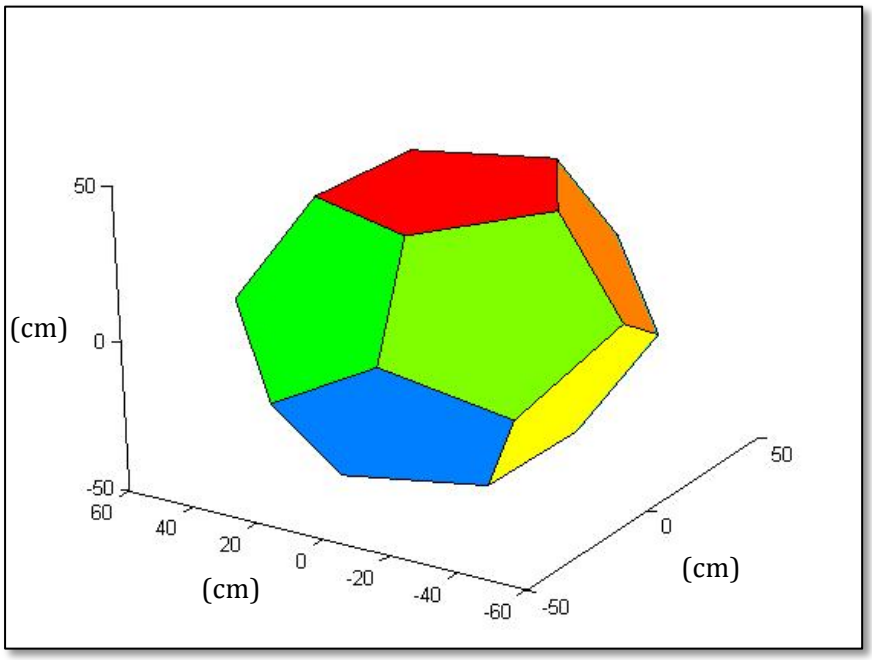

Figure 20: Matlab dodecahedron model

The Dodecahedron, seen in Figure 19 and 20, is any twelve sided three dimensional shape. The design for this research however uses the *regular* dodecahedron. It is a platonic solid, exhibiting faces that are congruent regular polygons, with the same number of faces meeting at each vertex. The *regular* Dodecahedron is symmetric in all directions. It can be rotated by a specific angle any amount of times and still maintain the same orientation. It has parallel and opposing planes and a three dimensional shape that makes it very sturdy and resistant to warping or deformations.

An initial design using pins to hold the film, shown in Figure 21, was devised. By placing the short edge of a film along each edge, it is possible to orient film in 5 different orientations. With this rotation of the film on each face, nearly every radiation beam from all gantry and couch rotation combinations will intercept an entrance and exit film. However, the final design did not use pins to hold the film, it was decided instead to use a machine grooved section was which would allow the film to sit flush against accurately carved edges.

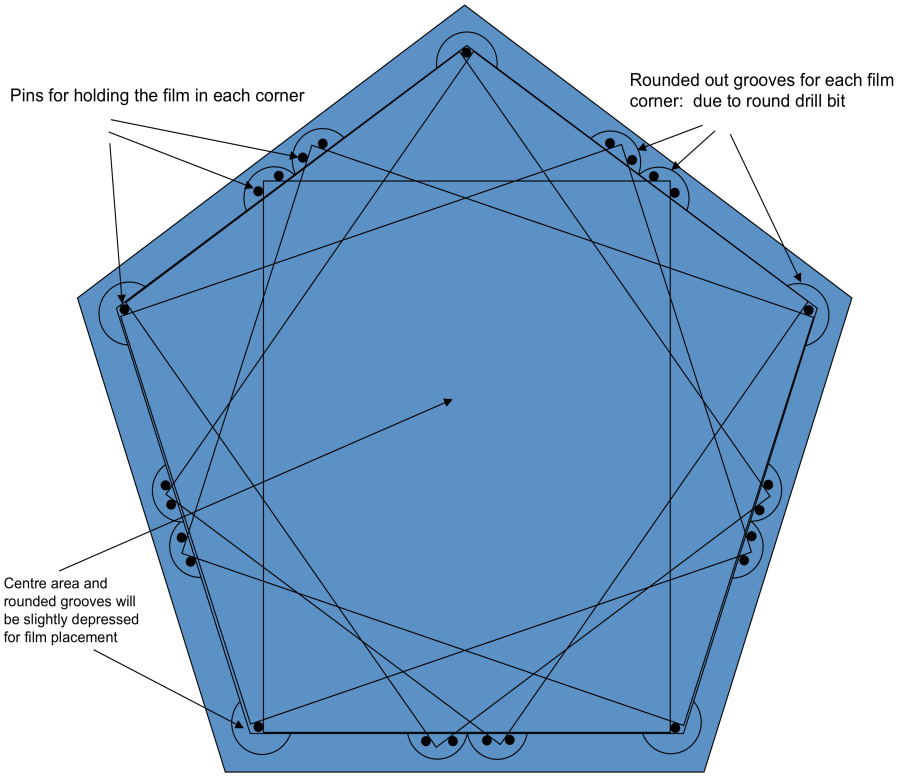

Figure 21: Dodecahedron Single face placement of film

Phantom Size and Material

The dodecahedron shape was used because it allowed for a larger phantom to be fabricated due to the fact that a dodecahedron has a more rounded shape than a cube, thus facilitating more adequately the concentric rotation of the treatment cone around the isocentre. However, it was necessary to have each sheet of Gafchromic film (20.3cm x 27.9cm) cut in half (width wise) as a dodecahedron with full sized film on the phantom faces would have created collisions between the phantom and the treatment unit. Only one corner and edge of the cut film on the un-cut edge is used for orientation therefore accurate cutting of the film is not necessary. With each film edge (the shorter edge) placed parallel to each phantom face edge it is possible to have five different orientations of the film on each face. To locate the film to the correct position on the phantom, the film is placed on a face of the phantom in the grooved out section. The film is pushed against the reference edge and then into the reference corner. This is best depicted visually and can be seen in Figures 22 and 23. It can be seen how the film sits flush with the reference edge on the phantom face. On the opposite side of the film (cut side) there is some space to allow for un-accurate cutting of the film. The film is attached to the phantom using masking tape along each edge.

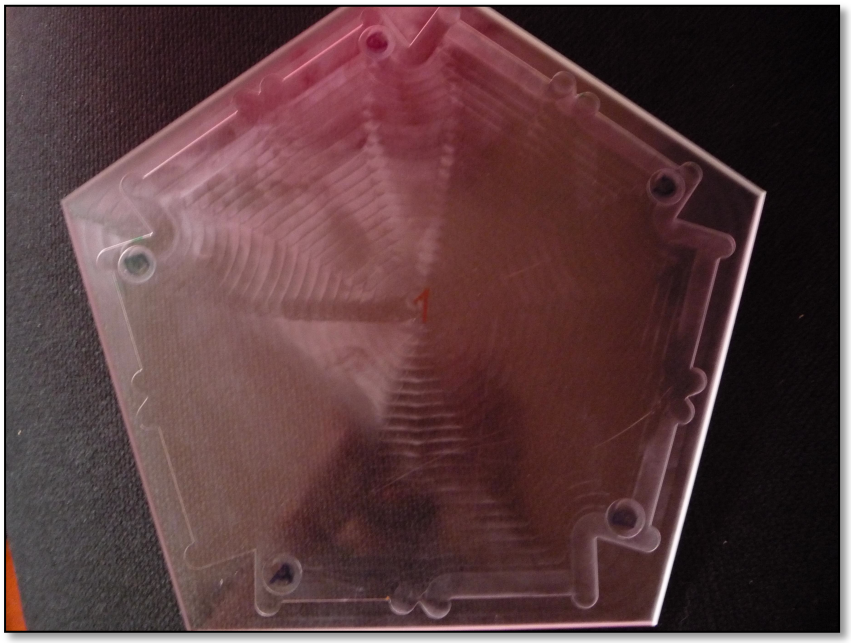

Figure 22: Phantom face showing grooved out centre to allow precise placement of Gafchromic film

This grooved out design feature allows for independent offset calculations for the same beam and gives coverage for the beam to enter from any location only missing the ones that fall on the edges of the phantom where there is no film (which actually can be measured if the phantom is shifted).

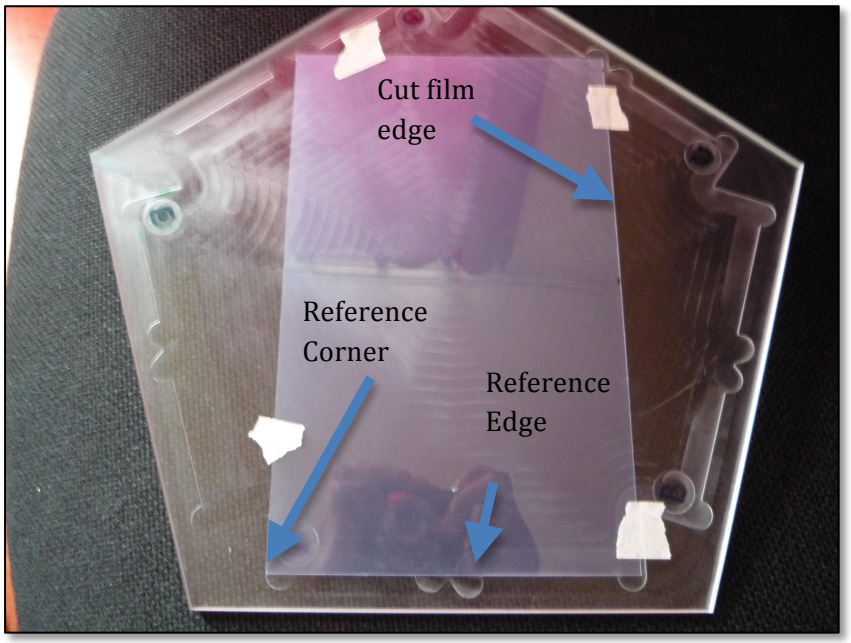

Figure 23: Phantom face with film fixated flush against the bottom left corner

The phantom was constructed solely of acrylic. This material is widely available in medical physics machine shops as it is already used as phantom material due to its charge build-up properties and it's ability to be easily machined. The phantom consists of an inner shell of 5.5mm thickness with a grooved out section to accommodate for different film orientations. The inner shell gives the phantom it's stability and provides for additional exposure of the film from backscattered radiation. The phantom also was constructed with an outer shell to provide the majority of the film dose build-up for adequate film exposure.

Measurements to determine the inner and outer shell thickness were first taken at DKFZ using the same stereotactic setup as that would be used during regular phantom use. The criteria for inner and outer shell thickness was based on phantom structural stability and weight and adequate exposure of the film. Constructing a phantom with too thin walls would lead to poor structural stability and poor film exposure while advantageously maintaining a low weight. Constructing a phantom with walls too thick would yield an unwanted high weight but provide for good structural stability. Therefore it can be seen that an optimal inner and outer shell thickness can be achieved.

The inner shell thickness was determined in collaboration with Prof. Gernot Echner, head engineer at the DKFZ, and was based solely on phantom weight and stability. It was decided to use an inner shell thickness of 5.5mm as this would provide for a light but structurally strong phantom while at the same time provide for some backscattered radiation.

The outer shell thickness was based solely on adequate exposure level for Gafchromic film. In order to determine the thickness, films were sandwiched between 8mm of solid water (essentially square acrylic pieces of known thicknesses used for quality assurance) for the inner shell (determined above) and various thicknesses of solid water on top for the outer shell and was irradiated with different amounts of radiation. Radiation doses emitted from the Linac are calibrated under known conditions and geometries. The Primus Linac used for the measurements is calibrated to deliver 1 cGy/MU at a known depth in water medium. MU here stands for Monitor Unit and is the numerical value inputted to the machine for radiation dose. Although the Linac is capable of delivering therapeutic photons and electrons at several energies, the clinical radiation used for SRS and this research at DKFZ and O.C.C. is 6MV photons delivered at a rate of 300 cGy/min. Figures 24 and 25 are the scanned Gafchromic films showing the different exposure levels obtained at different build-up thicknesses. The written values to the left of each row of beams is the thickness of build-up in centimetres used while the values on the top of each column are the dose delivered in Monitor Units. As can be seen from these three figures, increasing build-up thickness leads to increases in film exposure.

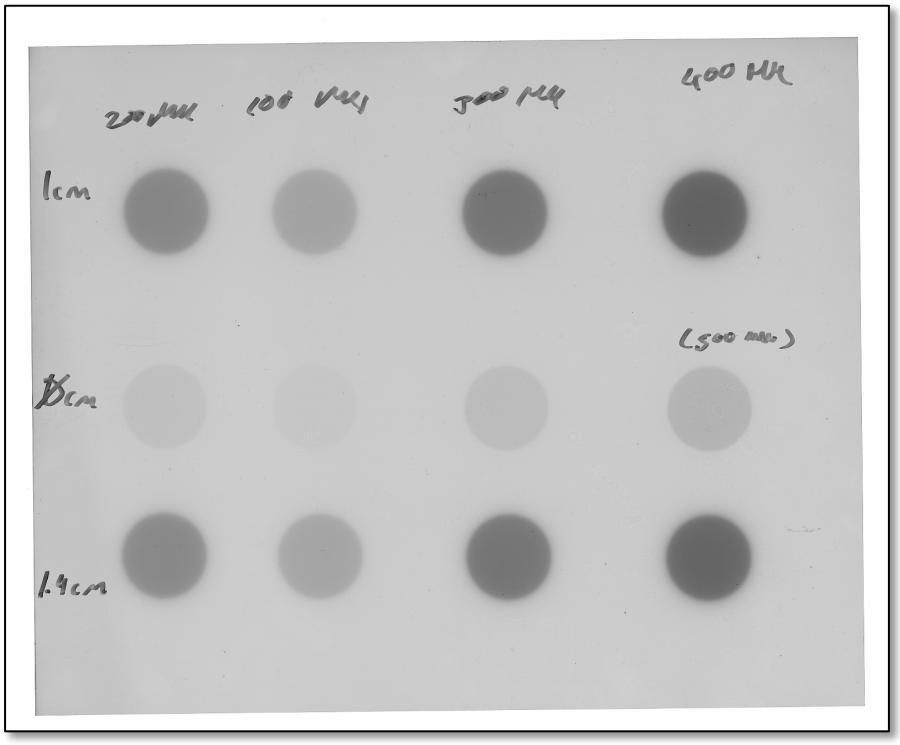

Figure 24: Gafchromic radiation exposures for various doses and build-up thicknesses

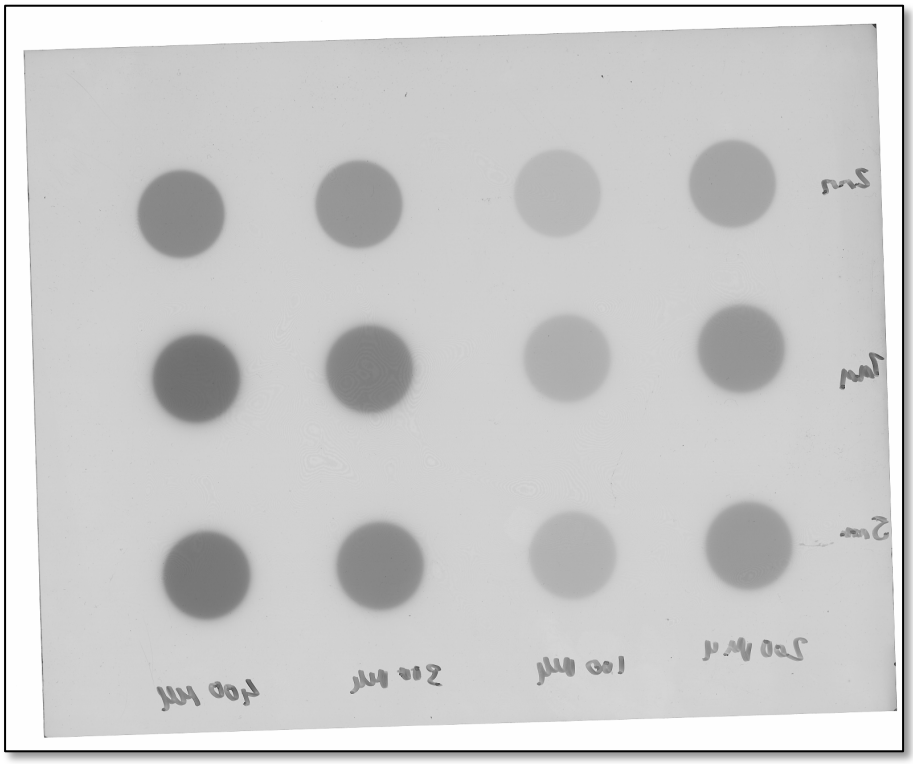

Figure 25: Gafchromic radiation exposures for various doses and build-up thicknesses

We also see that with no build-up, doses as large as 500MU, which takes up to a minute and a half to deliver, does not provide adequate exposure even for long irradiation times. Taking into account the exposure levels above, and again phantom weight, and outer shell structural stability, it was decided that an outer shell thickness of 5.5mm was to be used.

Phantom Fabrication

It is worth noting here that the individual phantom faces were constructed at the machine shop at the DKFZ in Heidelberg, Germany. Prof. Echner was concerned about shipping a completed phantom from Germany to Canada due to the possibility of deformations and/or cracks during transportation. Therefore, the individual phantom faces were shipped not attached to each other. Consequently, Mr. Harry Easton, head of the machine shop at O.C.C. assembled the pieces using a glue filled syringe to adhere each piece in place. The final product, seen in Figure 26, included a hollow inner dodecahedron shell with grooved out sections for film placement with two outer shells used for radiation build-up.

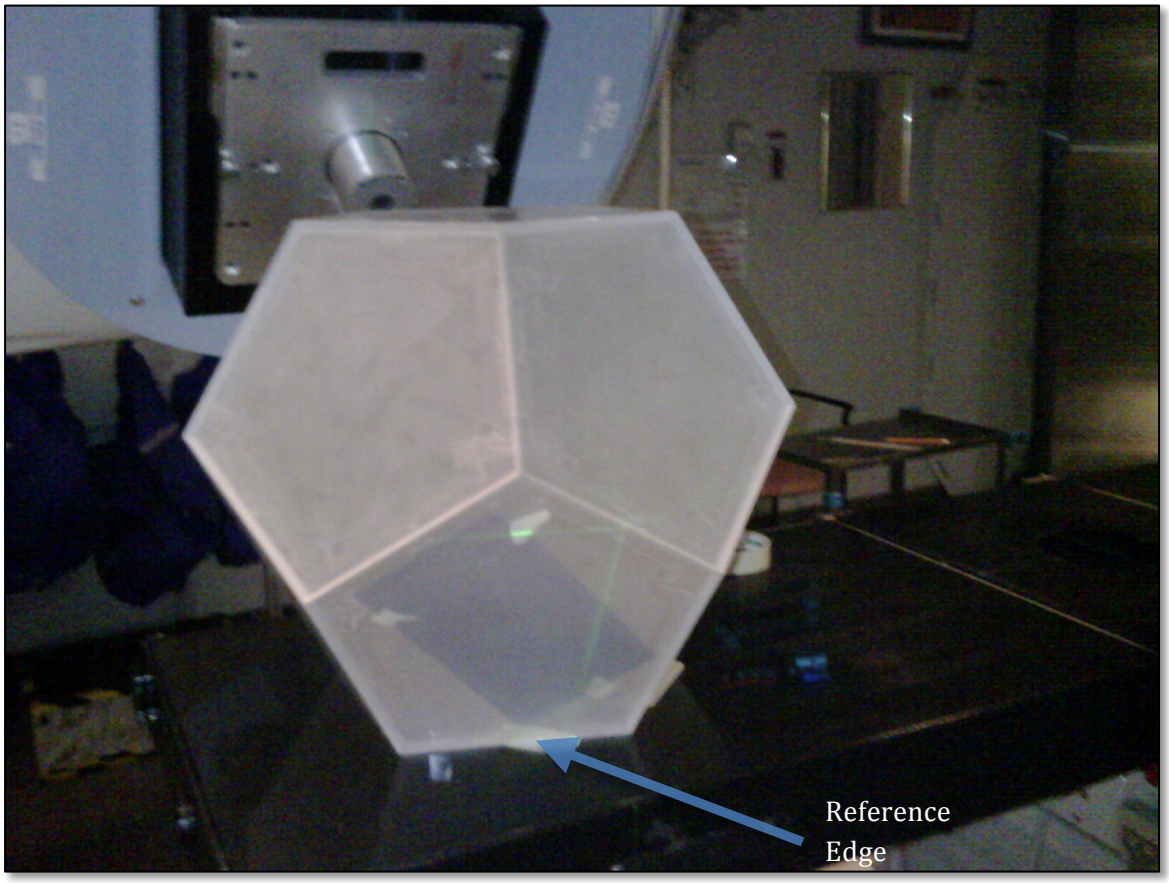

Figure 26: Completed Phantom

Once completed, each phantom face was designated a number (1 through 12) and each orientation possibility of the film on a single face was given a letter (A through E).

Software Design and Testing

A software program was written to analyse the irradiated films and provide an isocentre variability map for various treatment couch and gantry angles. The programming language used was Matlab, and this was chosen due to it's mathematics and 3-D plotting capabilities.

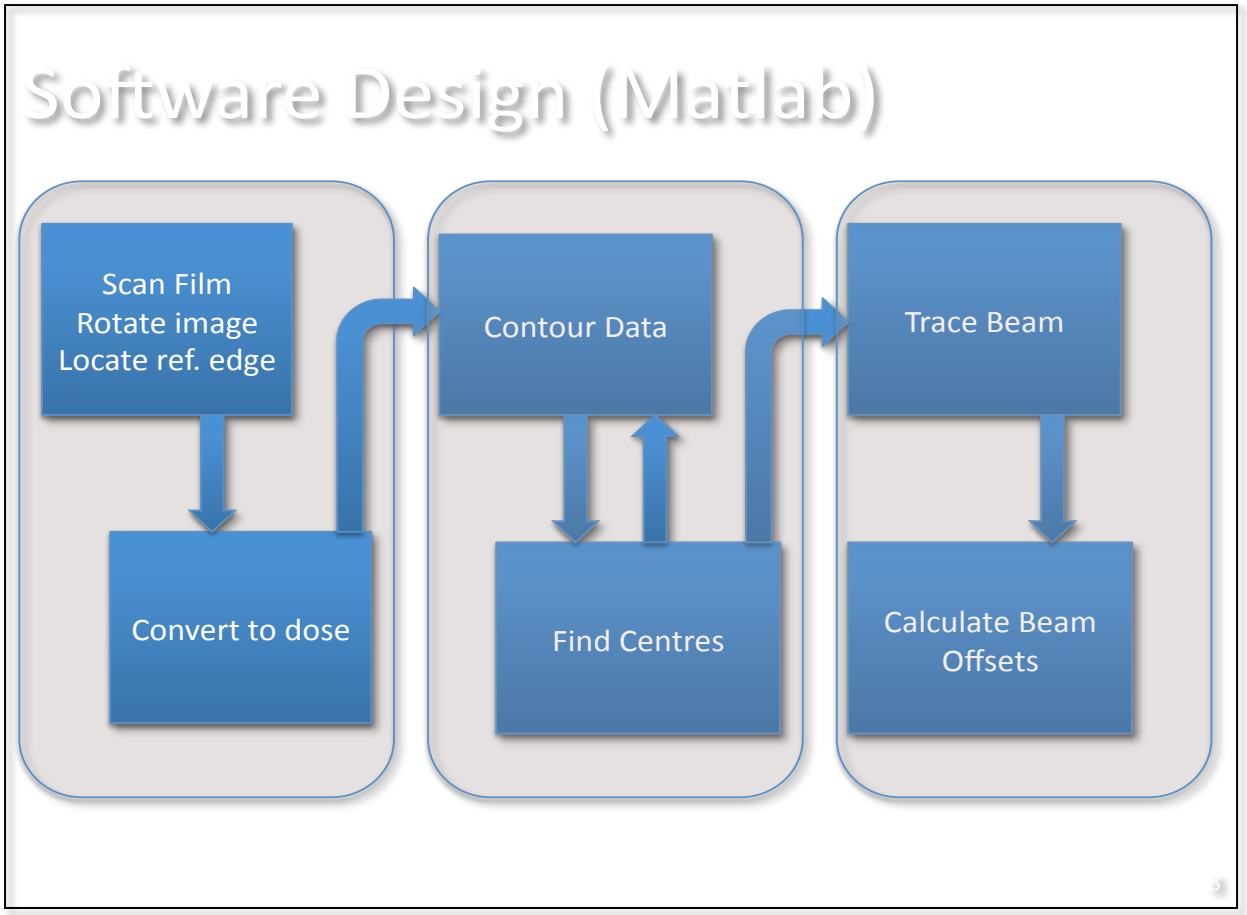

Figure 27: Software Flow Diagram

The software developed essentially calculates the isocentre variability map for various treatment couch and gantry angles by ray tracing the individual beams based on radiation beam spots on the film. Figure 27 shows the block diagram depicting the logical flow of the software each of which are described below in detail. The Matlab code (4 Matlab .m files) has been included in the Appendix.

Film Digitization

The input to the software is a series of image files (TIFF format) taken during a set of measurements. Figure 28 shows how an image file is created by scanning into a computer the individual films on a 16-bit flat bed scanner. The parameters used for scanning on the Vidar 16 bit flatbed scanner at The Odette Cancer Centre are as follows:

Resolution: 150 dpi

Bit depth: greyscale 16-bit

Figure 28: 16-bit Flat bed scanner. Adapted from http://scanner-review.blogspot.com/2007/11/umax-mirage-iise-114-x-17-9600-dpi.html with slight modification.

It was not necessary for the user to visually align the film on the scanner as straight as possible as the software does this for the user (explained below). For this research, the files were named with the following convention: 'face number–face letter.TIF'. For example, as can be seen from the Figure 30 below, films orientated with their reference corner located on face 11, spot E would have a file name '11-E.TIF'. Similarly, its opposing film would be named '3-B.TIF'. The user is able to change the file name and location for the entrance and exit film files in the code, as well as the face number and film orientation. It must also be noted here that some of the films scanned did not lie completely flat on the scanner bed and were not compressed by the top lid of the scanner in the closed position. Therefore, it was necessary to place a thin transparent piece of plastic over the film to weigh it down (the amount of scanner light attenuation was found to be negligible).

Image Rotation/ Locate reference edge

The software calculates beam spot locations on the film based on the distance or number of pixels from each beam spot to the reference corner. In order to properly calculate this distance it is necessary to rotate the image such that the reference edge is parallel to the rows in the image array matrix. From here the reference point is then located on the image to calculate the proper distance from each radiation spot centre to the reference point. This is best explained with three figures. The reference edge point and it's location can be seen in Figure 26 and 29 on the Matlab modelled phantom as well as the actual phantom.

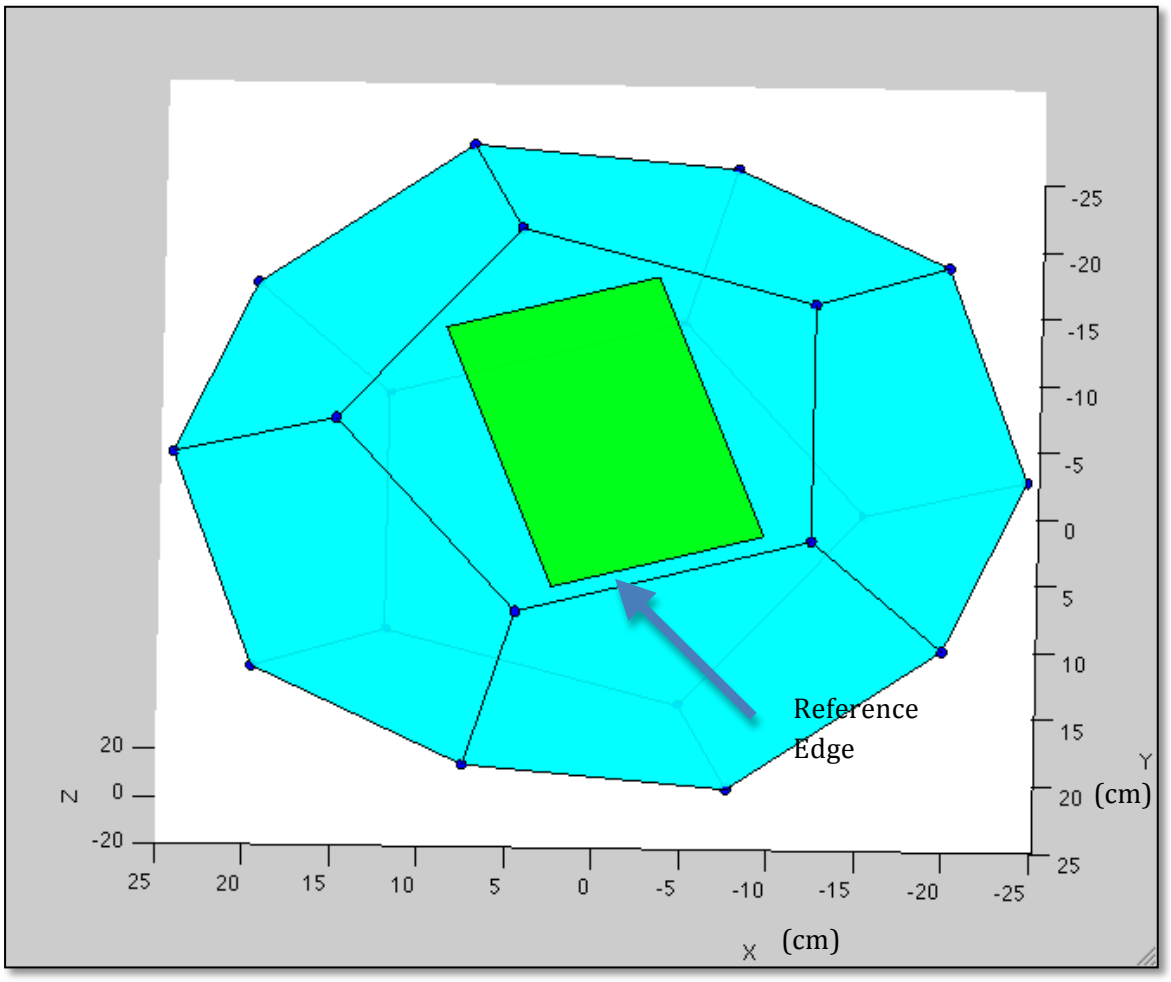

Figure 29: Matlab dodecahedron model with the location of a film

Since the film is firmly pushed against the reference edge and reference corner, it is necessary to know the location of each film relative to the white image background.

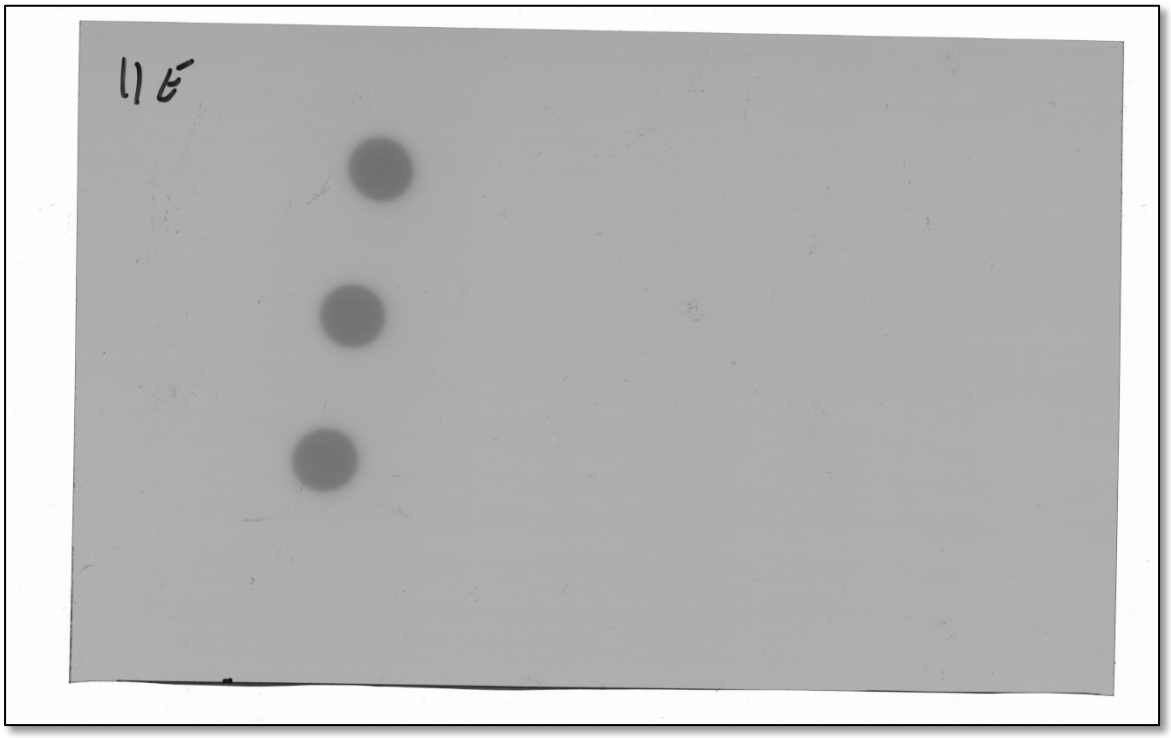

Figure 30: Un-rotated film Image

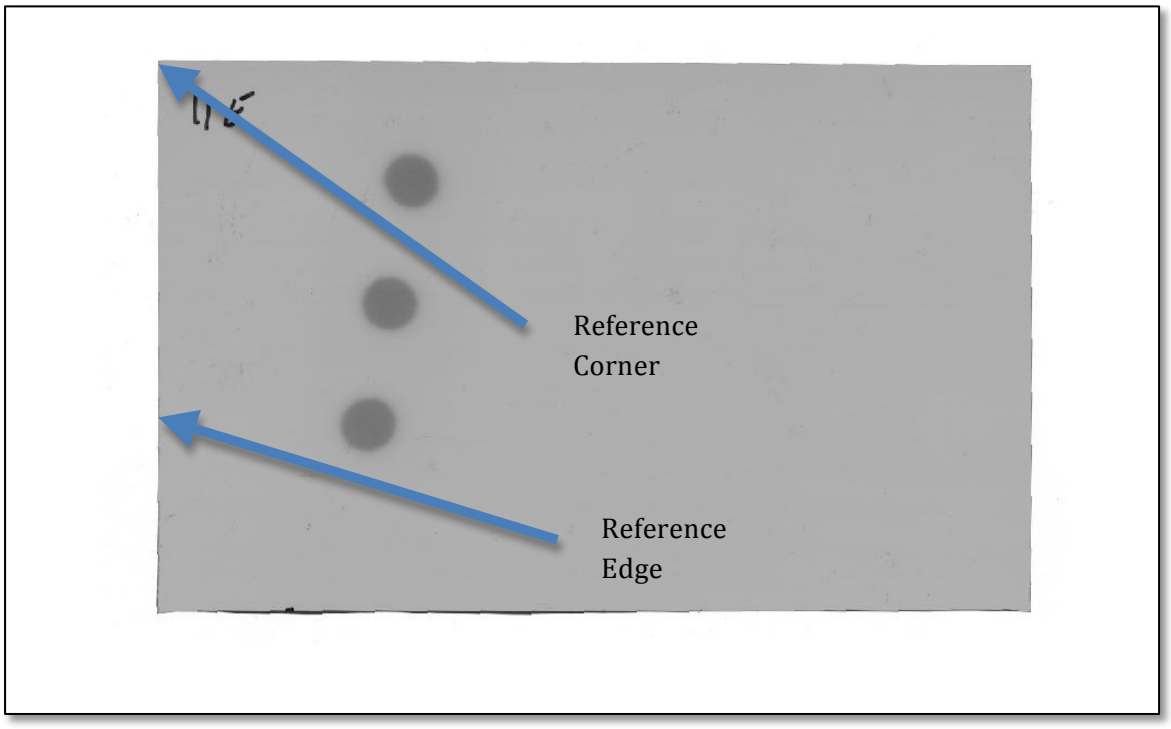

Figure 31: Rotated Film Image

For this research, all films were scanned with the reference corner located in the upper left hand corner of the screen. Matlab takes this corner to be the 0,0 for images where each pixel is an

element of an array or matrix containing the pixel values for an entire image. The matrix or array is defined here as a full representation of the two dimensional film space.

A subroutine is used to allow the user to select any point on the image with high precision by zooming in on selected regions.

Another subroutine performs image rotations. This is useful given that the reference edge of the film must be aligned with the pixel column of the image to allow for x and y distances to be easily calculated on the film. This subroutine allows the user to rotate the image based on two points selected along the reference (left) edge of the film. A line is then created along this edge which allows the software to rotate the image based on the angle between the user defined line and the vertical rows. Figure 30 shows a raw image file before any rotation has taken place and Figure 31 shows how the image looks following this transformation.

For the reference edge selection, or background removal, the user once again uses the above subroutine to select the reference corner (upper-left) of the film. An example can be seen in Figure 32.

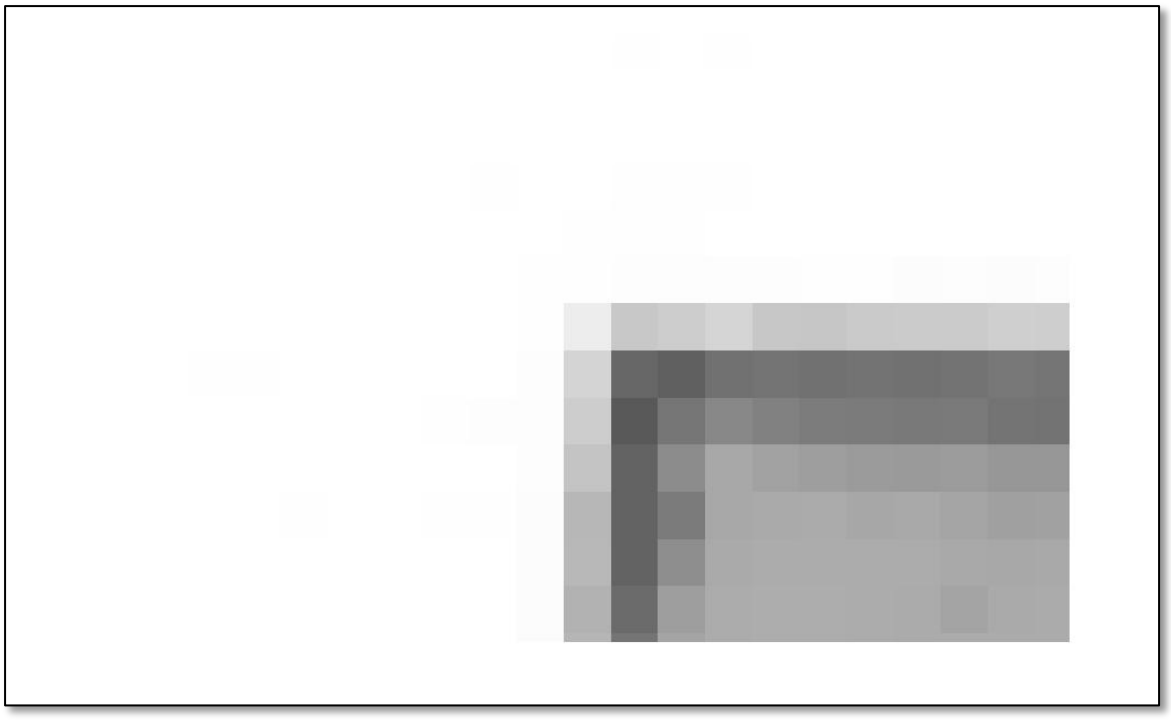

Figure 32: Reference corner selection (magnified)

Once the image has been rotated and the reference corner was selected, the voxel values are now converted to dose and then contoured to find the radiation spot centres.

Convert to Dose

The raw images created by the scanner is simply a array of gray-scale values ranging from 0 to 65535 based on the attenuation of light through the film. However, to correctly contour the beam

spots, the image must be converted to radiation dose. Dose response curves covering several energies and doses over large ranges have been created for the Gafchromic film previously at O.C.C. using the software ScanQA By PTW Inc. The dose response curve for 6MV is seen in Figure 33.

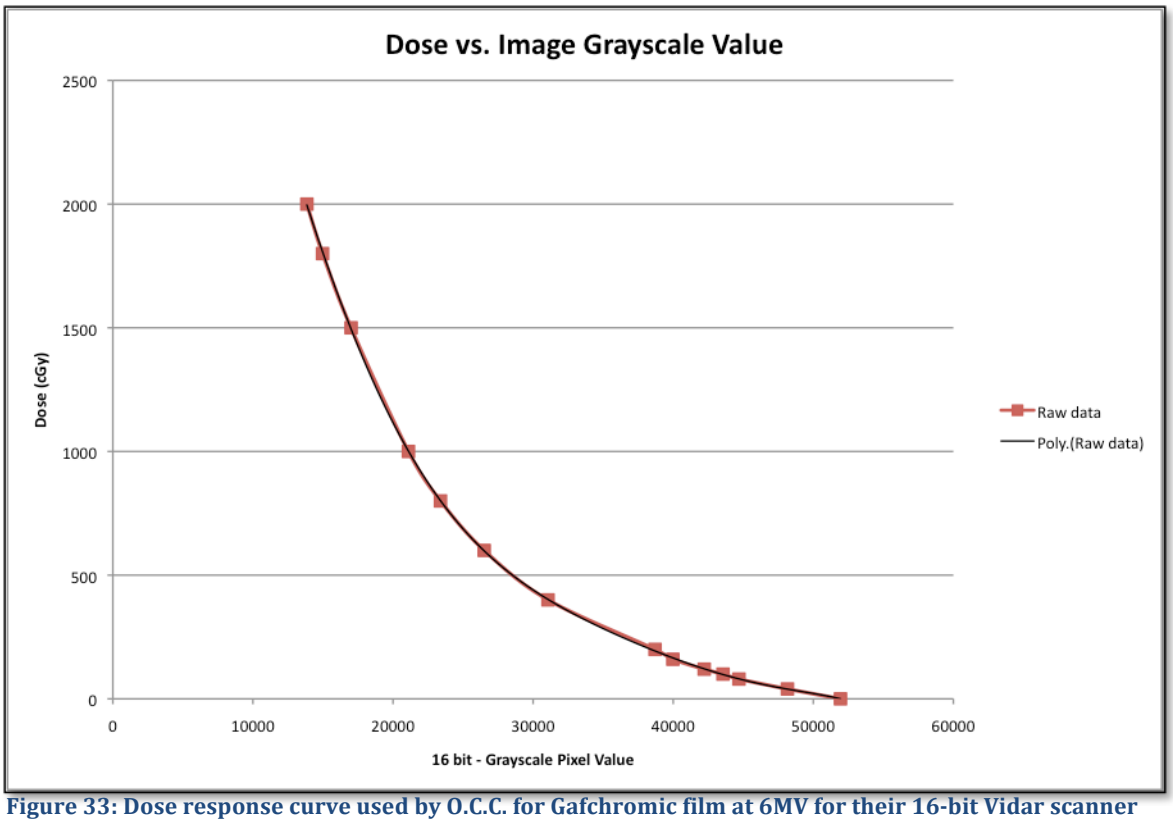

Figure 33: Dose response curve used by O.C.C. for Gafchromic film at 6MV for their 16-bit Vidar scanner

Equation 1 was used to convert each pixel in the film image into dose. Poly. (Raw Data) in Figure 33) was derived from a sixth degree polynomial fit of a range of data read into in the ScanQA software.

Eq. (1)

$$y = -3.97\times10^{-24}x^6 + 7.98\times10^{-19}x^5 - 6.31\times10^{-14}x^4 + 2.43\times10^{-9}x^3 - 4.31\times10^{-5}x^2 + 1.61\times10^{-1}x + 3539.74$$

Figure 34 shows a sample raw image before any conversion to dose has taken place while Figure 35a is the image after conversion.

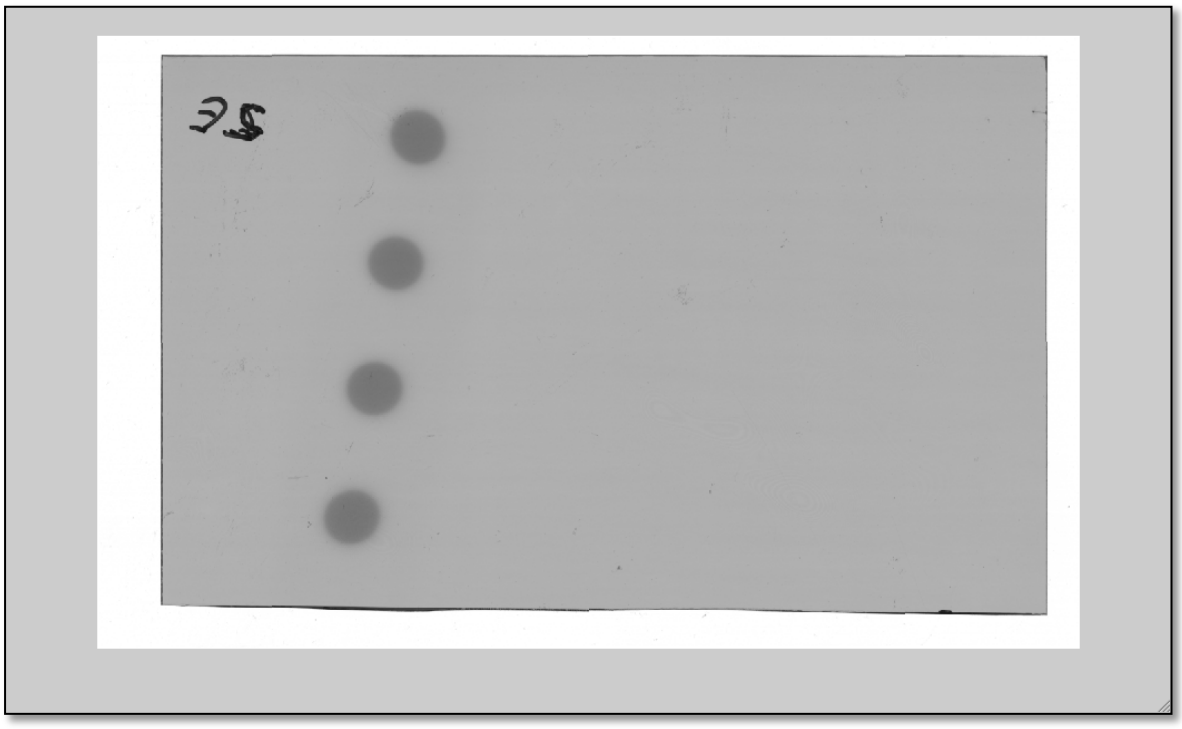

Figure 34: Film image (Greyscale) before conversion to dose (cGy)

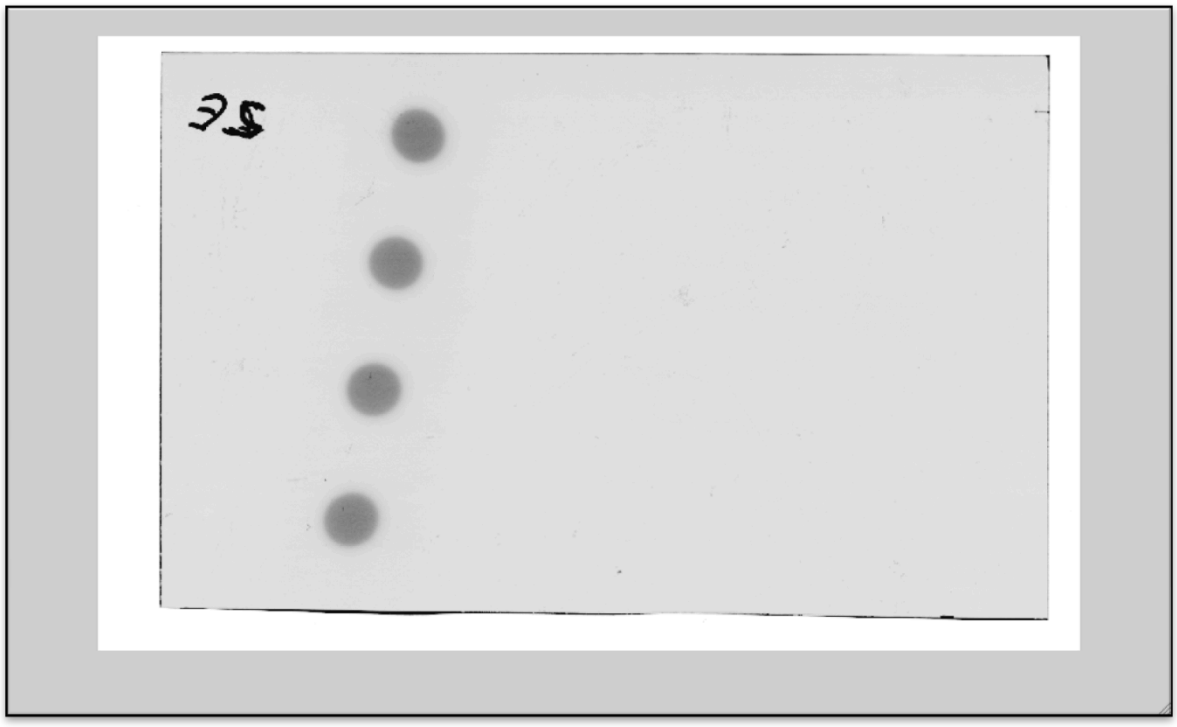

Figure 35a: Film image converted to dose (cGy)

As can been seen in the two above figures, the pixel values outside the irradiated area has become considerably lighter (low dose region).

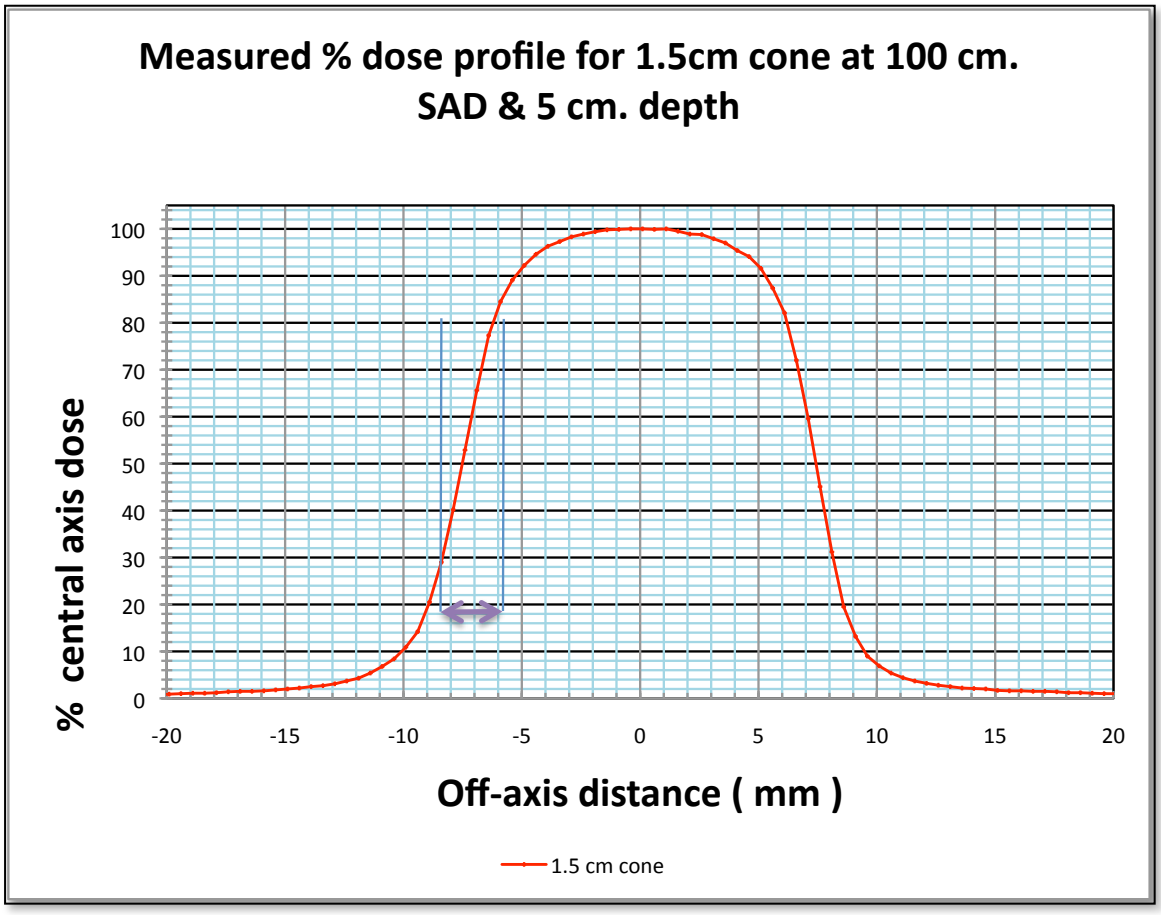

Figure 35b: Plot of the SRS cone research Linac profile at a typical clinical depth. The 80%-20% dosimetric penumbra here is 2.7 mm (indicated by violet arrow). At the depth of maximum dose or for the acrylic build-up (outer shell) thickness or for no build-up at all, the 80%-20% penumbra is typically 2.4 - 2.5 mm.

The plot in Figure 35b shows the percentage of the central axis dose as a function of off-axis distance for the 1.5cm cone at O.C.C. on the machine used for this research. The profile shown was measured at 5cm depth in water at 100cm distance from the source. As can be seen from this plot, there is a 2.4mm - 2.5mm range for which a dose threshold can be chosen for the data contouring.

Contour Data

The first steps of the software development were to have the software properly read in a film and locate the radiation beam spots by thresholding the image at an optimal pre-determined dose level.

The optimal dose threshold level, explained below, was determined by calculating the contours over a wide range of doses. The Matlab function Im2bw converts a greyscale image to a binary image based on this dose threshold. The output image replaces all pixels in the input image with luminance greater than the dose threshold level with the value 1 (white) and replaces all other pixels with the value 0 (black).

Find Radiation Spot Centres

Based on each individual contour, the central axis of the beam is found through two methods. Note that for both methods, the reference edge location is subtracted from the found beam centres. The first is done simply by calculating the average or median of the contour data. The second, however is done by performing a least squares fit of the contoured data to an ellipse (Fitzgibbon, 1999). The ellipse fit is done due to the circularly collimated radiation beam intersecting a flat film plane. From this fit, the centres are calculated from equation 2 based on the best parameters found (a,b,c,d,f,g), in the least square sense for the quadratic form of an ellipse:

Eq. (2) $$ax^2 + 2bxy + cy^2 + 2dx + 2fy + g = 0$$

Figure 36 shows the contour plots (in red) and the corresponding least-squares ellipse fits (in green) over a range of dose threshold values for a single radiation spot.

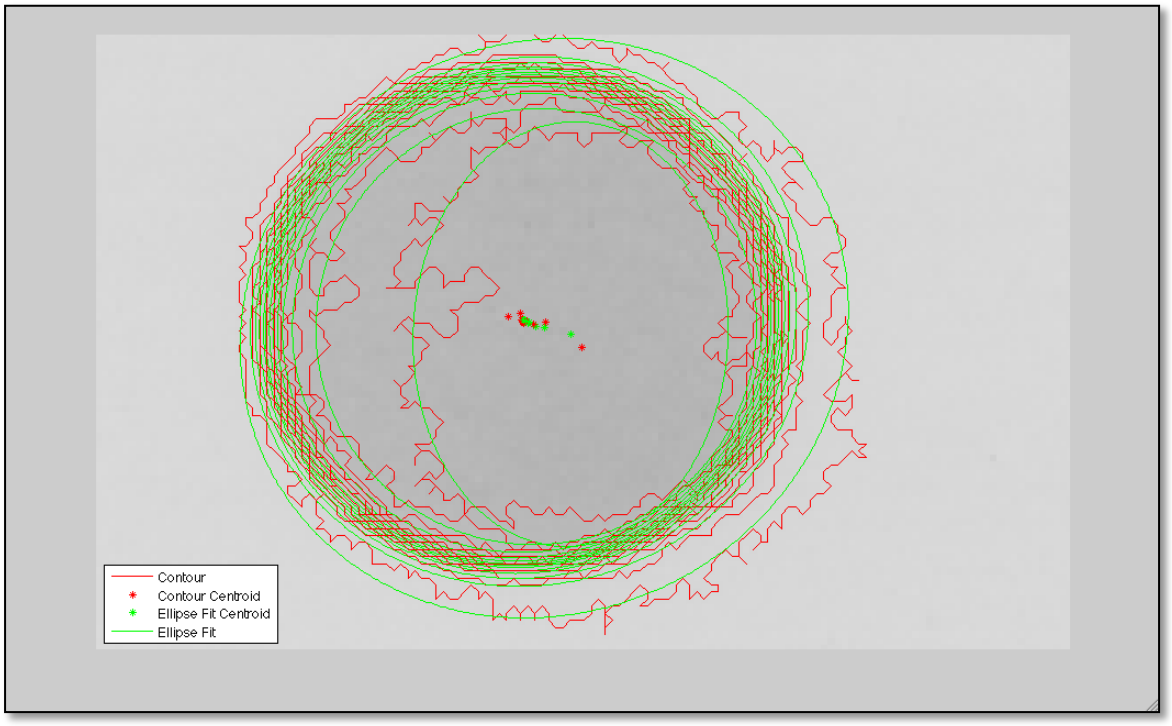

Figure 36: Plotted contours, fit, and centre data

To see how the radiation spot centre changes over a dose threshold range, two plots Figure 37 and 38 were produced. Each plot shows how the radiation spot centre pixel value changes in both the column and row directions.

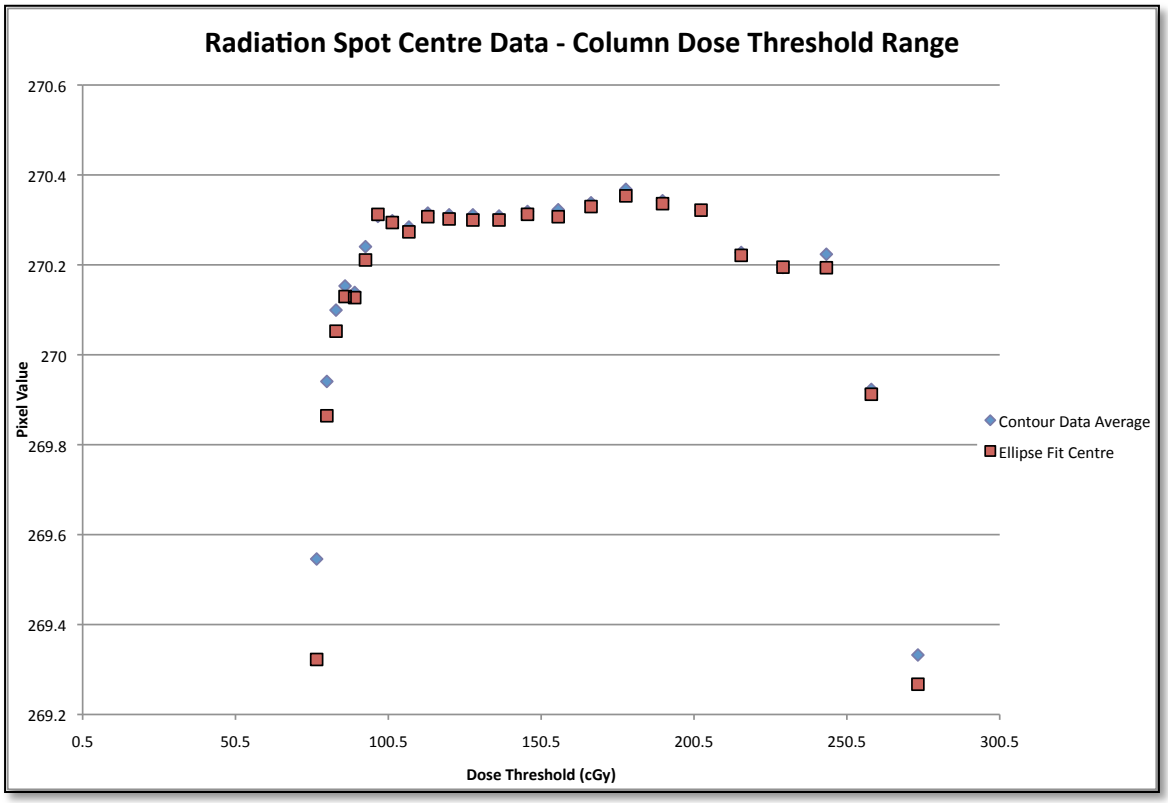

Figure 37: Calculated Radiation spot centres as a function of film dose threshold for the column pixel values

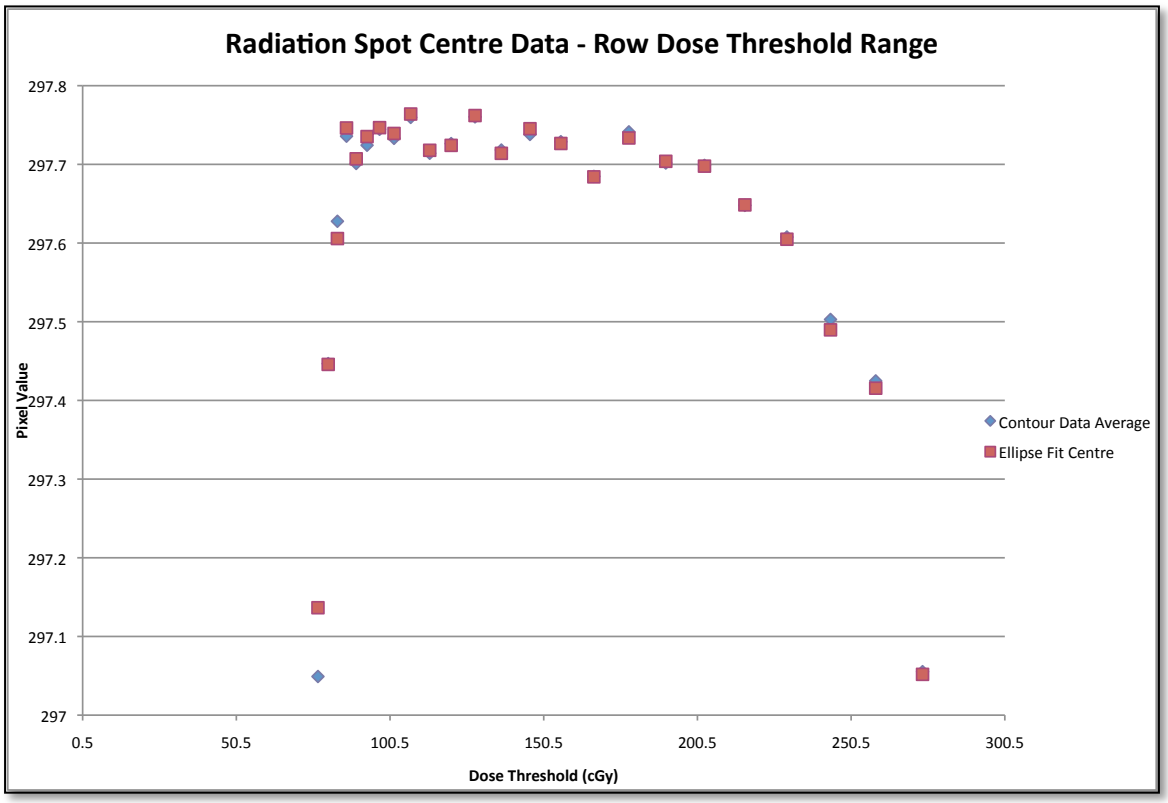

Figure 38: Calculated Radiation spot centres as a function of film dose threshold for the row pixel values.

As it can be seen from these two plots there is an optimal range of dose thresholds for which the radiation spot centre (both ellipse fit and contoured data) does not change. A properly contoured film from a set of rotation measurements can be seen in Figure 39.

Figure 39: Contoured film from a set of Couch rotation measurements

It is worth while to note here the case for an ellipse with a high eccentricity. In this scenario, the beam intersects one of the film planes at a high incident angle (away from the perpendicular, direct hit); however, the radiation field now intersects the plane at different distances from the source across the major axis of the elliptical field. Radiation in the field delivered closer to the source will be higher than that further from the source due to the inverse square law. Due to this the radiation profile will be slanted and not symmetric about the beam central axis. Figure 40 shows how changing the dose threshold level on a highly elliptical field changes the ellipse centre.

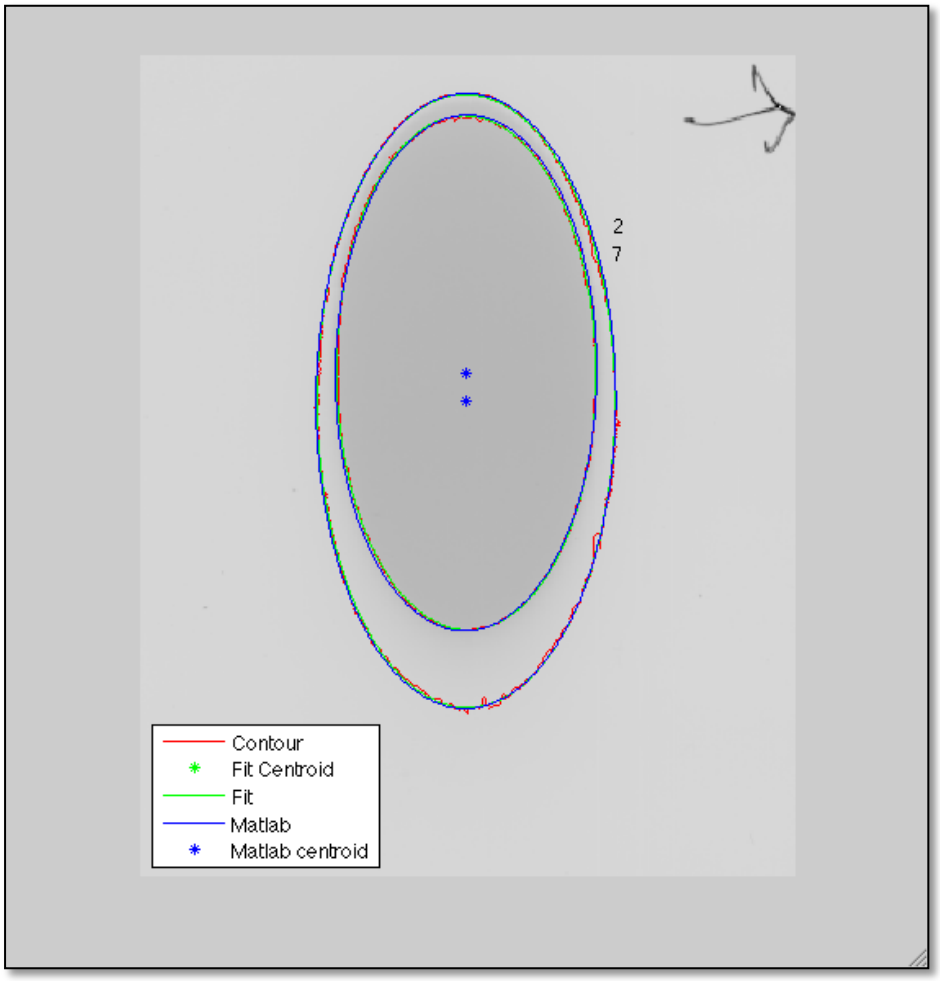

Figure 40: Highly elliptical field shape due to high incident angle

However, due to the nature of the dodecahedron, its symmetry, and its large number of phantom faces, the phantom will never encounter an highly elliptical field unless the phantom is shifted to collect data. Due to the fact that the incident angle remains low, it was found that a correction for the inverse square law on each pixel was not needed.

Once each radiation beam spot centre has been found, the two dimensional film space data matrix containing these points is passed to the trace beam function (explained below) along with the film location and orientation to find their locations in three dimensional phantom space.

The contouring and location of the radiation centres occurs for every film file included. The software uses pairs of opposing film files (entrance film and exit film) to allow the tracing of beams to occur.

Trace Beam

For visualization purposes, the phantom and the film are modeled and displayed in a Matlab plot which is also used to display the traced radiation beams. This plot sets up the three dimensional phantom coordinate system used for ray tracing. The computer modeled phantom contains angles and indices which make the model a perfect dodecahedron. The 20 indices of a dodecahedron are as follows:

$$(\pm 1, \pm 1, \pm 1)$$

$$(0, \pm 1/\varphi, \pm \varphi)$$

$$(\pm 1/\varphi, \pm \varphi, 0)$$

$$(\pm \varphi, 0, \pm 1/\varphi)$$

Where φ is equal to $(1+\sqrt{5})/2$ and is also called the golden ratio. These indices connect to form the 30 edges of the dodecahedron. A numerical factor is applied to all the above indices to magnify its size to that of the real phantom. Figures 41 through 44 show the modeled phantom and the three dimensional phantom coordinate system used.

This next step of the trace function inputs the radiation spot two dimensional data for each film and converts them into three dimensional phantom coordinates based on film locations and orientations. This can easily be done as each of the dodecahedron faces is connected to the surrounding others by the dihedral angle of 2 arctan(φ) or approximately 116.565 degrees. Furthermore, each face is pentagonal in shape allowing the five film orientations to easily rotated by 72 degrees. Through matrix rotation transformations of the film image data around the phantom centre, it is then possible to locate the film on one plane and then rotate it to the correct location and orientation on the phantom.

The 3D phantom space coordinate system convention used is defined in Figure 41. With the dodecahedron phantom sitting on the treatment couch, the centre of the phantom is placed at the isocentre. From here the X axis lies along the long axis of the couch (In-plane, positive x towards the gantry), the Y axis lies perpendicular to the couch long axis (Cross-plane, positive Y to the left, facing the gantry), and the Z axis is orthogonal to the couch plane (positive Z towards the gantry head). When modelled in Matlab, the phantom mapped onto this coordinate system is seen in Figures 42 through 44.

Figure 41: Phantom coordinate System convention. Adapted from http://www.radiology-equipment.com/oncology.cfm with slight modification.

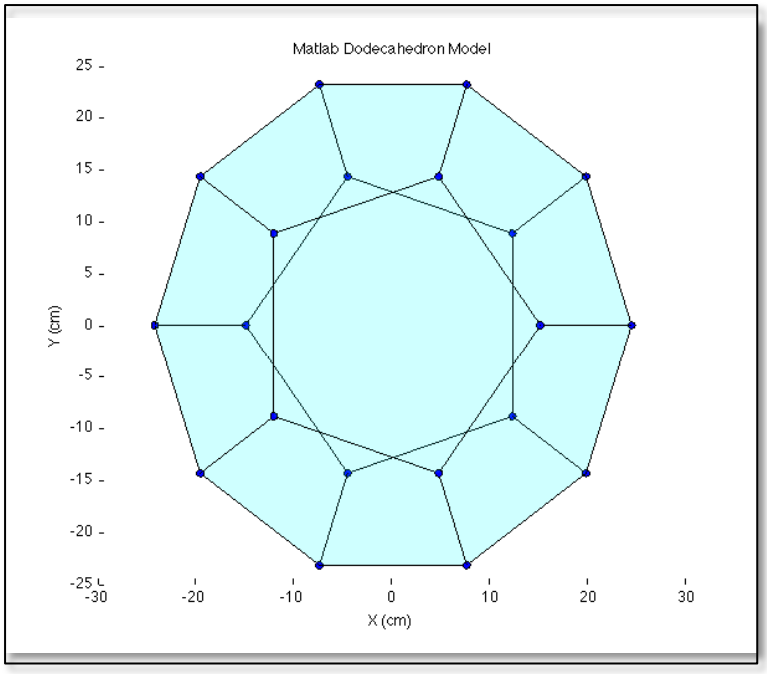

Figure 42: Dodecahedron model in the XY phantom coordinate system plane

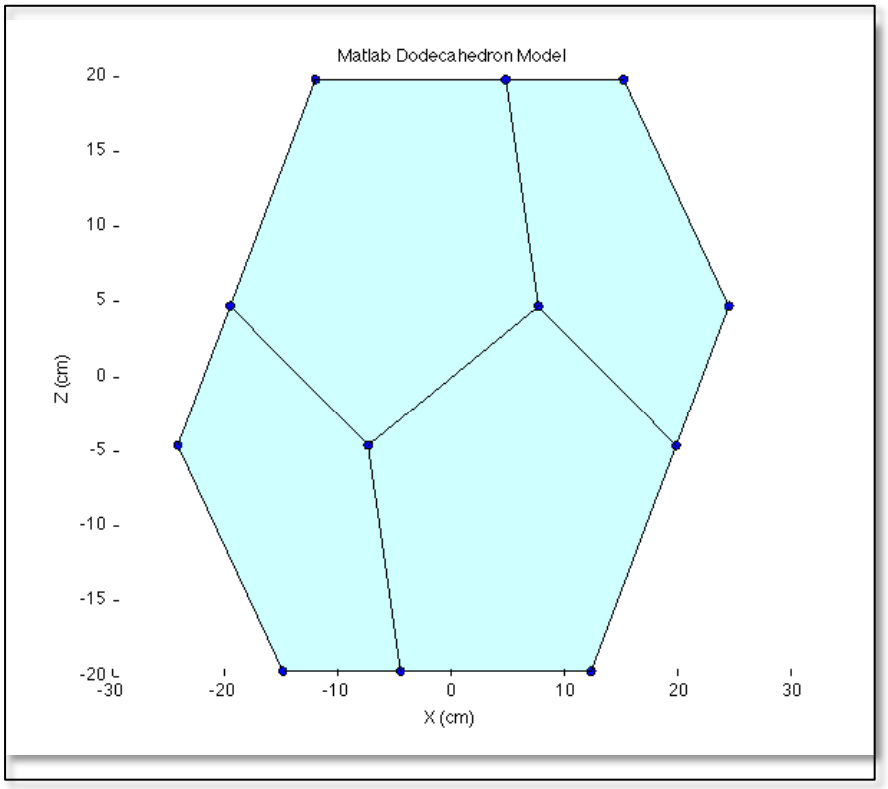

Figure 43: Dodecahedron model in the XZ phantom coordinate system plane

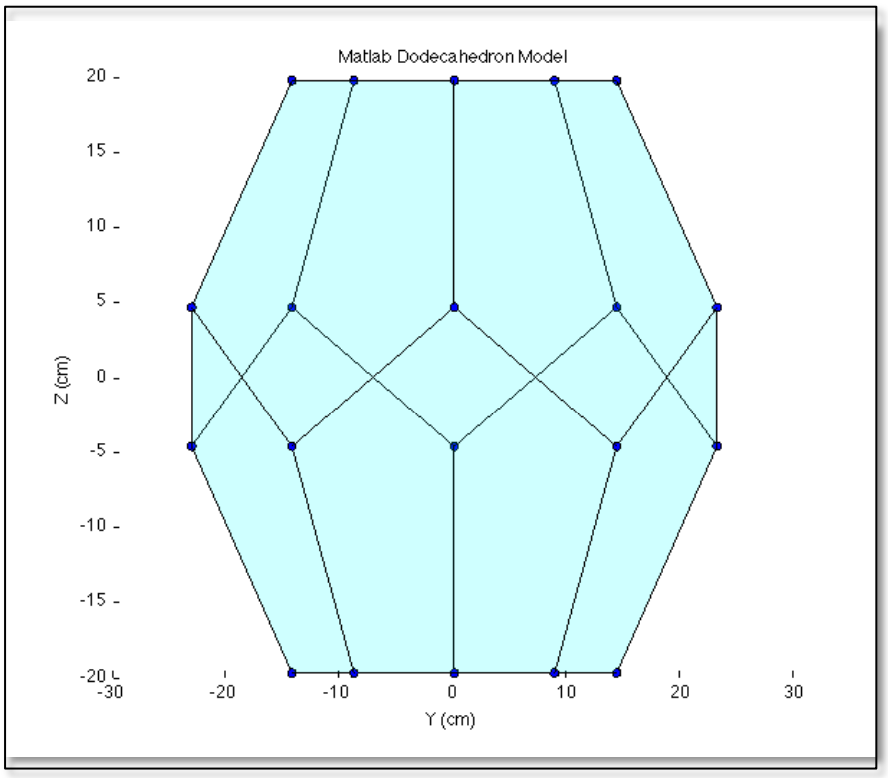

Figure 44: Dodecahedron model in the YZ phantom coordinate system plane

The array of two dimensional film data is first located on the top plane of the phantom (with the phantom situated on the treatment couch). The 2-D film data is then added to the starting location of the film (reference edge location) on the top plane to convert it to 3-D phantom coordinates, but not at the correct location. To rotate the new 3-D data to the correct position, two rotation axes are defined. The first rotation occurs about the positive Z axis (0,0,1) and is given by the rotation matrix:

$$R_Z(\theta) = \begin{bmatrix} \cos\theta & -\sin\theta & 0 \\ \sin\theta & \cos\theta & 0 \\ 0 & 0 & 1 \end{bmatrix}$$

By using multiples of 72 degrees, the data is rotated to its correct orientation on the top pentagonal face, but still on the incorrect face. To rotate the film and its data to the correct face, two rotations occur, the first about the positive Y axis, and then again about the positive Z axis. The rotation matrix used for the Y axis rotation is given by:

$$R_y(\theta) = \begin{bmatrix} \cos\theta & 0 & \sin\theta \\ 0 & 1 & 0 \\ -\sin\theta & 0 & \cos\theta \end{bmatrix}$$

Once the two opposing films and their two dimensional radiation spot data has been located, the software matches the corresponding beam spots on the entrance and exit films and traces the beam from the entrance film through the phantom to the opposite exit film side. Parametric equations given in Equation 3 are defined for each beam in three dimensional phantom space.

Eq. (3) $$RadiationSpot_{Entrance} + t \cdot (RadiationSpot_{Exit} - RadiationSpot_{Entrance})$$

The beam tracing procedure occurs for every pair of opposing entrance and exit film files at which point the beam trace analysis takes place and the beam offsets are calculated.

Calculate Beam Offsets

The analysis of the entire ray traced set involves examining the beams and finding how they are offset from each other and from the nominal isocentre. The method that was chosen to do this

analysis involves looking at single points along the path of the beam and how they relate to each other in 3-D phantom space.

The algorithm used in the software is a four step process which finds the distribution of single points on each beam path which is at a minimum distance to a specific point.

The first step in this process involves finding the point along each beam path that is at a minimum distance to the centre of the modeled phantom (0,0,0). This is done by using the beam parametric equations and solving for the parameter t which minimizes this distance. This is given by equation (4):

Eq. (4) $$t = \frac{(x_1 - x_0) \cdot (x_2 - x_1)}{\left|x_2 - x_1\right|^2}$$

Where x_0 is (0,0,0), x_1 is the radiation entrance spot, and x_2 is the radiation exit spot. This produces a set of minimum distance points (one for each beam) to the (0,0,0) phantom centre.

The second step in the offset calculation process finds the centre point or centroid between the distribution of minimum distance points in step one. This is simply done by searching for the point which minimizes the distance between itself and the surrounding points.

The third step is similar to the first step as in finding the point along the beam path which minimizes the distance to a point, however, this point is now the centre point found in step two and not (0,0,0). Again, this is done for all beams by solving for t in the equation above, producing a second distribution of points.

The final step in this algorithm is to shift the found centroid point found in step three to (0,0,0).

The resulting plot of the dodecahedron and the modelled radiation beams from a gantry rotation is shown in Figure 45 and a magnified view of the offsets near the isocentre in Figure 46. Depicted in Figure 46, the blue dots represent the minimum distance points calculated and the red dot represents the centre of the modeled phantom. The blue sphere is the smallest sphere which encompasses all minimum distance points.

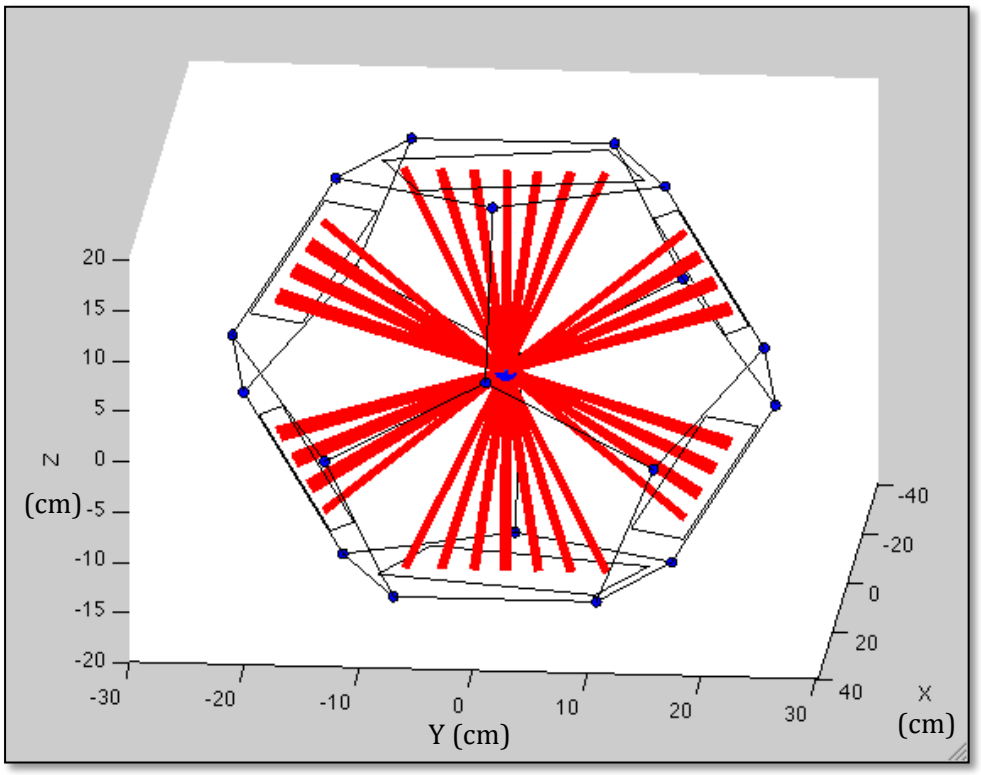

Figure 45: Matlab modeled gantry rotation measurements

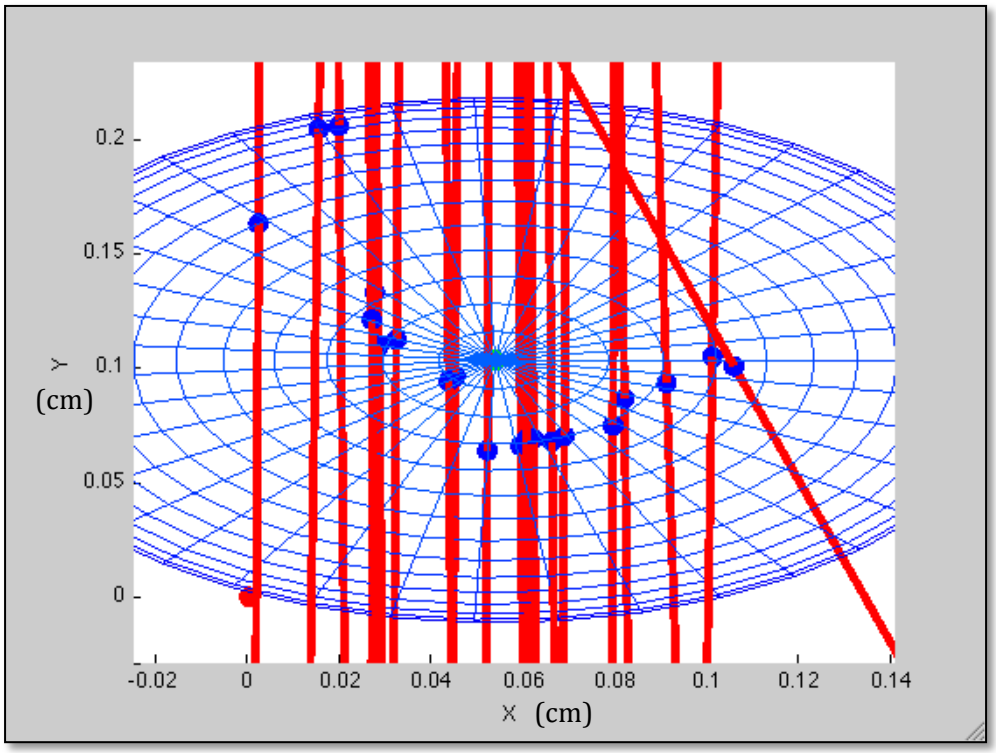

Figure 46: Matlab modeled gantry rotation measurements magnified to the isocentre

Phantom Testing

Testing of the Dodecahedron phantom involved placing the phantom at known location and orientation and taking measurements that would ensure it's robustness and validity in its offset measurements. Furthermore, measurements were taken to characterize the phantom in the calculation software.

Phantom orientation/ Measurement Setup

The placement of the phantom to measure the radiation beam offsets involved positioning the phantom on the treatment couch in a known location to be input into the calculation software. For most measurements, the phantom was placed at the isocentre such that the phantom centre is aligned with the machine isocentre. This was done by visually aligning the treatment room lasers to outer scribe marks on the phantom indicating the phantom centre. In order to fix the phantom to the treatment couch, the bottom of the phantom was taped (masking tape) to the treatment couch ensuring no movement of the phantom took place.

Note: for these measurements and for all SRS treatments, the treatment couch is locked into place via rubber brakes that completely restrict any motion.

The original intention was to have the phantom fixated to the treatment couch through a rigid attachment which would place the phantom in the exact same position every time. The attachment would have been located at the end of the treatment couch where normally the stereotactic head frame would be attached. Note: The treatment couch for the Linac used for this research at O.C.C. was modified to allow the stereotactic head frame to be attached to the end of the couch.

The first tests of the phantom revealed that with the bottom outer shell (build-up material) fixated to the couch, it was very difficult (if in fact impossible) to remove the phantom from the shell to replace film without moving the lower shell and thus the phantom from its measurement position. Therefore, for all measurements following this, the outer shell build-up was not used. This led to longer irradiation times to adequately expose the film, but ensured phantom position during measurements.

Phantom Robustness

To find if the phantom is robust, i.e. can it be moved from its measurement setup position and still yield the same results, the phantom was first placed at the isocentre then a series of film measurements were taken at various gantry and couch angles. For these measurements the resulting minimum distance points were then plotted in the XY, XZ, and YZ planes.

The phantom was then rotated and shifted from the isocentre by a known amount. The same beams were again measured but now at some distance and rotation from the phantom centre. A plot in each plane of the two minimum distance points for both the shifted and un-shifted phantom can be found in Figures 47, 48, and 49.

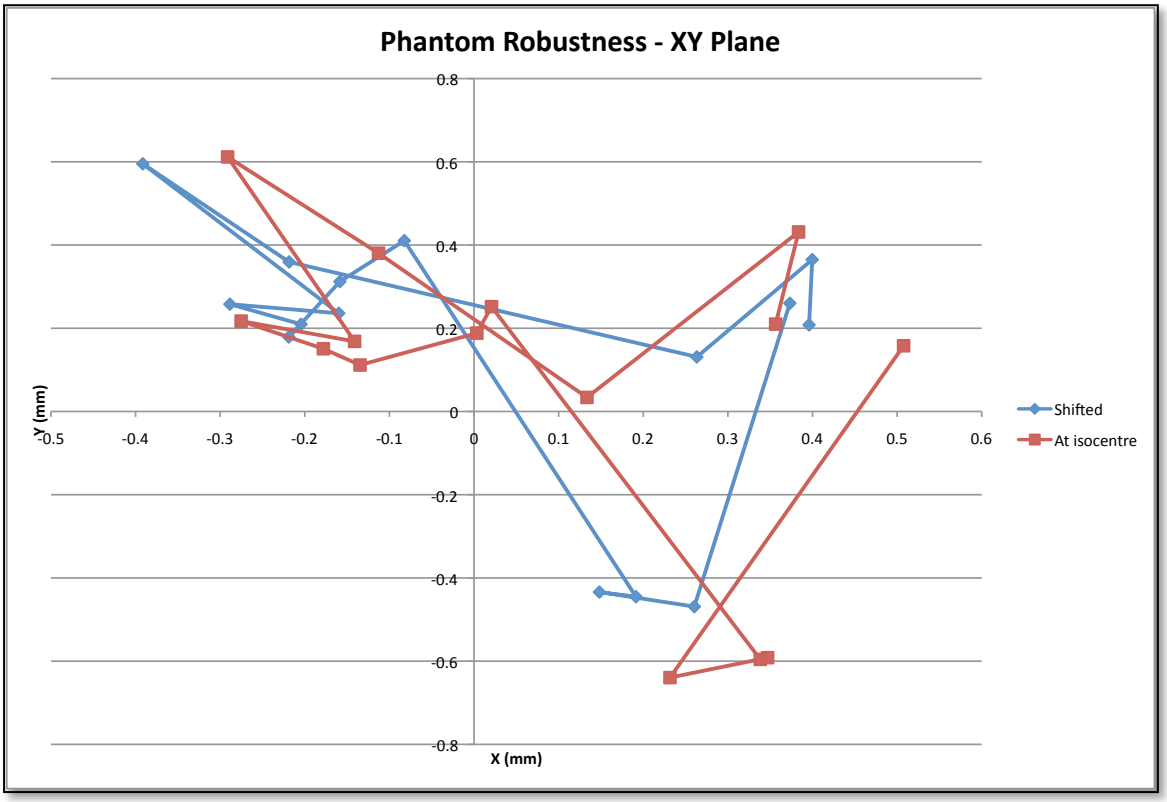

Figure 47: Phantom shifted and un-shifted data in the XY phantom plane

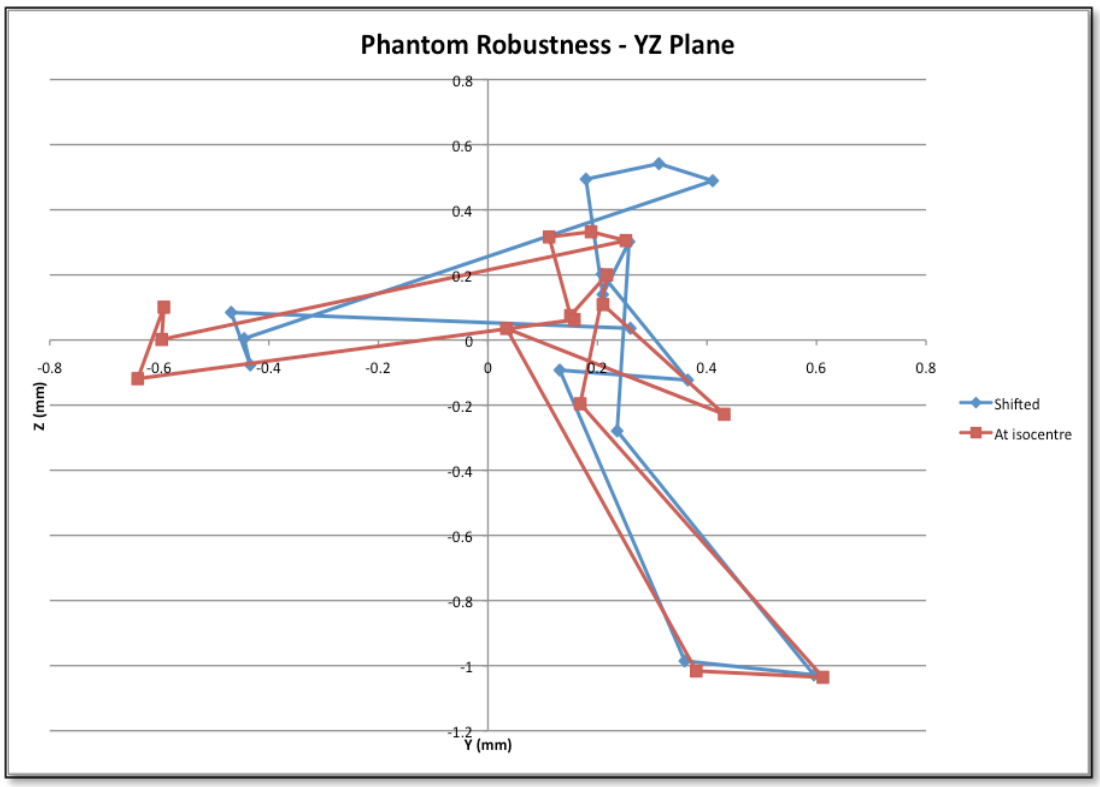

Figure 48: Phantom shifted and un-shifted data in the YZ phantom plane

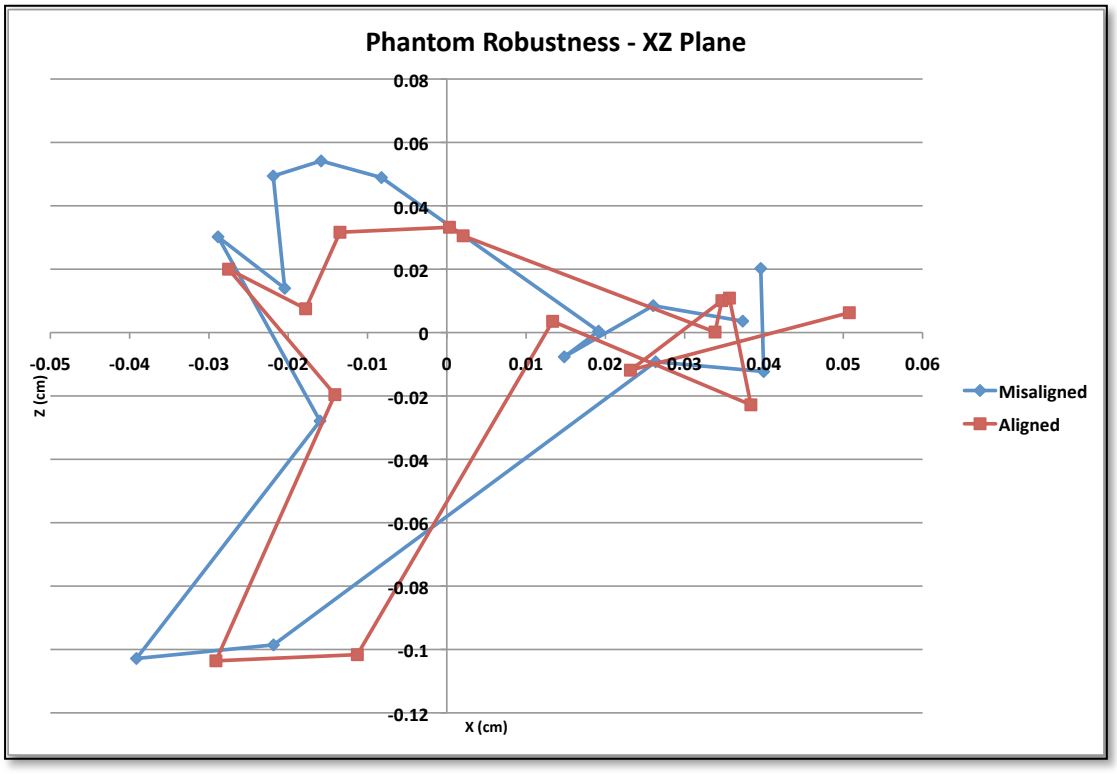

Figure 49: Phantom shifted and un-shifted data in the XZ phantom plane

As can be seen from these three figures, the minimum distance points calculated for the phantom at the isocentre and at the shifted/rotated place are within 0.2mm of each other. Therefore the phantom is robust such that any positioning errors (rotational or shifted) will not affect the minimum distance points distribution. The plots seem to indicate that the phantom detected a small additional rotation, due to the fact that the phantom has been aligned after rotation by eye, a misalignment uncounted for in the calculations. It was also hypothesised but not investigated that alignment can be discerned from the centres of the entrance and exit beams for irradiations taken at the same gantry angle. In the future, rotation and translation of the phantom relative to a point of closest approach of the 0 and 90° gantry beams with axes defined by the 0 entrance / exit and 90° entrance / exit should give a rigid body fixed frame for the room and thus could be used for phantom alignment.

The final step of the phantom testing was to confirm it's validity. This was done to see if the offset beams are calculated to be where they are in reality. To validate the phantom it was necessary to characterize this particular phantom in the calculation software.

Phantom Characterization

In order to ensure that the radiation beams are properly modelled in the software to their true locations, certain parameters needed to be adjusted to their true values. These parameters are true dimensions and angles applied to the modelled dodecahedron which is assumed to be completely perfect in shape and size. The characterization process was very time consuming due to the phantoms multiple film location and orientations. Adjustments in the parameters below as small as 0.1mm and 0.1 degrees yielded beam offset results differing greater then 0.5mm. Due to this, the complete characterization of the phantom was not complete during this thesis and this is explained in more detail below in the discussion section.

These adjustable parameters in the calculation software are as follows and are explained in detail below:

Dodecahedron size: Each vertex of the modelled phantom is multiplied by a factor determining the overall size of the phantom and thus each edge length.

Rotations about Z-axis: These are the angles (described in the Trace Beam Section) the software uses to rotate the film about the Z-axis to place the film on the correct phantom face (1 through 12). For a perfect dodecahedron this angle is 72 degrees.

Rotations about Y-axis: These are the angles (also described above) the software uses to rotate the film about the Y-axis to place the film on the correct film face. (1 through 12) For a perfect dodecahedron this angle is 180 subtract the dihedral (≈116.565 degrees).

Rotations of film on each phantom face: These angles (described above) used by the software rotate the film within each face to their correct orientation (A through E). For a perfect

dodecahedron this angle is 72 degrees.

Reference edge location: the distance from each phantom vertex to the reference edge location where the film sits.

The overall dodecahedron size was determined by using a micrometer scale at the O.C.C. machine shop. The phantom top to bottom distance was determined (i.e. parallel and opposing film distance separations) to be 39.354cm (measured to the face inner film groove). The measurement of the vertex to vertex distance also confirmed the modelled dodecahedron size.

The next characterization that took place was the reference edge location on each phantom face. The x and y distances seen in Figure 50 below were measured by hand to be 2.20cm and 1.15cm respectively. However, it was found that the hand measurements were not accurate enough and further measurements were needed.

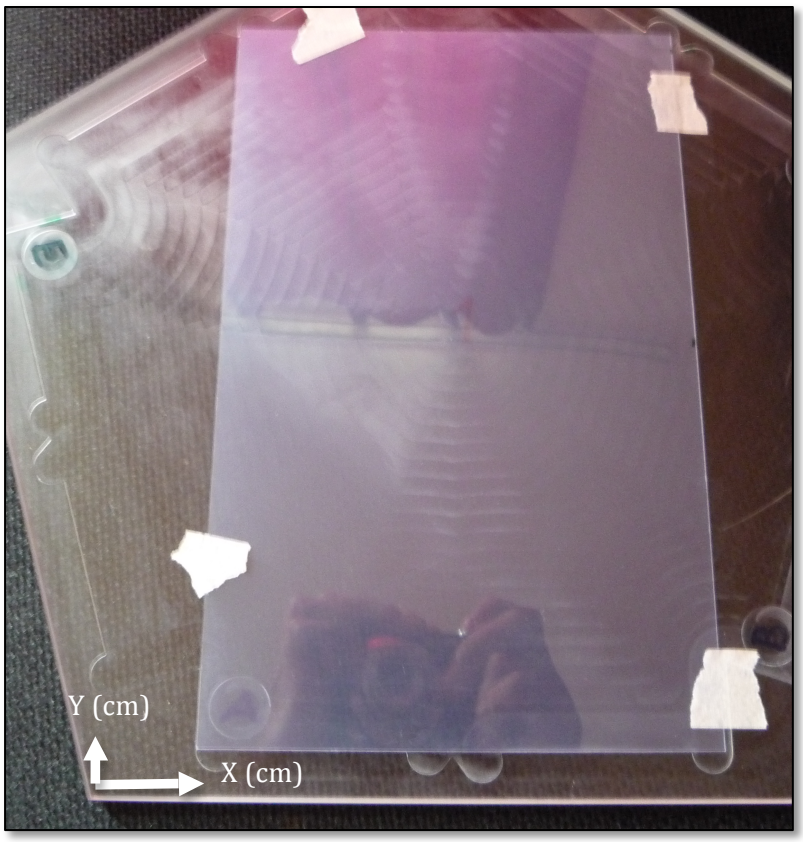

Figure 50: Reference Corner Location

To characterize a single phantom face, measurements of a single beam (no rotation of the gantry and couch) were taken by rotating the film through each orientation (A through E). Ideally, each film orientation should produce the same beam offset, however it was found that the hand measurements above produced offset differences (of the same beam) of 0.5mm. By adjusting the x and y distances to the reference edge location it was possible to minimize the distance between

each ray trace from the different orientations. The adjusted value of the reference edge location was found to be x: 2.48cm and y: 1.36cm. The minimum distance points plot can be seen in Figures 51, 52, and 53 and confirms that each film orientation produces offsets of a maximum of 0.085mm for the same beam.

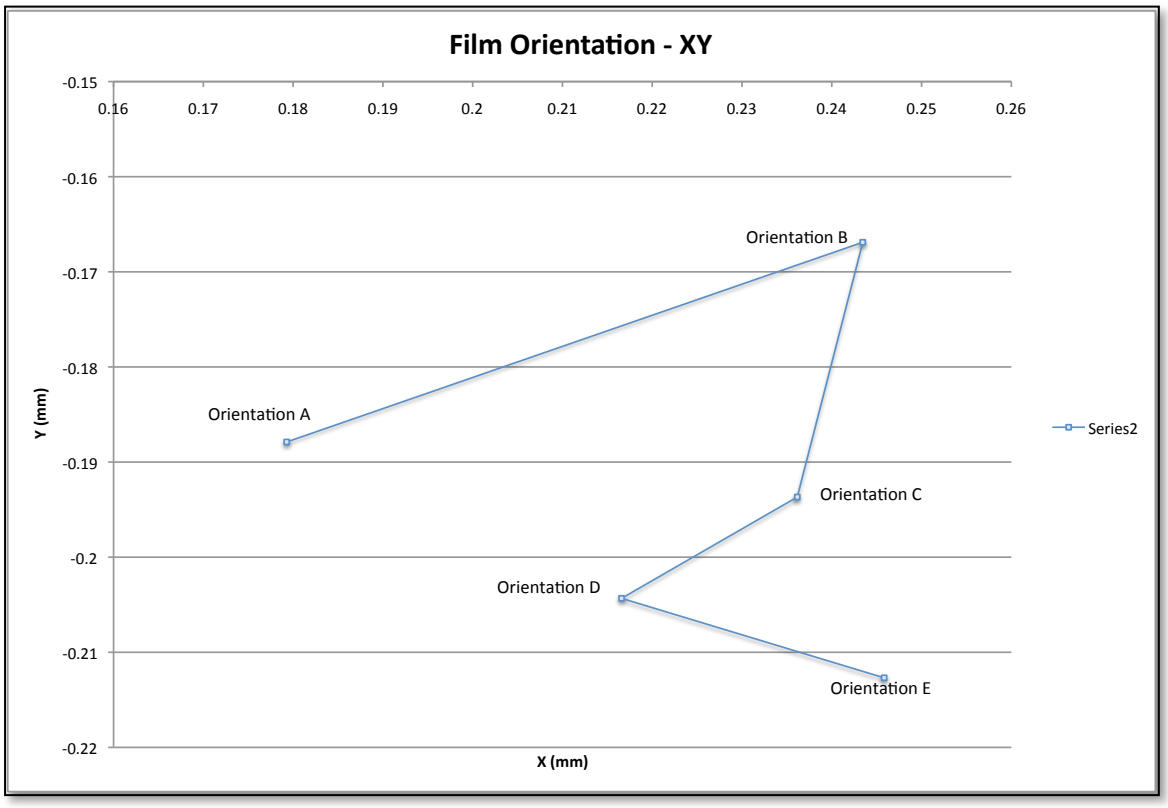

Figure 51: Different film orientation data for the same radiation beam in the XY plane

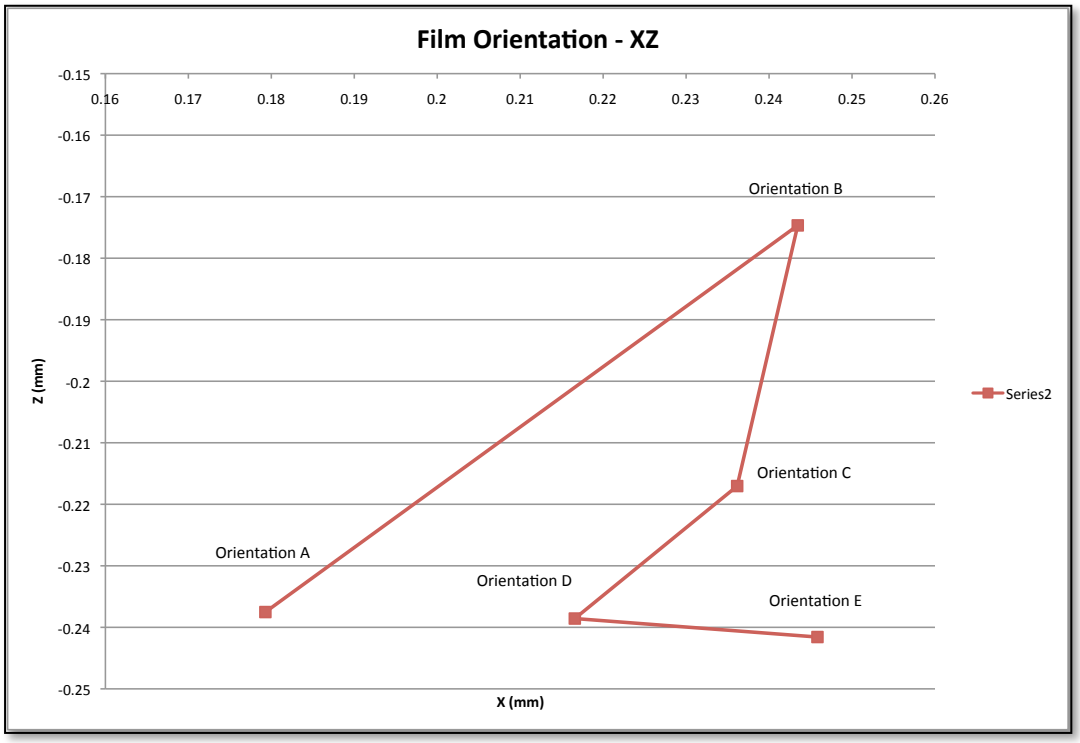

Figure 52: Different film orientation data for the same radiation beam in the XZ plane

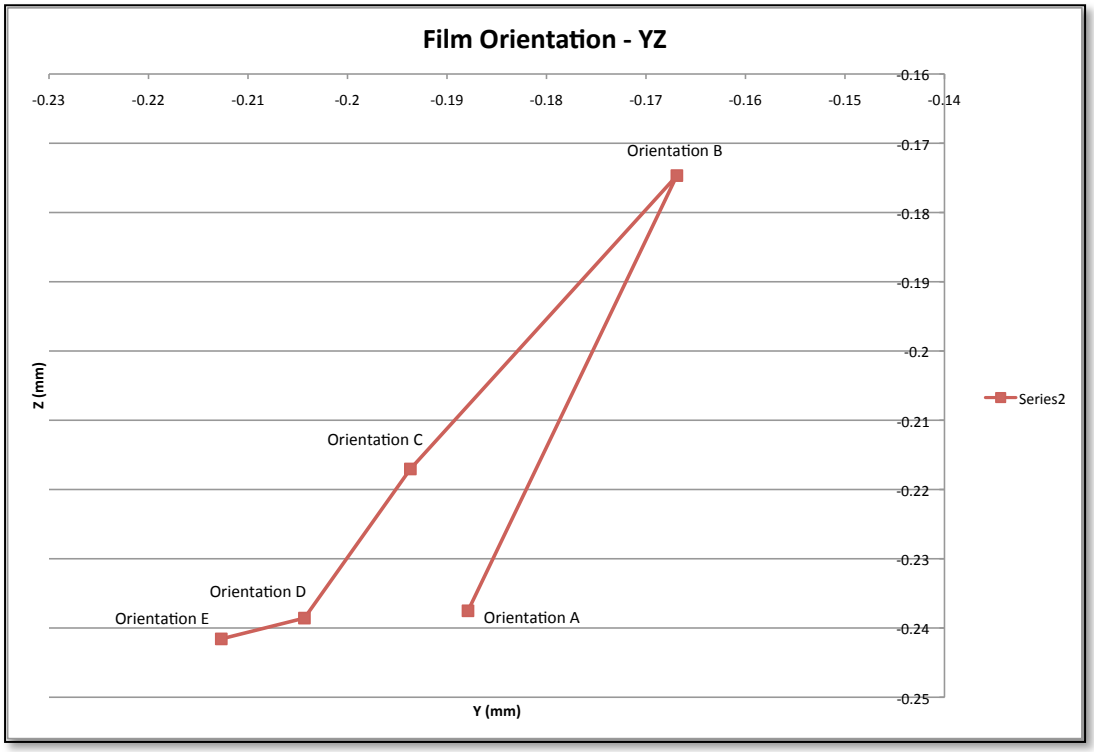

Figure 53: Different film orientation data for the same radiation beam in the YZ plane

The angle of rotation between film orientations on a single face was left at 72 degrees. This was not altered due to the fact that the reference edge location change was all that was needed to properly model the same beam with different film orientations.

The final two parameters that can be changed to characterize the phantom, the rotation of the film about the Z and Y axes to properly place the film on its correct face were not investigated due to time constraints for this research. It is hypothesised that the vertices for each face (and the reference edge) on the phantom has a specific location slightly different than a perfect dodecahedron due to slight machining and fabrication imperfections. These locations can be implicitly input into the software or can be defined by exact rotations (angles between each phantom face) with possible shifts. This will be discussed further in the following sections below.

Data Results

Gantry Rotation Data

The radiation beam offsets due to the motion of the gantry alone was measured on three different dates. Multiple films were oriented on the phantom to allow for the gantry rotation measurements. Since parallel and opposing beams will traverse over the same location on the film, it was necessary to remove the phantom and replace films to measure the opposing gantry angles. For the first two measurements (June 9, 2010 and June 19, 2010) the build-up shell was used. It was determined however after the analysis of these measurements that the location of the phantom after removal to replace the films could not be reproduced with the necessary accuracy. Therefore, for all measurements taken after whereby the phantom was needed to be replaced during measurements, the outer build-up shell was removed. Although this increased the irradiation times for sufficient film exposure, the film could be replaced without movement of the phantom on the treatment couch during measurements. Therefore due to time constraints, the gantry rotation data was only measured once without build-up to ensure that data taken between film replacements was accurate.

The offset data due to gantry rotation was taken (without build-up layer) on June 27, 2010. The gantry was rotated from -126° to +126° in 8 degree intervals. The Matlab model of the phantom and the resulting beam traces can be seen in Figures 54 and 55.

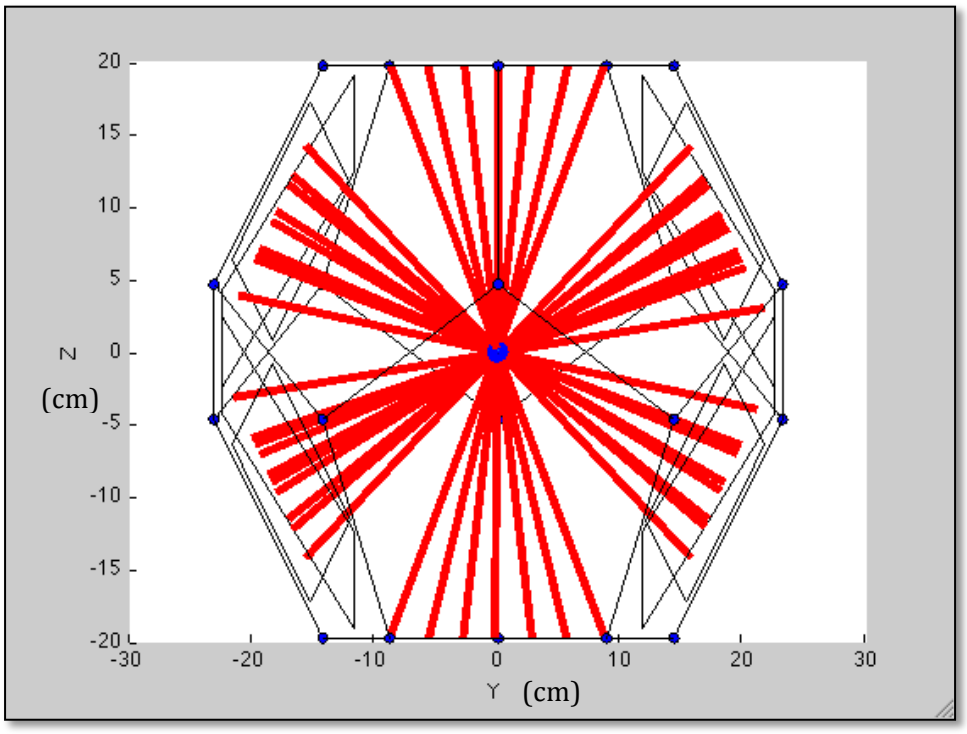

Figure 54: Modeled gantry rotation Data set

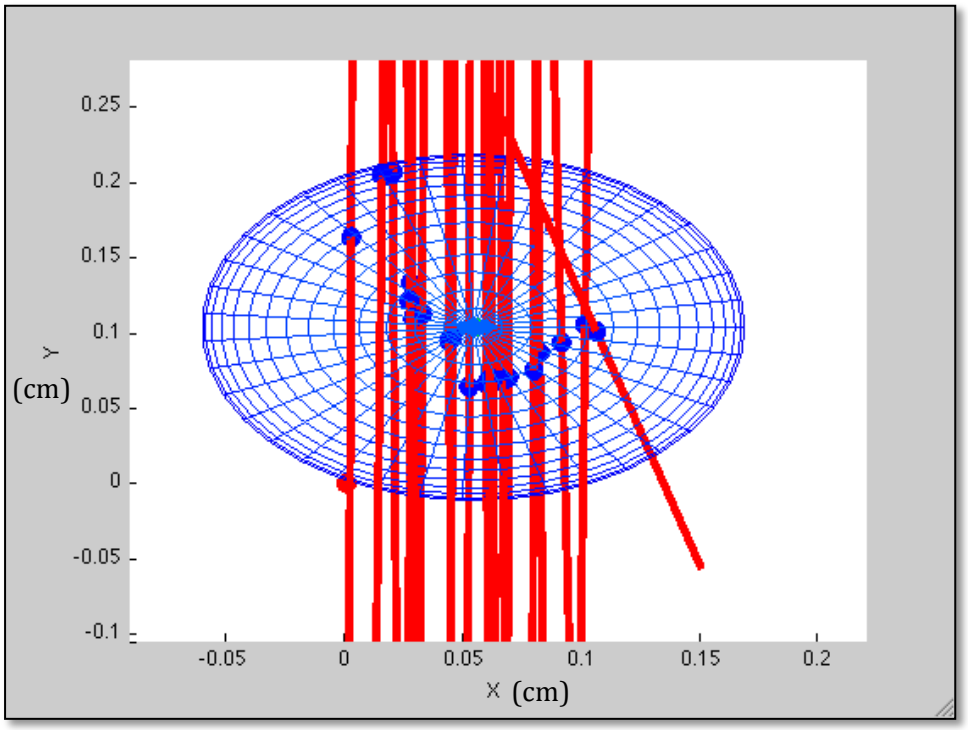

Figure 55: Modeled gantry rotation data magnified to the isocentre

The plots of the minimum distance points projected onto the XY, XZ, and YZ phantom coordinate system are found in Figures 56, 57 and 58. Denoted on the plots are the first and last gantry angle exposed on a single film, these are connected by a single series. In parentheses in the legend is the film face entrance number and it's orientation is followed by the exit face number and it's orientation. The gaps A, B, and C denoted by the red arrows should not be there. The red arrows join points in the plots that should appear close together because they correspond to similar beams. Our analysis suggests that they are the consequence of the translation in the positional data from it's true location due to the phantom not being a perfect dodecahedron and not yet completely characterized in the calculation software. This is examined further in the Gantry Rotation Data Discussion Section.

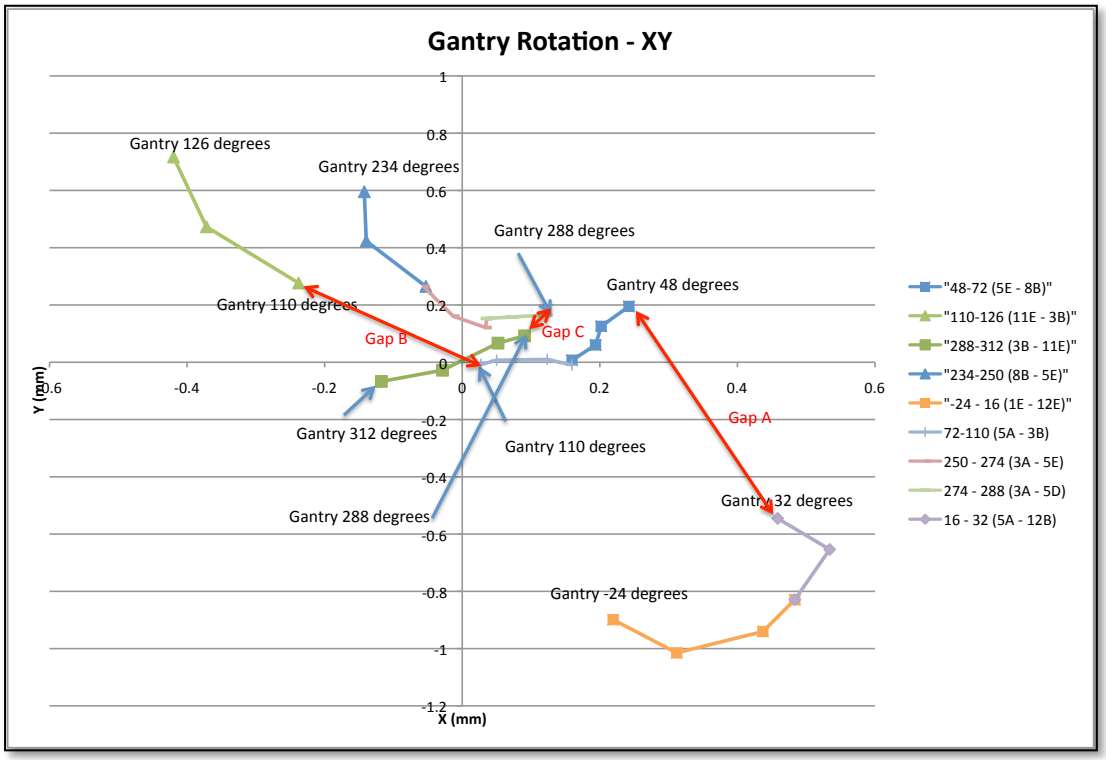

Figure 56: Minimum distance points for Gantry rotation in the XY phantom plane

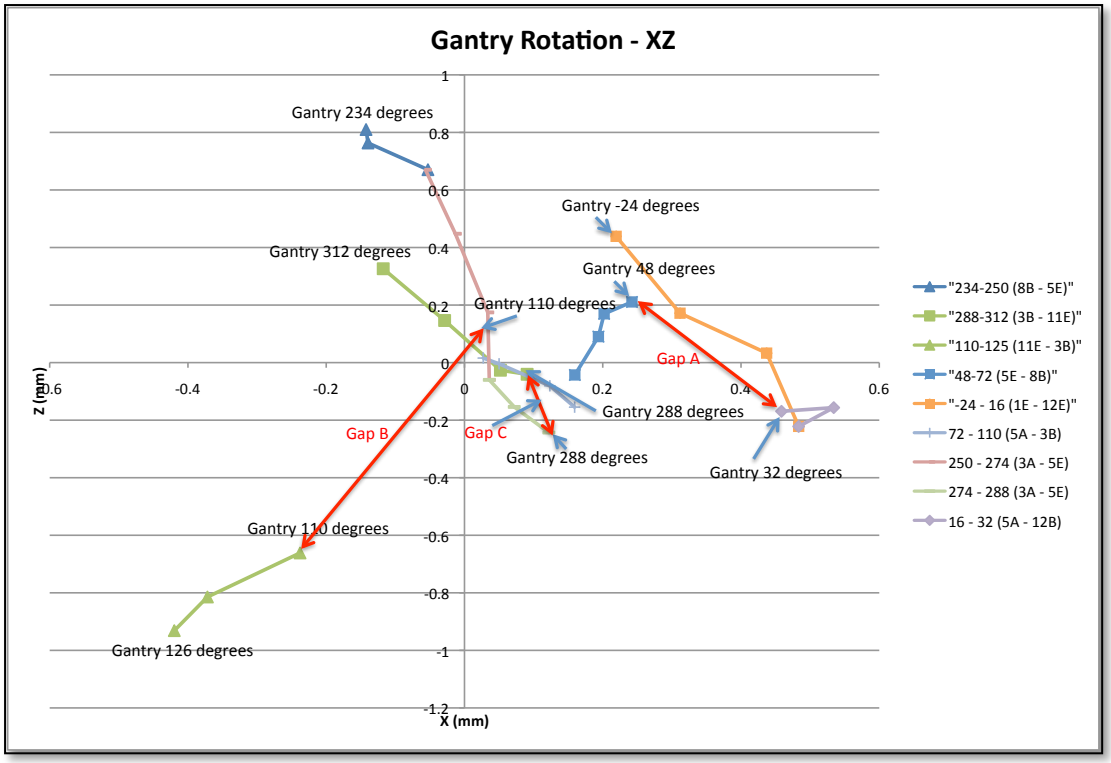

Figure 57: Minimum distance points for Gantry rotation in the XZ phantom plane

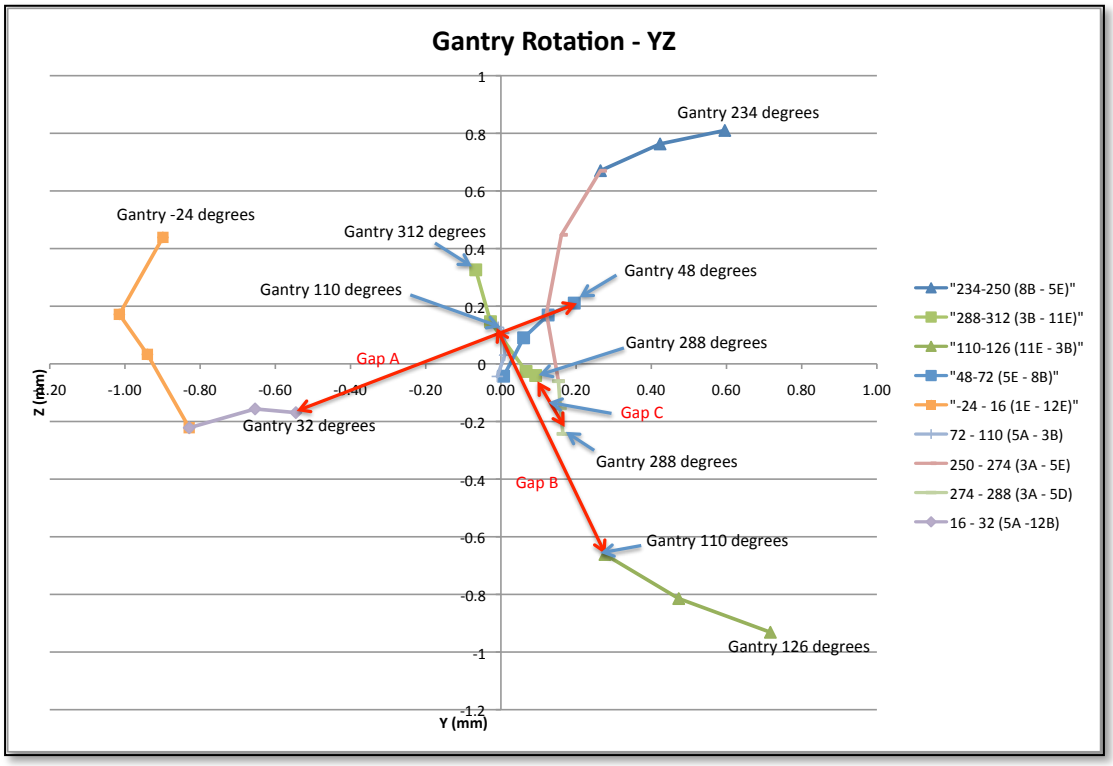

Figure 58: Minimum distance points for Gantry rotation in the YZ phantom plane

Also measured was the variation in gantry reproducibility. Measurements were taken of a single gantry angle exposure. The gantry was then moved away from that angle and then moved back again using the Linac's digital reading hand control. The exposure was then taken again using another set films in the same orientation as the first. This was repeated five times. Due to the same film orientations be used for all the repeated data, any inconsistencies in the phantom not being a perfect dodecahedron would not effect the data. The standard deviation of the offsets from this data in all three principle planes of the phantom coordinate system were found to be: StdDev(x)=0.11mm, StdDev(y)=0.12mm, 0.16mm.

Couch Rotation Data

The radiation beam offsets determined by couch rotation alone were performed on three different days. Set 1 on June 3, 2010, Set 2 on June 14, 2010, and Set 3 on June 26, 2010. The measurements all were taken using the exact same phantom setup. Films were placed on the phantom in the same orientations on all three days and the phantom centre was visibly aligned to the treatment room lasers.

The minimum distance points were calculated for a series of couch rotations in the range used by O.C.C. This range, from 66° to -64° was measured in 8° intervals (the smallest angle resolution of the rotation whereby exit beam spots do not overlap). The gantry was kept stationary at 65°, however any gantry angle could be used and this angle was chosen as to maximize the amount of data taken from couch rotations on a single film.

The Matlab model of the phantom and the resulting beam traces can be seen in Figures 59 and 60.

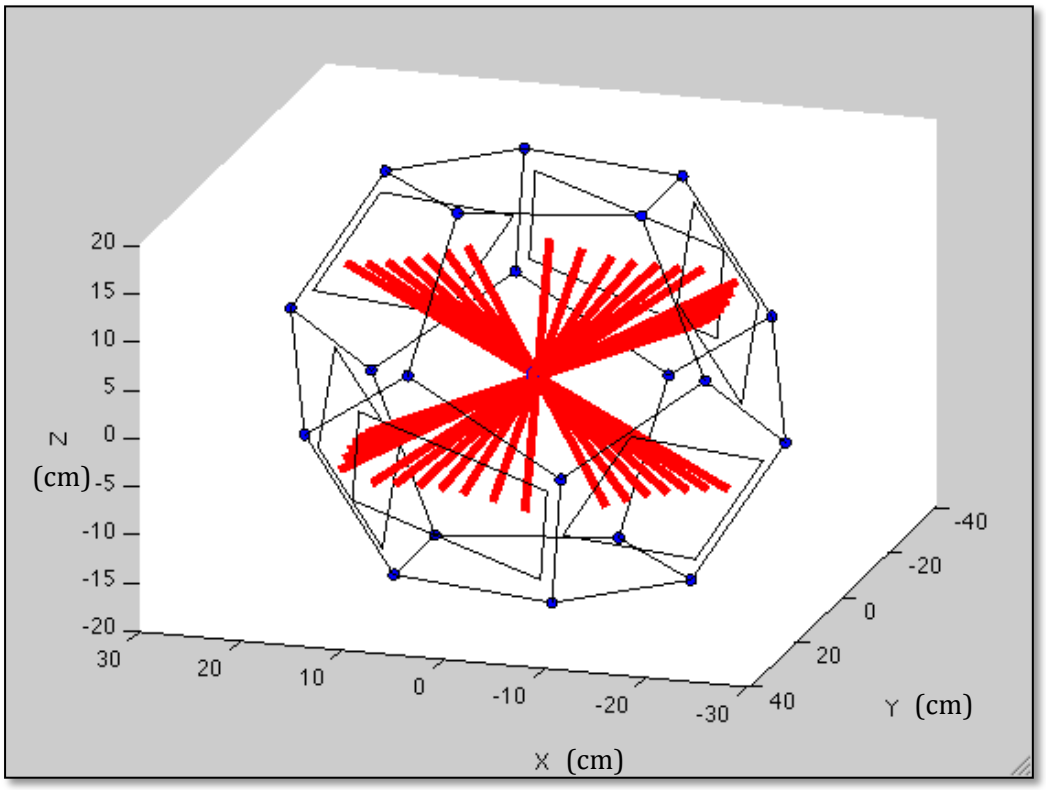

Figure 59: Modeled treatment couch rotation Data set

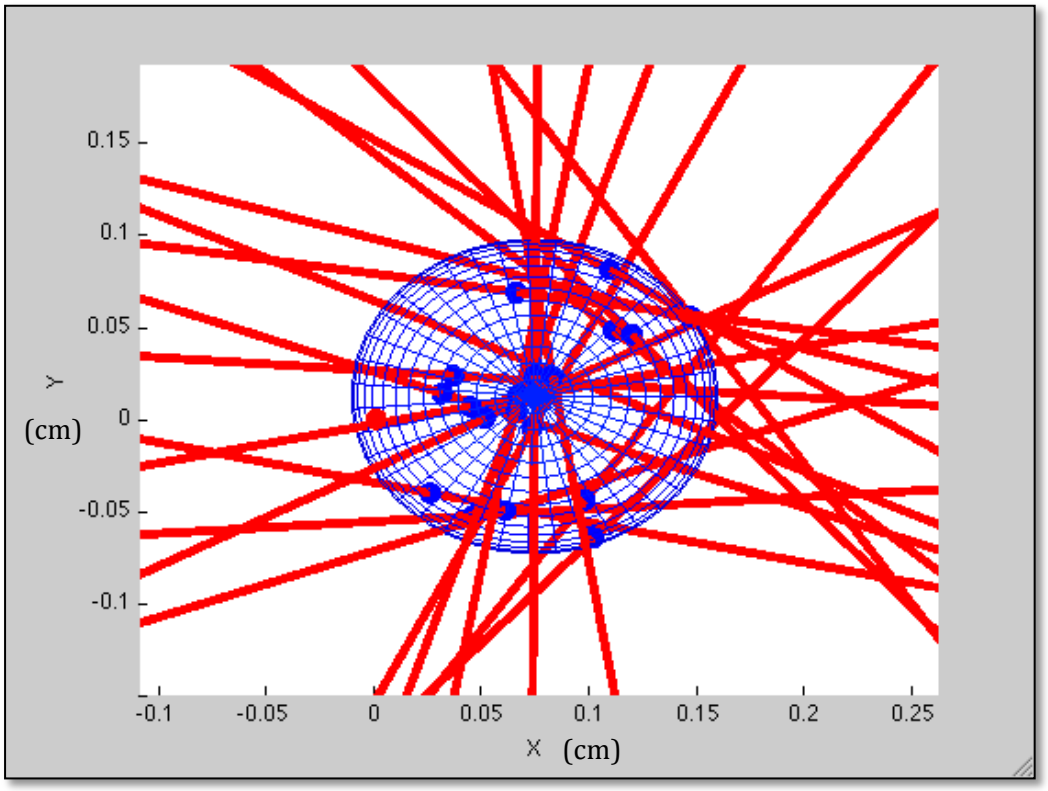

Figure 60: Modeled treatment couch rotation data magnified to the isocentre

Figures 61, 62, and 63 show the minimum distance points projected on the XY, XZ, and YZ planes of the phantom coordinate system. The information in the legend gives the couch angles measured, then in parentheses the entrance film face and its orientation, the exit film face and its orientation and followed by the Set number. The couch start and finish point on each film face is denoted on the plots. The motion of the calculated offset can be seen across each film face. It is evident from the gaps between the data from different film faces that further phantom characterization is needed to produce a continuous offset curve for the entire couch rotation range. This is examined further in the Couch Rotation Data Discussion Section.

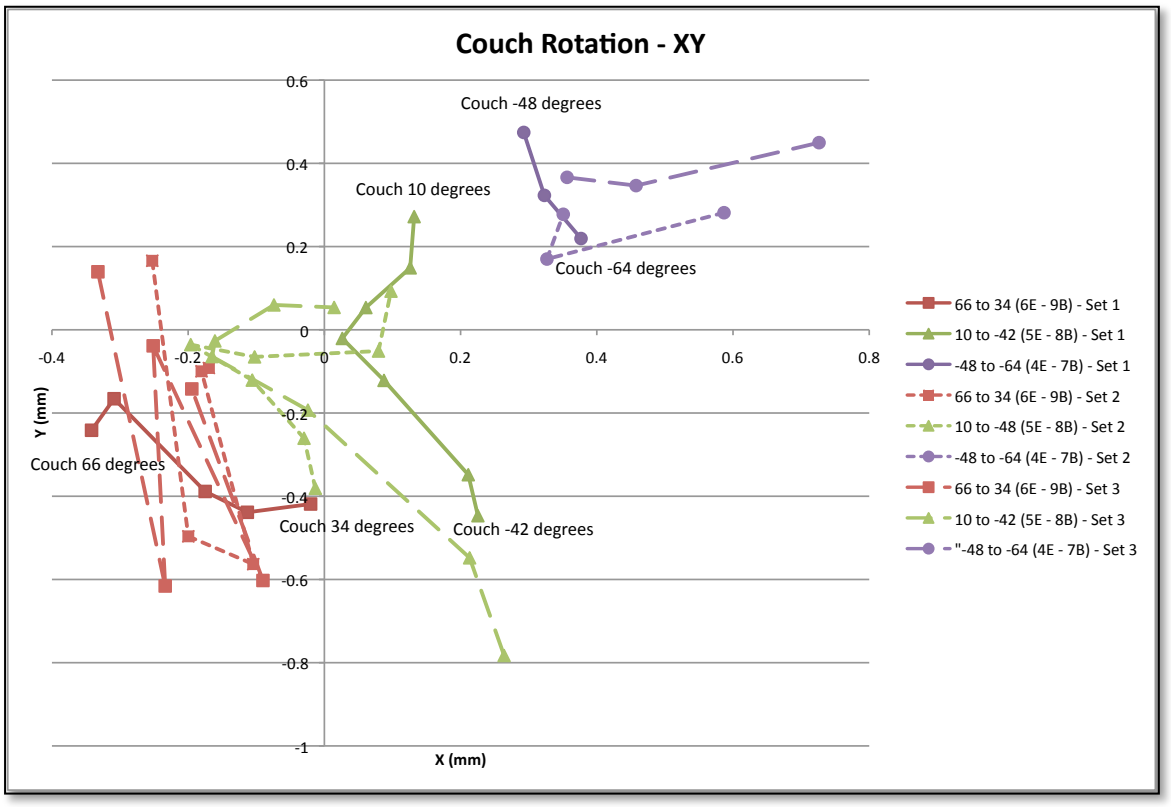

Figure 61: Minimum distance points for Couch rotation in the XY phantom plane

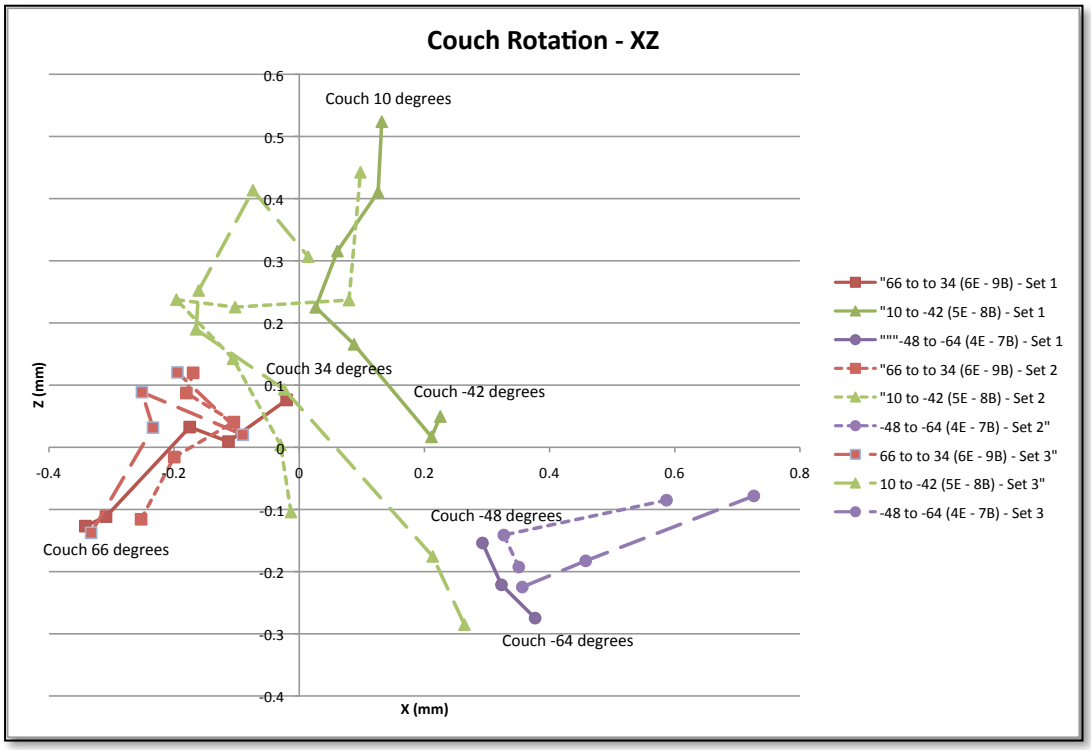

Figure 62: Minimum distance points for Couch rotation in the XZ phantom plane

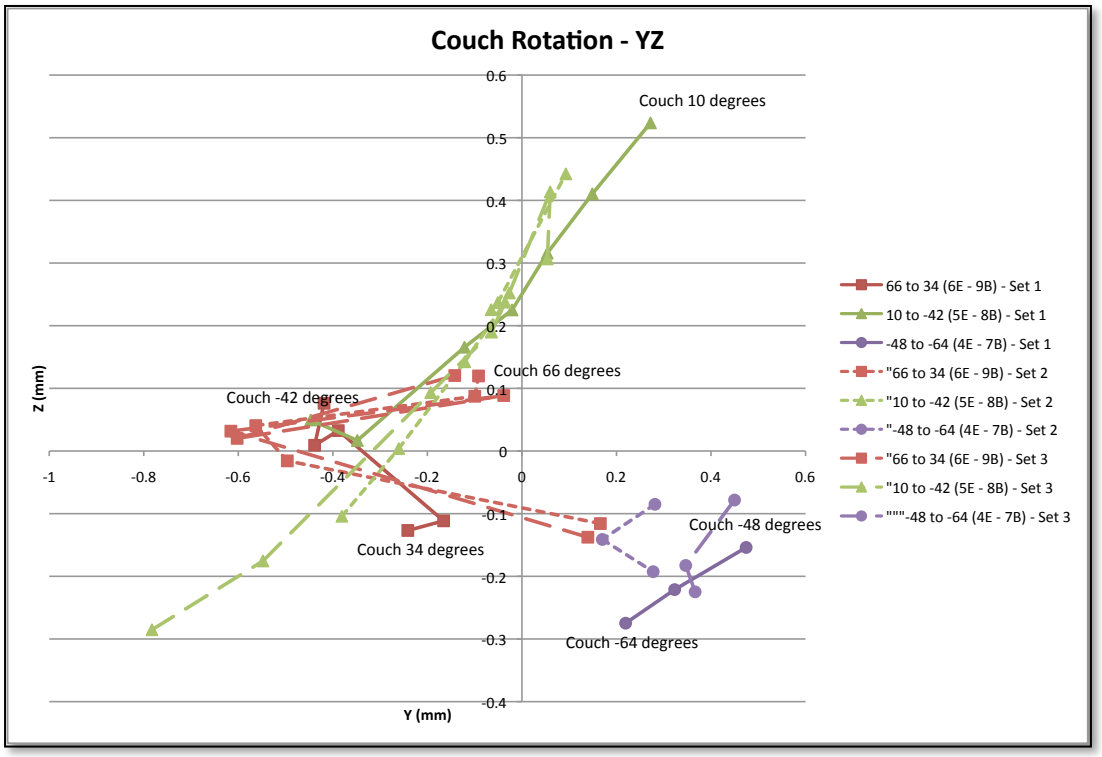

Figure 63: Minimum distance points for Couch rotation in the YZ phantom plane

Also measured was the variation in couch reproducibility. Measurements were taken of a single couch angle exposure. The couch was then moved away from that angle and then moved back again using the couch's digital reading hand control. The exposure was then taken again using another set films in the same orientation as the first. This was repeated five times. Due to the same film orientations be used for all the repeated data, any inconsistencies in the phantom not being a perfect dodecahedron would not effect the data. The standard deviation of the offsets from this data in all three principle planes of the phantom coordinate system were found to be: StdDev(x)=0.28mm, StdDev(y)=0.14mm, 0.25mm. This would be the uncertainty in film digitization and the uncertainty associated with the random error from the couch rotation due to its mechanical instabilities.

The couch angles 'missed' by the film were not taken due to time constraints. It was also evident from the gantry rotation data that phantom characterization was needed to accurately know the location of beams when exposed on different phantom faces.

Error Analysis

The error analysis will examine the uncertainties involved with determining the true position of the modelled radiation beams and their relative offsets. It must be noted here that, at this stage, when trying to characterize the phantom itself, we must separate the errors that are not due to the phantom itself like the yet inadequate methods to consistently and accurately position the phantom or the films thus resulting in a lack of phantom position reproducibility or unwanted phantom movements, which are not errors associated with the intrinsic uncertainties of the phantom to accurately determine radiation offsets. These extraneous effects can be controlled (e.g. by fixating phantom to the couch) and thus are not part of this error analysis. The errors that were examined, *i.e.* those associated with the phantom's determination of the radiation spots, were divided into two sections:

1) Uncertainties in film digitization and radiation spot determination.
2) Uncertainties associated with the phantom and its characterization.

1. Uncertainties in film digitization and radiation spot determination

As mentioned above the film was scanned with a resolution of 150 dpi. This is equivalent to 0.16933 mm per pixel. The calculation of the offsets is determined by the location of the radiation beam spots centres on both entrance and exit planes. However, the radiation spot centre depends on the determination of the film reference point and the rotation of the film within the software. Even though it was shown in Figures 37 and 38 that the radiation spot centre can be determined to within 1% the size of a pixel size or 0.017mm and that the ellipse fit to the data matches the contoured data average to within 0.1% the size of pixel, the uncertainty due to film scanning resolution is much larger.

In examining the radiation beam spot positional error due to film rotation in the software, it must be noted here that the Gafchromic film did not exhibit complete right angles on the uncut edges some of the time. Due to this, the shorter edge of the film was used for image rotation as the film was aligned with the short edge (reference edge) parallel to the sides of each pentagonal face. The largest source of uncertainty to image rotation derives from the fact that the line of rotation cannot be known to better accuracy than one pixel at the start and end points of the rotation line. The line of rotation was always measured near the corners of the short film edge to maximize the line of rotation length and thus minimize this uncertainty. This was determined to 0.12mm.

The uncertainty due to film digitization is of the order of one pixel or 0.17 mm, and is the main source of uncertainty in the determination of the location of the image and thus of the reference corner. Given that this uncertainty is much larger than the uncertainty in the determination of the center of the radiation spots, and given that the calculation of film rotation simply reproduces uncertainties in the initial conditions, the uncertainty in digitization is the main source of uncertainty in determining the true position of individual beams on a single film.

2. Uncertainties associated with the phantom and its characterization

The uncertainties due to imperfections in the dodecahedron can be divided into uncertainties associated with the individual faces and uncertainties associated with the shape of the entire phantom. This is because the individual faces were all precision machined in the same manner at DKFZ while they were 'glued' together at O.C.C.

The uncertainties associated with measuring the same radiation beam using different film orientations on the same face are likely due to very small machining imperfections in the fabrication process. It was shown in the Phantom Characterization Section that the offsets of radiation beams exposed (only on the same film) can be measured with an high degree of accuracy. The maximum deviation of the minimum distance points in Figures 51, 52, and 53 in Results Section is 0.085mm. Since the uncertainty due to film digitization is larger than this deviation, the relative motion of the beam on a single film near the isocentre as either the couch or gantry are rotated cannot be known better than 0.16933mm or one pixel.

The uncertainty due to slight phantom imperfections from an imperfect fabrication were not systematically investigated in this research due to time constraints. Therefore, true uncertainties involving the relative and absolute location of all the radiation beams cannot be known until full phantom characterization takes place. Due to the complexity of the dodecahedron shape when compared to simpler shapes such as a cube, the characterization process of any machined dodecahedron phantom will inevitably take considerable time in order to properly have the phantom clinically ready to model radiosurgical beam offsets. The dodecahedron shape is composed of 12 regular pentagonal faces, with three meeting at each vertex, 20 vertices, and 30 edges. To characterize these parameters would require a procedure to locate the 20 individual vertices. Based on the gaps in the plots from the gantry rotation data section, an uncertainty can only be estimated as true locations and rotations of data originating from different film faces cannot be known until the characterization has taken place. Given that a large fraction of the thesis work involved the design and fabrication of the phantom at two different cancer centres, our work in the characterization of the phantom, including the identification of unexpected sources of error, constitutes the beginning of a longer process.

Although individual radiation beams can be localized on a single film to 170 microns, the uncertainty when determining the locations of all the beams from multiple films can only be determined once the phantom has been properly characterized. Therefore, in this thesis research, true error bars which, aside from the voxel uncertainties would involve a knowledge of the limitations of the phantom, including QA tests on the accuracy of the film-holding grooves, the accuracy of the relative positions of all vertices and a rigid and consistent positioning of the phantom, have been left out of the plots only to be added in the future once they can be determined following phantom characterization. As of now, these uncertainties would not represent the true nature of the uncertainties of the phantom but rather the conditions of the manufacturing process of this very first prototype. By presenting the discrepancies found outside error bounds, we have

rather been able to identify several critical aspects that need to be resolved in the manufacturing, assembling and positioning aspects of this phantom.

3. Other Uncertainties

Another source of error that must be taken into consideration is the uncertainty involved with the placement of the phantom. Although careful alignment of the phantom to the treatment room lasers (which were checked against a calibrated mechanical pointer before each measurement) was done, small misalignments without doubt still occurred that influenced the results. It became evident that further phantom characterization was necessary, therefore any means to reliably align the phantom to the same orientation with an accuracy of less than 1mm was not pursued. Therefore, the uncertainty associated with phantom positioning could only be estimated at this point and would be pointless to investigate until a reliable method of positioning the phantom is found. As stated earlier in the Phantom Robustness Section, a means to align the phantom using gantry 0° and 90° reference beams will be investigated in the future as shall the design and construction of a phantom couch adaptor.

Discussion

The measurement of isocentric radiation beam offsets from a modified Linac is an integral part of the quality assurance program that is used for SRS. The highest degree of accuracy and precision for all aspects of a SRS treatment should always be sought after. The data presented here has shown that it would be possible to accurately determine the offsets for any gantry or couch angles from a properly characterized phantom. However, for this accuracy to be obtained, the phantom must be machined and fabricated with the highest possible precision and must be carefully characterized using measurements which shall apply only to this specific phantom. Moreover it is crucial to accurately position the phantom with a rigid phantom support that allows changing the films without any involuntary displacement or rotation of the phantom or use the hypothesised method described earlier employing 0° and 90° reference beams.

The data presented here for relative offsets of the radiation beams has been given separately for the gantry and couch rotations. For the Linac based SRS treatments, the gantry and couch are independent of each other as neither is mechanically or physically related to the other.

Gantry and Couch reproducibility data was taken and shown in the Data Results section. It was found that the gantry and couch do not reproduce the exact same beams when rotating either of the two. The digital readout for the gantry and couch allows for tenths of degrees in resolution of rotational movement. The maximum deviations in all principle directions for the gantry data was 0.16mm and for the couch data 0.28mm. It would be difficult to ascertain whether or not these variations in reproducibility come from the slight difference in gantry or couch positions when they are rotated away from and back to the same angle using the digital readout, if they come from slight mechanical instabilities in the gantry and couch rotation mechanisms, or if they come from the uncertainty in film digitization.

Gantry Rotation Data Discussion

The offset data from gantry rotation alone was presented in Figures 56, 57, and 58 above. For these measurements the couch was left stationary at angle 0 degrees. Films were placed all around the phantom in orientations to maximize the coverage of the gantry rotation as in Figure 54. In order to measure the offsets from the missed gantry angles a second data set was acquired where the phantom removed from its position, film was replaced, and then the phantom was then placed at a shifted location by a known amount. The missing gantry angles were measured with the previous gantry data such that any placement errors when the data is registered from previous data set will be factored out. However it was found that the missing gantry data did not completely 'bridge' the gap over the missed gantry angles from the initial measurements. The Gaps, A, B, and C noted in Figures 56 through 58 show that characterization of the phantom is needed to accurately know the offsets of the radiation beams due to gantry and/or couch motion. Also with the introduction of an attachment to rigidly fixate the phantom to the end of the treatment couch, registration of data between measurements when the phantom is removed for film placement would not be needed. Furthermore, using an attachment would greatly simplify the phantom characterization process

allowing for exact repositioning of the phantom during measurements as would using the gantry 0° and 90° reference beam method mentioned earlier. It can also been seen from the plots in the gantry rotation data section, that if the gaps are closed and correct rotations are applied to data captured on the same film plane using phantom characterizations, a continuous and smooth plot of the offsets can be obtained. This is what would be expected as the motion of the radiation beam due to gantry motion is a systematic error. This is due to gravity acting on the head of the treatment machine where the radiation originates. Although there will be small unpredictable deviations due to the gantry rotating on a set of bearings, the offsets which occur due to gravity acting on the head of the machine will be dominant. Furthermore, since the gantry rotates about a much larger drum than the treatment couch, it will exhibit a more stable motion during rotation (D,Souza, 1999).

Once a characterization of the phantom is complete and an attachment to the treatment couch is constructed, full data sets can be obtained for all gantry treatment angles with a high degree of accuracy and precision.

Couch Rotation Data Discussion

The analysis of the offset data from couch rotation data section shows the motion of the couch through it's isocentric rotation. The measured data was taken identically on three different days. The plots show that the offsets measured on different days is not repeatable and is also evident in the couch reproducibility results showing that the couch offsets cannot be reproduced better than a maximum of 0.28mm. This would be expected as the bearings on which the couch rotates produces small unpredictable movements of the couch (and thus the treatment target). This random error is not affected by gravity during the couch's rotation as it does the gantry as the couch's plane of rotation is perpendicular to the force of gravity.

The gaps in the offset data is evident that more data is needed to be taken at shifted phantom locations to acquire all couch treatment angle and also that phantom characterization is needed. It was shown that modelling of beams falling on the same film opposing film faces can be done with precision better than 0.17mm. Therefore, it can be said that the relative offsets of the beams on the same film are accurately reproduced. However, beams modelled on different faces are not accurately offset relative to each other due to the phantom not being completely characterized.

A method to determine the offset from treatment couch rotation was investigated by Hartmann et al examining the rotation of a sphere mounted on the couch at the isocentre as the couch rotates. From this, they were able to determine the mean radial distance between the couch rotation axis and isocentre and the mean inclination of the couch axis in two principle planes. These were found to be 0.25 ± 0.25mm, -0.03 ± 0.02°, and -0.04 ± 0.01° (Karger, 2000). True comparisons can only be done once phantom characterization is complete and all offsets including uncertainties from couch rotation is known.

Phantom Characterization Discussion

In the phantom characterization section above, it was shown that each phantom face had a unique set of coordinates for the reference point. By altering the reference point location, the offset data taken at each film orientation using a stationary gantry and couch converged together to distances smaller than the film resolution. It was evident from the offset convergence that small changes in the reference point location (as small as 0.1mm) yielded very large changes in the offsets (up to 0.3mm). This is proof that a very careful characterization procedure must occur for the phantom. In fact, since any dodecahedron phantom will not be exactly fabricated the same, a unique characterization will be needed for each future phantom. Measurement data would need to be taken with care to place the film properly while not moving the phantom. Further characterization of the phantom would involve doing repeated measurements of partial arcs with the phantom rotated in such a way that beams that have appeared on two film sets show up on one film set in a second run. The relation between the two faces can be deduced by making the results agree (as they should for the gantry at the same set of angles). Also, for a accurate phantom characterization to take place, it would be best to have an attachment fabricated to allow reproducible positioning of the phantom at the end of the treatment couch.

In regards to the phantom characterization work which needs to be completed for this research in the future, the accurate positions of each individual phantom vertex need to be implicitly inputted into the calculation software. This would accurately define the reference point location and the angle at which each phantom face sits in the shape. Once this is complete, this characterized phantom should be able to properly calculate the offsets with an accuracy similar to that of a single film face above (less than 0.17mm).

Conclusions

A radiosurgical dodecahedral phantom was designed and fabricated for this research. The design and fabrication occurred at the German Cancer Research Centre (DKFZ) in Heidelberg, Germany and at the Odette Cancer Centre in Toronto, Canada. Unexpected issues arose during the fabrication process that required several reassessments of the construction and of the details of the phantom, which led to the need of extra time needed for construction and thus for a delay in the characterization experiments.

It was shown that with a proper characterization of the phantom, uncertainties of 0.17mm can be achieved in localizing the radiation beams.

The work here also shows that any future phantoms made must be individually characterized with extreme accuracy in order to consistently achieve this levels of uncertainty. It is also possible that any future phantoms made would not need as much characterization if the fabrication process could consistently achieve dodecahedrons that are closer to their perfect shape and if a mechanism for accurate positioning and flatness of the films is devised.

Given the exceptional accuracies that are possible to achieve, a completely characterized phantom will give medical physicists a quality assurance tool to accurately know the isocentric variation of their linear accelerator treatment machines. Furthermore, based on the future plans for the phantom, it can potentially give physicists a tool to measure the radiation dose distributions from SRS treatments. To be able to know both the isocentric variation and dose distribution would be a invaluable to the improvement of SRS. Moreover, given its accuracies of the order of a hundred microns, this phantom is an ideal tool for testing and calibrating iPet therapies in which beams of only hundreds of keV are used with penumbras of only hundreds of microns (Keller, 2007). Furthermore, this phantom in theory could be used beneficially to localize radiation beams from any isocentric treatment units including the Gamma-knife or proton therapy units.

The process of designing and fabricating a phantom for use in radiosurgery quality assurance was proven to be a large task. The research presented here represents the first step in the quest for an accurate construction and complete characterization of this phantom. Further steps will include, among others: the design of a consistent manufacturing process, including a strategy to accurately position the radiographic film both in placement and by avoiding bending; the design and construction of a rigid phantom support with micrometric positioning; and the introduction in the analysis software of an accurate and complete 3D positioning of all the phantom's vertices.

Future Considerations

For this radiosurgical phantom to function as a tool for measuring the offset radiation, the characterization process needs to be completed. It was shown that by assuming the phantom is a perfect dodecahedron leads to an incorrect beam localization of the order of 0.5 mm and that a unique characterization is needed for this specific phantom. Furthermore, a mechanical device to reproducibly fixate the phantom to the treatment couch is needed. Due to time constraints it was not constructed as part of this project. Once the characterization process and the attachment are completed, the phantom will be able to determine radiation beam offsets from any gantry and couch rotation (relative to each other and relative to a fixed point) with 0.17 mm uncertainty.

Another SRS quality assurance application which can be pursued with this phantom is the ability to determine the radiation dose delivered from the Linac. The use of Gafchromic films on the phantom to expose the radiation beams is possible as calibration for dose has been done. It has been shown that radiochromic film can reliably be used for radiosurgery dosimetry (Robar, 1999). If the software is modified to determine the offsets for a beam moving continuously over the phantom and thus a film sheet, it would be able to calculate the amount of radiation dose delivered and the dose distribution for an entire treatment or for individual gantry arcs. This would be invaluable information to the medical physicists as the phantom would not only give positional information in regards to the treatment beams, but would yield dosimetric information as well.

Implementing the resulting isocentre variability map in practice to achieve greater radiation isocentre accuracy and precision, is hypothesised to be done using two methods. The first method will involve mapping the radiation isocentre as it varies with collimator rotation. Treatments typically use only one collimator angle and the treatment fields are usually circular in shape. By exploiting these two characteristics, it will be assessed whether or not certain converging beams can be corrected by rotating the collimator and directing them closer to a common radiation isocentre point. This would provide a corresponding collimator angle to use for each gantry and couch angle during treatment translating into less radiation isocentre variability. The second method hypothesised will be to shift the collimator by small distance where by the radiation beam will be aimed in the direction of collimator shift. By designing a device that can translate the individual cones by small distances it will be possible to direct the converging beams to a radiation isocentre with less variation.

If reducing the isocentre variation can not be possible using the methods above, it will be determined if it is possible to model the offsets into the treatment planning system. By doing this in theory, the dose calculation algorithm will account for all the offsets when determining the optimal treatment plan.

Appendices

Appendix A1. *Matlab code: callFunc.m – Main function with distance calculations.*


```
%%%%%%%%%%%%%%%%%%%
%%% Appendix A1
%%%%%%%%%%%%%%%%%%%


%%% orientationLet and Num are the orientations of the film on the dode
%%% (see rayTrace.m)

global orientationLet
global orientationNum
global face

%%% minDistPts :  the minumum distance between each pair of beams and their
%%%     points
%%%% entranceData: the beam locations on the entrance in Dode coords,
%%%%    similarly for exitData
%%% minDist_vector : a vector pointing to the shortest distance on each ray↙
to the dode centre (0,0,0)
%%% v : parametrized vector between entrance and exut beams
%%% minDist_vector_centroid - shorttest distance points from calculated
%%%     centriod of data
%%% normalized_vector_centroid - shorttest distance points from calculated
%%%     centriod of data normalized to centroid


minDist_vector=[];
minDist_vector_centroid=[];
normalized_vector_centroid=[];
minDistPts=[];
entranceData=[];
    exitData=[];
    minDist=[];
    v=[];


%%%% Run thru each film and call readFilm to calculate the entrance and exit↙
data pionts
for face= [1 2 3]% 4 5 6]% 6 7]

    if face==1;
    %%%%  Entrance parameters
        entrance_File='/Users/rob/Research/Film Data/June26-CouchSet3/6-E.↙
tif'
        orientationLet='e';
        orientationNum=6;

        %%% Run readFilm.m
        entranceCoords=readFilm(entrance_File, 2);

        %%%% Exit Parameter
        exit_File='/Users/rob/Research/Film Data/June26-CouchSet3/9-B.tif'
        orientationLet='b';
        orientationNum=9;
    elseif face==2
        entrance_File='/Users/rob/Research/Film Data/June26-CouchSet3/5-E.↙
tif'
```

```
        orientationLet='e';
        orientationNum=5;

        %%% Run readFilm.m
        entranceCoords=readFilm(entrance_File, 2);

        %%%% Exit Parameter
        exit_File='/Users/rob/Research/Film Data/June26-CouchSet3/8-B.tif'
        orientationLet='b';
        orientationNum=8;
    elseif face==3
        entrance_File='/Users/rob/Research/Film Data/June26-CouchSet3/4-E.↙
tif'
        orientationLet='e';
        orientationNum=4;

        %%% Run readFilm.m
        entranceCoords=readFilm(entrance_File, 2);

        %%%% Exit Parameter
        exit_File='/Users/rob/Research/Film Data/June26-CouchSet3/7-B.tif'
        orientationLet='b';
        orientationNum=7;
    elseif face==4
        entrance_File='/Users/rob/Research/Film Data/June09-Set2/12-E.tif'
        orientationLet='e';
        orientationNum=12

        %%% Run readFilm.m
        entranceCoords=readFilm(entrance_File, 2);

        %%%% Exit Parameter
        exit_File='/Users/rob/Research/Film Data/June09-Set2/1-E.tif'
        orientationLet='e';
        orientationNum=1;
    elseif face==5
        entrance_File='/Users/rob/Research/Film Data/June09-Set2/3-B.tif'
        orientationLet='b';
        orientationNum=3;

        %%% Run readFilm.m
        entranceCoords=readFilm(entrance_File, 2);

        %%%% Exit Parameter
        exit_File='/Users/rob/Research/Film Data/June09-Set2/11-E.tif'
        orientationLet='e';
        orientationNum=11;
    elseif face==6
        entrance_File='/Users/rob/Research/Film Data/June09-Set2/8-B.tif'
        orientationLet='b';
        orientationNum=8;

        %%% Run readFilm.m
        entranceCoords=readFilm(entrance_File, 2);

        %%%% Exit Parameter
```

```
        exit_File='/Users/rob/Research/Film Data/June09-Set2/5-E.tif'
        orientationLet='e';
        orientationNum=5;

    elseif face==7
        entrance_File='/Users/rob/Research/Film Data/July22-Gantry_gaps/5-E.↙
tif'
        orientationLet='e';
        orientationNum=5;

        %%% Run readFilm.m
        entranceCoords=readFilm(entrance_File, 2);

        %%%% Exit Parameter
        exit_File='/Users/rob/Research/Film Data/July22-Gantry_gaps/3-C.tif'
        orientationLet='c';
        orientationNum=3;
    end
    %%% Run readFilm.
    exitCoords=readFilm(exit_File,3);



    %%%% RUN Plots
    [c,d]=size(entranceCoords);




    for j = 1:c
        %%%  Parametrize each entance beam thru the centre to a spot on the
            %%%  other film to compare to real spots to figure which spots
            %%%  match

            %v_orig=[0 0 9.45]-entranceCoords(j,:);
            v_orig=[0 0 0]-entranceCoords(j,:);
            %v_orig=[2.8 -1.8 -1]-entranceCoords(j,:);
            compCoordX=entranceCoords(j,1)+2*v_orig(1,1);
            compCoordY=entranceCoords(j,2)+2*v_orig(1,2);
            compCoordZ=entranceCoords(j,3)+2*v_orig(1,3);

            %scatter3(compCoordX,compCoordY,compCoordZ,100,'g','filled')
            %scatter3(v_orig(1,1), v_orig(1,2), v_orig(1,3),↙
100,'g','filled')

        [e,f]=size(exitCoords);

        for k = 1:e


            comparison=((compCoordX-exitCoords(k,1))^2+(compCoordY-↙
exitCoords(k,2))^2+(compCoordZ-exitCoords(k,3))^2)^(0.5);
```

```
            if (comparison) < 0.5

                %%%% now parametrize the spots that match up
                v=[exitCoords(k,:)-entranceCoords(j,:); v];

                %%% EntranceData and exitData hold the coordinates of the↙
beams
                %%% in order such that beam 1 in entranceData matches beam 1
                %%% exitData
                entranceData=[entranceCoords(j,:); entranceData];
                exitData=[exitCoords(k,:); exitData];

                %%Para(numBeams)=entranceCoords(j,1)+t*v;

                Entrance_Beam=j;
                Exit_Beam=k;
                %%%Distance_to_iso=((entranceCoords(j,1)+0.5*v(1,1))^2+↙
(entranceCoords(j,2)+0.5*v(1,2))^2+.....
                %%%    (entranceCoords(j,3)+0.5*v(1,3))^2)^(0.5)
                xtrace=[entranceCoords(j,1) exitCoords(k,1)];
                ytrace=[entranceCoords(j,2) exitCoords(k,2)];
                ztrace=[entranceCoords(j,3) exitCoords(k,3)];

                %%% Calculate shortest distance to dode centre for each
                %%% beam
                %%% the parametrized time this happens occurs at minDist_t
                minDist_t = -1*dot(entranceCoords(j,:)-[0 0 0], exitCoords↙
(k,:)-entranceCoords(j,:))/......
                    dot(abs(exitCoords(k,:)-entranceCoords(j,:)),abs↙
(exitCoords(k,:)-entranceCoords(j,:)));

                %%% Calculate the gantry and couch treatment angle
                %%%% calculate gantry angle and couch angle based on↙
entrance
        %%%% coords

                if entranceData(1,3)>0
                    gantryAngle=asind((sqrt(entranceData(1,1)^2 +↙
entranceData(1,2)^2))/(sqrt(entranceData(1,1)^2 + entranceData(1,2)^2 +↙
entranceData(1,3)^2)));
                else
                    gantryAngle=acosd((sqrt(entranceData(1,1)^2 +↙
entranceData(1,2)^2))/(sqrt(entranceData(1,1)^2 + entranceData(1,2)^2 +↙
entranceData(1,3)^2)));
                end

                couchAngle=acosd(entranceData(1,2)/(sqrt(entranceData(1,1)^2↙
+ entranceData(1,2)^2)));
```

```
                couchAngle=-1*(couchAngle-180);

                if entranceData(1,2) > 0 & entranceData(1,3) > 0;
                    gantryAngle=gantryAngle-2*gantryAngle + 360;
                elseif entranceData(1,2) > 0 & entranceData(1,3) < 0;
                    gantryAngle=270-gantryAngle;
                elseif entranceData(1,2) < 0 & entranceData(1,3) < 0;
                    gantryAngle=90+gantryAngle;

                end

                if entranceData(1,1) < 0 & entranceData(1,2)<0;
                    couchAngle=couchAngle-2*couchAngle+360;
                elseif entranceData(1,1) < 0 & entranceData(1,2) > 0;
                    couchAngle=180 - couchAngle;
                elseif entranceData(1,1) > 0 & entranceData(1,2)>0;
                    couchAngle=180 + couchAngle;
                end


                %%%% Shortest distance calc
                minDist_vector=[(entranceCoords(j,:)+minDist_t*v(1,:))↙
gantryAngle couchAngle; minDist_vector];

                %%% Plot beams
                plot3(xtrace,ytrace,ztrace,'Color','r','LineWidth',3);


            end

       %%text(entranceCoords(j,1),entranceCoords(j,2),entranceCoords(j,3),↙
int2str(j),'Color','w');

        end
    end
end


%



%%% Find centroid of data using k-means clustering

kmeanDist=[minDist_vector(:,1) minDist_vector(:,2) minDist_vector(:,3)];
[IDX,C,sumd,D] = kmeans(kmeanDist,1);


[g,h]=size(entranceData);
for b = 1:g


                %%% Calculate shorttest distance for each beam again now
                %%% from the centroid c
                minDist_t = -1*dot(entranceData(b,:)-C, exitData(b,:)-↙
```

```
entranceData(b,:))/......
                    dot(abs(exitData(b,:)-entranceData(b,:)),abs(exitData↙
(b,:)-entranceData(b,:)));

                minDist_vector_centroid=[(entranceData(b,:)+minDist_t*v↙
(b,:)); minDist_vector_centroid];


end



%%% Find the new centroid of the new data now
kmeanDist2=[minDist_vector_centroid(:,1) minDist_vector_centroid(:,2)↙
minDist_vector_centroid(:,3)];
[IDX2,C2,sumd2,D2] = kmeans(kmeanDist2,1);

for r=1:g
    normalized_vector_centroid=[(minDist_vector_centroid(r,1)-C2(1,1)) .....
        (minDist_vector_centroid(r,2)-C2(1,2)) .....
        (minDist_vector_centroid(r,3)-C2(1,3)); normalized_vector_centroid];

end

minCentreX=C2(1,1);
minCentreY=C2(1,2);
minCentreZ=C2(1,3);

%%% Append gantry and couch data calculated above

minDist_vector_centroid=[minDist_vector_centroid minDist_vector(:,4)↙
minDist_vector(:,5)];
normalized_vector_centroid=[normalized_vector_centroid minDist_vector(:,4)↙
minDist_vector(:,5)];


%%% Plot centroid
scatter3(C2(1,1),C2(1,2),C2(1,3),100,'g','filled')

%%% Plot shortest distance to centroid points
scatter3(0,0,0,100,'r','filled')
scatter3(minDist_vector_centroid(:,1), minDist_vector_centroid(:,2),↙
minDist_vector_centroid(:,3), 100, 'b', 'filled')%% ,'b','LineWidth',1,↙
'MarkerSize',10);


%%% Calculate distane from centroid to all points to find sphere radius
[num_minDist, num_col]=size(minDist_vector_centroid);
minSphere=0;

for q=1:num_minDist
    DisttoAvg=sqrt((minDist_vector_centroid(q,1)-minCentreX)^2 +↙
(minDist_vector_centroid(q,2)-minCentreY)^2 + (minDist_vector_centroid(q,3)-↙
minCentreZ)^2);
```

```
    if DisttoAvg > minSphere
        minSphere=DisttoAvg;
    end
end


%%%%%%%%%%%%%%%%%%%%%%%%%%%%%%%%%%%%%%%%%%%%%%%%%%%%%%%%%%%%%%%%%%%%%%%%%%%%%%%↙
%%%%%%%%%%%


%%%% display min dist points, min sphere, avg centre of points
%minDist_vector_centroid
minSphere
minCentreX
minCentreY
minCentreZ


phi=linspace(0,pi,30);
theta=linspace(0,2*pi,40);
[phi,theta]=meshgrid(phi,theta);


x=minCentreX+minSphere*sin(phi).*cos(theta);
y=minCentreY+minSphere*sin(phi).*sin(theta);
z=minCentreZ+minSphere*cos(phi);
mesh(x, y, z);
alpha(0.0);
%%%%%%%%%%%%%%%%%%

%%%%%%%%%%%%%%%%%%%%%%%%%%%%%%%%%%%%%%%%%%%%%%%%%%%%%%%%%%%%%%%%%%%%%%%%%%%%%%%
%%% plot min dist points in 3 plames


%figure(5)

%scatter(minDistPts(:,1), minDistPts(:,2),35,'filled');
%%%scatter3(minDistPts(:,1),minDistPts(:,2),minDistPts(:,4),35,minDistPts(:,↙
5),'filled');
%Legend(minDistPts(:,4))


%%%%%%%%%%%%%%%%%%%%%%%%%%%%%%%%%%%%%%%%%%%%%%%%%%%%%%%%%%%%%%%%%%%%%%%%%%%%%%%


%
```

Appendix A2. *Matlab code: readFilm.m – Function to read and contour film data.*


```
%%%%%%%%%%%%%%%%%%%
%%% Appendix A2
%%%%%%%%%%%%%%%%%%%


%%%%% This function opens the film file and calculates the coordinates in 2d
%%%%% film coordinates of all the found beam spots. It then calls the
%%%%% rayTrace function to convert the film spot centres to 3d global coords

function [beamCentre]=readFilm(filmFileName, filmIndex);
global orientationLet;
global orientationNum;
global face;



    %%%%%%% open film image
    %   filmIndex=1
   % I = imread('/Users/rob/Research/Film Data/pri5-ellipse001.tif');
    I=imread(filmFileName);

   %imageInfo=imfinfo(filmFileName);
   %imageInfo.ColorType;


   %%%% Starts the centroid difference matrix for excel and the beamCentre
   %%%% matrix whixh holds the coords of each beam spot
   diff_matrix=[];
   beamCentre=[];




   %%% convert to grayscale and display image

     figure(1), imshow(I);
     %hold on;
    %if imageInfo.ColorType ~= 'grayscale'
    %    I = rgb2gray(I);
    %end

    %%%%%%%%%%%%%%%%%%%%%%%%%%%%%%%%%%%%%%%%%%%%%%%%%%%%%%%%

    %figure, imshow(I);







%%%%%%%%%%%%%%%%%%%%%%%%%%%%%%%%%%%%%%%%%%%%%%%%%%%%%%%%%%%%%%%%%%%%%%%%%%%
%%%% Calculate rotation angle based on user input by calling ginput2
```

```
datacursormode on
lineAngle=ginput2(2);

close(1);

deltaX=lineAngle(2,1)-lineAngle(1,1);
deltaY=lineAngle(1,2)-lineAngle(2,2);
topAngle = -atan(deltaY / deltaX) * 180 / pi
%%%%%%%%%%%%%%%%%%%%%%%%%%%%%%%%%%%%%%%%%%%%%%%%%%%%%%%%%%%%%%%%%%%5

%%%%%%%%%%%%%%%%%%%%%%%%%%%%%%%%%%%%%%%%%%%%%%%%%%%%%%%%%%%%%%%%%%55
%%%%%%%%%% Rotate the image back.
if topAngle < 0
    IRot = imrotate(I, topAngle+90, 'loose', 'bicubic');
else
    IRot = imrotate(I, topAngle-90, 'loose', 'bicubic');
end
IRot(IRot == 0) = 65534;
[sizeRow,sizeCol] = size(IRot);

%%% get rid of white border using selected point above
figure, imshow(IRot)
removeborder_pt=ginput2(1)




close(1);
    %figure(filmIndex), imshow(IRot);
    %hold on;


%%%%%% plot grid lines %%%%%%%%%%%%%%%%%%%%%%%
% for grd = 1:1051
%         plot ([1 1371],[grd grd], '-k', 'linewidth', 1);
% end
%
% for grd = 1:1371
%         plot ([grd grd],[1 1051], '-k', 'linewidth', 1);
% end
%%%%%%%%%%%%%%%%%%%%%%%%%%%%%%%%%%%%%%%%%%%%%%%%%%%%


%%%%% Convert to dose%%%%%%%%%%%%%%%%%%%%%%%%%%%%
%%%% Parameters from FilmQA software
%%% coefficients

a0= 3.5397461361e3;
a1=1.6105333329e-1;
a2=-4.3147580666e-5;
a3=2.4260634827e-9;
a4=-6.3080751711e-14;
a5=7.9783970065e-19;
a6=-3.9699153037e-24;
```

```
[c,d]=size(IRot);
IRot2=ones(c,d);


for i = 1:c
    for j=1:d

        gs=double(IRot(i,j))-9000;
        if gs >13850


            IRot(i,j)=65532-32.7*(a0 + a1*gs + a2*gs^2....
                + a3*gs^3 + a4*gs^4....
                + a5*gs^5 + a6*gs^6);
        else
            IRot(i,j)=2000;
        end

    end
end




figure(filmIndex), imshow(IRot,[1 65532]);



hold on;
%%%%%%%%%%%%%%%%%%%%%%%%%%%%%%%%%%%%%%%%%%%%%%%%%%%%



%%%%%%%%%%%%%%%%%%%%%%%%%%%%%%%%%%%%%%%%%%%%%%%%%%%%
%%%%%%  inverse square law fix

% theta = 15;
% D=1949;
%
% xCentre=986;
% yCentre=206;

% for row=44:206;
%     for col=986%850:1128;
%         newD=(D^2+((row-yCentre)^2+(col-xCentre)^2)-2*D*((row-yCentre)^2+↙
(col-xCentre)^2)^0.5*cosd(90-theta))^0.5;
%
%         IRot(row, col)=IRot(row,col)*((D/newD)^2);
%         test=((D/newD)^2)
%     end
% end
%
% for row = 206:393
```

```
%    for col=986%850:1128;
%         newD=(D^2+((row-yCentre)^2+(col-xCentre)^2)-2*D*((row-yCentre)^2+(col-xCentre)^2)^0.5*cosd(90-theta))^0.5;
%         IRot(row, col)=IRot(row,col)*((newD/D)^2);
%    end
% end
%%%%%%%%%%%%%%%%%%%%%%%%%%%%%%%%%%%%%%%%%%%%%%%%%%%%%%%%%%%


%%%%%%%%%%%%%%%%%%%%%%%%%%%%%%%%%%%%%%%%%%%%%%%%%%%%%%%%%%%%%%%%
%%%%%%   find, calculate, and Plot Contour, least squars fit, matlab parameters %%%%%
%%%%

%

% %%%% New green gafchromic levels
 if filmIndex==2;

     level = 0.8

    else

        level = 0.71


    end
%


    %%%%%%%threshold the image and create a binary image
    bw = im2bw(IRot,level);
    bw=(~bw);


    %%%%%%%%%%%%%%%%%%%%%%%%%%%%%%%%%%%%%%%%%%%%%%%%%%%%%%%%%%%


    %%%%%%% remove all objects containing less than 5000 pixels
    bw = bwareaopen(bw, 2000);
    %%%%%%%%%%%%%%%%%%%%%%%%%%%%%%%%%%%%%%%%%%%%%%%%%%%%%%%%%%%%%%%%

    %%%%%%%fill in holes within the image
    bw = imfill(bw,'holes');
    %%%%%%%%%%%%%%%%%%%%%%%%%%%%%%%%%%%%

    %%%%%%% determine the size of the film image
      %col = round(dim(2)/2)-90
      %row = find(bw(:,col), 1)
      %row = min(find(bw(:,col)))
      %contour = bwtraceboundary(bw,[row, col],'N');
      %  hold on;
      %plot(contour(:,2),contour(:,1),'r','LineWidth',1);
%%%%%%%%%%%%%%%%%%%%%%%%%%%%%%%%%%%%%%%%%%%%%%%%%%%%%%%%%%%%%%%%
```

```
    % %%%%%%locate boundaries using bwboundaries method
     [B,L,N,A]=bwboundaries(bw);
     %%%%%%%%%% plot boundaries

     [m,n] = size(bw);



     %%%%% for film spots on an edge, get rid of contours at the borders

     %%% first determine where film ends in y direction at x=750(750th↙
column frmo
     %%% left, any would work as image is rotated now)
     rowSearch=m;


     while IRot(rowSearch,750)>64000

         rowSearch=rowSearch-1;
     end

     colSearch=n;
     while IRot(300,colSearch)>64000
           colSearch=colSearch-1;
     end

     m = rowSearch;
     n= colSearch;


     length(B);



     for l=1:length(B)
         boundary=B{l};
         p=1;



        while length(boundary)>p
            if (boundary(p, 1) == 1) || ....
                    (boundary(p, 1) == 2) || ....
                    (boundary(p, 1) == 3) || ....
                    (boundary(p, 1) == 4) || ....
                    (boundary(p, 1) == 5) || ....
                    (boundary(p, 1) == 6) || ....
                    (boundary(p, 1) == 7) || ....
                (boundary(p, 1) == 8) || ....
                    (boundary(p, 1) == 9) || ....
                    (boundary(p, 1) == 10) || ....
                    (boundary(p, 1) == m) || ....
                    (boundary(p, 1) == m-1) || ....
                    (boundary(p, 1) == m-2) || ....
```

```
                 (boundary(p, 1) == m-3) ||  ....
                     (boundary(p, 1) == m-4) || ....
                     (boundary(p, 1) == m-5) || ....
                     (boundary(p, 1) == m-6) ||  ....
                     (boundary(p, 1) == m-7) ;



                  boundary(p,:)=[];
             else
                 p=p+1;
             end

         end
         p=1;

         while length(boundary)>p
             if  (boundary(p,2) == 1) ||....
                      (boundary(p,2) == 2) ||....
                      (boundary(p,2) == 3) ||....
                   (boundary(p,2) == 4) ||....
                    (boundary(p,2) == 5) ||....
                      (boundary(p,2) == 6) ||....
                      (boundary(p,2) == 7) ||....
                  (boundary(p,2) == 8) ||....
                      (boundary(p,2) == 9) ||....
                      (boundary(p,2) == 10) ||....
                      (boundary(p,2) == n) || ....
                      (boundary(p,2) == n-1) || ....
                      (boundary(p,2) == n-2) || ....
                  (boundary(p,2) == n-3) || ....
                      (boundary(p,2) == n-4) || ....
                      (boundary(p,2) == n-5) || ....
                      (boundary(p,2) == n-6) || ....
                      (boundary(p,2) == n-7);



                  boundary(p,:)=[];
             else
                 p=p+1;
             end
         end


         %%% plot countour data
          plot(boundary(:,2),boundary(:,1),'r','LineWidth',1);



         %%%%%%%%%%%%%%%%%%%%%%%%%%%%%%%%%%%%%%%%%%%%%%%%%%%%%%%%%%%



         %%%%%% fit each ellipse or parabola to a contour of an ellipse
equation
```

```
        %for m=1:length(B);
            contour=boundary;
            X = contour(:,2);
            Y = contour(:,1);


            %%%%%%%%%%%%%%%% use ellipse_fit.m
             XY =[X Y];

             centroid = mean(XY);   % the centroid of the countoured data set
             %%% plot the centroid of contour data
 plot(centroid(1,1), centroid(1,2),'r*');



            %Construct M
            M = [2*X.*Y Y.^2 2*X 2*Y ones(size(X))] ;

            % Multiply (-X.^2) by pseudoinverse(M)
            e = M\(-X.^2);

            %Extract parameters from vector e
            a = 1;
            b = e(1);
            c = e(2);
            d = e(3);
            f = e(4);
            g = e(5);

            %Use Formulas from Mathworld to find semimajor_axis, semiminor_axis, x0, y0
            %, and phi

            delta = b^2-a*c;

            x0 = (c*d - b*f)/delta;
            y0 = (a*f - b*d)/delta;

            phi = 0.5 * acot((c-a)/(2*b));

            nom = 2 * (a*f^2 + c*d^2 + g*b^2 - 2*b*d*f - a*c*g);
            s = sqrt(1 + (4*b^2)/(a-c)^2);

            a_prime = sqrt(nom/(delta* ( (c-a)*s -(c+a))));

            b_prime = sqrt(nom/(delta* ( (a-c)*s -(c+a))));

            semimajor_axis = max(a_prime, b_prime);
            semiminor_axis = min(a_prime, b_prime);

            if (a_prime < b_prime)
                phi = pi/2 - phi;
            end
```

```
%%%%%%%%%%%%%%%%%%%%%%%%%%%%%%%%%%%%%%%%%%%%%%%%%%%%%%%%%%%%%%%%%%%%%%%%%%%%%%%%%%%%%%%%%%%


            %%%%%%%plot the centroids and fitted boundary of connected↙
objects calculated


            %%%if (semimajor_axis ~= 0) || (semiminor_axis ~= 0)
                plot(x0, y0,'g*');


                theta = 0:0.01:2*pi;
                Xfit=x0+semimajor_axis*cos(theta)*cos(phi)-↙
semiminor_axis*sin(theta)*sin(phi);
                Yfit=y0+semimajor_axis*cos(theta)*sin(phi)↙
+semiminor_axis*sin(theta)*cos(phi);

                plot(real(Xfit), real(Yfit),'g','LineWidth',1);


                text(x0+75,y0-75,int2str(l));



               beamCentre=[x0-removeborder_pt(1,1) y0-removeborder_pt(1,2);↙
beamCentre];


                figure(filmIndex);

            %%%end
                %%text(boundary(1,2)-35,boundary(1,1)+13,'x','Color','g',...
      %%% 'FontSize',14,'FontWeight','bold');

            %%%%%%%%%%%%%%%%%%%%%%%%%%%%%%%%%%%%%%%%%%%%%%%%%%%%%%%%%%%%%%%%%%%%%%%%%%%%%%%%%%%%%




    %%%%%%calculate connected objects area properties and display using the
    %%%%%%regionprops meethod
%     centroid=regionprops(bw,'centroid');
%     centroids = cat(1, centroid.Centroid);
%     eccentr=regionprops(bw,'eccentricity');
%     eccentricities=cat(1,eccentr.Eccentricity);
%     majaxislength=regionprops(bw,'majoraxislength');
%     majaxislengths=cat(1, majaxislength.MajorAxisLength);
%     minaxislength=regionprops(bw,'minoraxislength');
%     minaxislengths=cat(1, minaxislength.MinorAxisLength);
%     orientation=regionprops(bw,'orientation');
%     orientations=cat(1,orientation.Orientation);
```

```
%     %XY
%      x0_RP=centroids(l,1);
%      y0_RP=centroids(l,2);
%      a_RP=majaxislengths(l)/2;
%      b_RP=minaxislengths(l)/2;
%      phi_RP=orientations(l)*(pi/180);
% %
% %     %%%%% Plot regionprops fit
%      %theta = 0:0.01:2*pi;
% %
%      %Xfit = c+(c/a)*cos(theta) + x0;
%      %Yfit = (c/a)*sin(theta) + y0;
%      Xfit_RP=x0_RP+a_RP*cos(theta)*cos(phi_RP)-b_RP*sin(theta)*sin(phi_RP);
%      Yfit_RP=y0_RP+a_RP*cos(theta)*sin(phi_RP)+b_RP*sin(theta)*cos(phi_RP);
%      plot(Xfit_RP, Yfit_RP,'b','LineWidth',1);
% %     %asind(eccentricities)
% %     %wcentroids
% %
%      plot(centroids(:,1), centroids(:,2), 'b*');
%
%      eccentricities(l);
%
%
%      %%%% Populate centroid difference matrix to plot in excel
%      diff_matrix=[diff_matrix;l level x0_RP y0_RP x0 y0];


    %%%%%%%%%%%%%%%%%%%%%%%%%%%%%%%%%%%%%%%%%%%%%%%%%%%%%%%%%%%%%%%%%%%%%%%

end

%%% ADD Plot Legend
h = legend('Contour','Contour Centroid','Ellipse Fit Centroid','Ellipse Fit',3);



%%%% Call raytrace to convert beam centres in film coord to global coordinates using beam
%%%% centre in film coordinates as input
beamCentre=rayTrace(beamCentre);
```

Appendix A3. Matlab code: rayTrace.m – Tracing a beam from entrance to exit points.


```
%%%%%%%%%%%%%%%%%%%
%%% Appendix A3
%%%%%%%%%%%%%%%%%%%

%%% this function patches the dodecahedron (with film) together and
%%% calculates the beam spots in global coordinates

function [globCoord]=rayTrace(beamCentre)
globCoord=[];
global orientationLet;
global orientationNum;
global zPlane;

%     I = imread('d:\robt\ImageFiles\test.tif');
%         figure, imshow(I);
%     hold on;




%%%%%%%%%  phi = golden ratio = (1+sqrt(5))/2
%%%%%%%%%  dihedral = dihedral angle is about 116.565 degrees
phi=0.5*(1+sqrt(5));
dihedral=acos((-1/5)*sqrt(5));
%%%%%%%%%%%%%%%%%%%%%%%%%%%%%%%%%%%%%%%%%%%%%%%%%%%%


%%% dode size factor for 1/2 film sheets in (cm)
dode_sizefactor=14.2962;
filmwidth=12.7;
filmheight=20.3;
edgeToedge=1;

%%% Dode size factor for full film sheets
% dode_sizefactor=19;
% filmwidth=20.3;
% filmheight=25.4;
% edgeToedge=1;

%%% filmshift_x and y is the distance from a dode vertex to the start of
%%% the film
filmshift_x=1.359;
%filmshift_x=1.15;
filmshift_y=2.475;

%%%%%%%%%%%%%%%%%%%%%%%%%%%%%%%%%%%%%%%%%%%%%%%%%%%%%%%%%%%%%%%%%%%%%%%
%%%%%%%%%%%%%   Dodecahedron %%%%%%%%%%%%%%%%%%%%%%%%%%%%%%%%%%%%%%%%
%%%%% vertex points of all points on the dodecahedron
vertex_matrix = [1 1 1; 1 -1 -1; 1 1 -1; -1 1 1; -1 -1 1; -1 1 -1; -1 -1 -1;↵
1 -1 1;....
     0 1/phi phi; 0 -1/phi phi; 0 1/phi -phi; 0 -1/phi -phi; .......
     1/phi phi 0; -1/phi phi 0; 1/phi -phi 0; -1/phi -phi 0;.........
     phi 0 1/phi; -phi 0 1/phi; phi 0 -1/phi; -phi 0 -1/phi];
%%%%%%%%%%%%%%%%%%%%%%%%%%%%%%%%%%%%%%%%%%%%%%%%%%%%%%%%%%%%%%%%%%%%%%%
```

```
%%%% Phantom orientation rotations %%%%%%%%%%%%%%%%%%%%%%%%%%%%%%%
%%% Rotate Dode about the yaxis
vertex_matrix=vertex_matrix*[1 0 0; 0 cos(dihedral/2) sin(dihedral/2); 0 -↙
sin(dihedral/2) cos(dihedral/2)];

%%% Rotate Dode about the zaxis 90 degrees
vertex_matrix=vertex_matrix*[cos(pi/2) sin(pi/2) 0; -sin(pi/2) cos(pi/2) 0;↙
0 0 1];
%%%%%%%%%%%%%%%%%%%%%%%%%%%%%%%%%%%%%%%%%%%%%%%%%%%%%%%%%%%%%%%%%%%%


%%%%%%%%  dodecahedron size factor multiplication
vertex_matrix=dode_sizefactor*vertex_matrix;
 %%%%%%%%%%%%%%%%%%%%%%%%%%%%%%%%%%%%%%%%%%%%%%%

 label_matrix=[1;2;3;4;5;6;7;8;9;10;11;12;13;14;15;16;17;18;19;20];
 label_matrix=[vertex_matrix label_matrix];



%%%%%  Dodecahedron Face matrix - specifies the connections of all faces
faces_matrix = [14 13 1 9 4; 9 1 17 8 10; 5 10 8 15 16; 4 9 10 5 18;.....
    18 4 14 6 20; 13 1 17 19 3; 17 8 15 2 19; 18 5 16 7 20;....
    7 12 2 15 16; 6 20 7 12 11; 14 13 3 11 6; 11 3 19 2 12];
%%%%%%%%%%%%%%%%%%%%%%%%%%%%%%%%%%%%%%%%%%%%%%%%%%%%%%%%%%%%%%%%%%%%

%%%%%%%%%%%%%  Patch the dodecahedron together and start new chart for↙
this%%%%%%%%%%%%%%%%%
figure(4)
patch('Vertices',vertex_matrix,'Faces',faces_matrix,...
    'FaceVertexCData',hsv(12),'FaceColor','c', 'Marker','o',↙
'MarkerFaceColor','b');
alpha(0.1);
%%%%%%%%%%%%%%%%%%%%%%%%%%%%%%%%%%%%%%%%%%%%%%%%%%%%%%%%%%%%%%%%%%%%




  hold on;

%%%arc radius (cm)
  a=30;
%%%%%%%%%%%%%

% Phantom radius
%%%%r=30;
%%%%%%%%%%%%%%%

%%%%%%%  plot of small cone arcs entry and exit%%%%%%%%%%%%%%%%%%%%%%%%%%
% %%%%%%%% SRS small cone Parameters %%%%%
%    couchStart=60;
%    couchDelta=30;
%    numArcs=5;
```

```
%%%%%%%%%%%%%%%%%%%%%%%%%%%%%%%%%%%%%%%%%%%%%%%%%%%%%%%%%%%%%%%


%%%%%%%  plot of large cone arcs entry and exit%%%%%%%%%%%%%%%%%%%%%%%%%
% gantryStart=300;
% gantryDelta=10;
% gantryArc=75;
%
%  for couch=[56, 22, -22, -56]
%
%      %%% rotate phantom...or couch
%      couch=couch+180;
%
%     for i = gantryStart:gantryDelta:gantryStart+(gantryArc-gantryDelta)
%
%         Xi=[a*sind(couch)*cosd(i) 0];
%         Yi=[a*cosd(couch)*cosd(i) 0];
%         Zi=[a*sind(i) 0];
%
%         Xf=[0 -a*sind(couch)*cosd(i)];
%         Yf=[0 -a*cosd(couch)*cosd(i)];
%         Zf=[0 -a*sind(i)];
%
%         plot3(Xi,Yi,Zi,'Color','r','LineWidth',22);
%         plot3(Xf,Yf,Zf,'Color','y','LineWidth',22);
%     end
%     gantryStart=gantryStart+gantryArc;
%  end
% %%%%%%%%%%%%%%%%%%%%%%%%%%%%%%%%%%%%%%%%%%%%%%%%%%%%%%%%%%%%%%%%%%%%%%%%%



%%%%%%%%%%%%%%%%%%%%%%%%%%%%%%%%%%%%%%%%%%%%%%%%%%%%%%%%%%%%%%%%%%%%%%%
%%%% Plot Mcgill technique
% gantryStart=300;
% gantryDelta=2;
% gantryArc=300;
% couch=75;
%
%
% %%%for couch=couchStart:-couchDelta:couchStart-(couchDelta*(numArcs-1))
%     for i = gantryStart:gantryDelta:gantryStart+(gantryArc-gantryDelta)
%
%         Xi=[a*sind(couch)*cosd(i) 0];
%         Yi=[a*cosd(couch)*cosd(i) 0];
%         Zi=[a*sind(i) 0];
%
%         Xf=[0 -a*sind(couch)*cosd(i)];
%         Yf=[0 -a*cosd(couch)*cosd(i)];
%         Zf=[0 -a*sind(i)];
%
%         plot3(Xi,Yi,Zi,'Color','b');
%         plot3(Xf,Yf,Zf,'Color','g');
%         couch=couch-1;
%     end
%%%%%%%%%%%%%%%%%%%%%%%%%%%%%%%%%%%%%%%%%%%%%%%%%%%%%%%%%%%%%%%%%%%%%%%
```

```
%%%%%%%%%%%%%%%%%%%%%%%%%%%%%%%%%%%%%%%%%%%%%%%%%%%%%%%%%%%%%%%%%%%%%%%%%%%%
%%%%%%%%%%% Plot arc lines and the normal surfaces to the lines%%%%%%%%%
%%%%%%%%%%%%%%%%%%%

%%% couchStart=60;
%%% couchDelta=30;
%%% numArcs=5;
% gantryStart=300;
% gantryDelta=2;
% gantryArc=60;

%%%for couch=couchStart:-couchDelta:couchStart-(couchDelta*(numArcs-1))
% for couch=[60, 30, 0 -30, -60]
%   faceCol=0.7;
%
%
%  for l=1:-2:-1
%
%      %%%%  plot arcs%%%%%%%%%%
%         X=[l*a*sind(couch)*cosd(gantryStart) l*a*sind(couch)*cosd↙
(gantryStart+gantryArc)];
%         Y=[l*a*cosd(couch)*cosd(gantryStart) l*a*cosd(couch)*cosd↙
(gantryStart+gantryArc)];
%         Z=[l*a*sind(gantryStart) l*a*sind(gantryStart+gantryArc)];
%     %%%%%%%%%%%%%%%%%%%%%%%%%
%
%       % plot3(X,Y,Z);
%     %%%% change positions of film planes if needed
%         if (couch == 30) || (couch == -30)
%
%             X(1,1)=
%             X(1,2)=
%             Y(1,1)=
%             Y(1,2)=
%             Z(1,1)=
%             Z(1,2)=
%         else (couch == 60) || (couch == -60)
%         else (couch == 0)
%
%         end
%  %%%%%%%%%%%%%%%%%%%%%%%%%%%%%%%%%%%%%%%

%         Xvert1=X(1,1)*(r/a)-(filmWidth/2)*cosd(couch);
%         Xvert2=X(1,1)*(r/a)+(filmWidth/2)*cosd(couch);
%         Xvert3=X(1,2)*(r/a)-(filmWidth/2)*cosd(couch);
%         Xvert4=X(1,2)*(r/a)+(filmWidth/2)*cosd(couch);
%
%         Yvert1=Y(1,1)*(r/a)+(filmWidth/2)*sind(couch);
%         Yvert2=Y(1,1)*(r/a)-(filmWidth/2)*sind(couch);
%         Yvert3=Y(1,2)*(r/a)+(filmWidth/2)*sind(couch);
%         Yvert4=Y(1,2)*(r/a)-(filmWidth/2)*sind(couch);
%
%         Zvert1=Z(1,1)*(r/a);
```

```
%         Zvert2=Z(1,2)*(r/a);
%
%         newPatch=[Xvert1 Yvert1 Zvert1; Xvert2 Yvert2 Zvert1; .....
%             Xvert3 Yvert3 Zvert2; Xvert4 Yvert4 Zvert2];
%         newFaces=[1 2 4 3];
%
%         patch('Vertices',newPatch,'Faces',newFaces,...
%             'FaceVertexCData',hsv(1),'FaceColor',[faceCol,0,0]);
%
%     faceCol=faceCol-0.7;
%
%  end
%      gantryStart=gantryStart+gantryArc;
%
% end

%filmLength=sqrt(Xvert1^2+Yvert1^2+Zvert1^2)

%%% patch couch
% couchVert=[-40 -40 -40; -40 40 -40; 100 40 -40; 100 -40 -40];
% couchFace=[1 2 3 4];
% patch('Vertices',couchVert,'Faces',couchFace,...
%            'FaceVertexCData',hsv(1),'FaceColor', 'y');

%%%%%%%%%%%%%%%%%%%%%%%%%%%%%%%%%%%%%%%%%%%%%%%%%%%%%%%%%%%%%%%%%%%%%%%%%%%%↵
%%%%%
%%%%%%%%%%%%%%%%%%%%%%%%%%%%%%%%%%%%%%%%%%%%%%%%%%%%%%%%%%%%%%%%%%%%%%%%%%%%↵
%%%%

xlabel('X');
ylabel('Y');
zlabel('Z');


%%%%%%%%%%%%%%%%%%%%%%%%%%%%%%%%%%%%%%%%%%%%%%%%%%%%%%%%%%%%%%%%%%%%%%%%%%%%
%%%% Test for cone collision by mapping a sphere

%
% r=33.4;
% phi=linspace(0,pi,30);
% theta=linspace(0,2*pi,40);
% [phi,theta]=meshgrid(phi,theta);
%
%
% x=r*sin(phi).*cos(theta);
% y=r*sin(phi).*sin(theta);
% z=r*cos(phi);
% mesh(x, y, z);
% alpha(0.4);
%%%%%%%%%%%%%%%%%%%%%%%%%%%%%%%%%%%%%%%%%%%%%%%%%%%%%%%%%%%%%%%%%%%%%%%%%%%%



%%%%% Find locations of points on film relative to 3d coordinates
%%% full film scan resolution = 1194x1500
```

```
%%%%%% Define start points for film measurement %%%%%%%%%%%%%%%%
%%% all units in cm
% point 1
[xSize, ySize]=size(beamCentre);



for i = 1:xSize

x0_RP=beamCentre(i,1);
y0_RP=beamCentre(i,2);
xStart=vertex_matrix(13,1);
yStart=vertex_matrix(13,2);
zStart=vertex_matrix(13,3);



%if isempty(orientationLet)==True
    %orientationLet='a'%input('Enter orientation Letter: ','s');
    %orientationNum=1%input('Enter orientation Number: ');
%end


%%%% distance per pixel (cm) = 0.016933

      Spot01=[(xStart+filmshift_x)+0.016933*x0_RP; (yStart-filmshift_y)↵
-0.016933*y0_RP; zStart];


      %%% Do Rotation to bring back to top plane

      %%% theta is rotation of film on one plane
      if orientationLet=='a'
          theta=0;
      elseif orientationLet=='b'
          theta=72;
      elseif orientationLet=='c'
          theta=144;
      elseif orientationLet=='d'
          theta=216;

      elseif orientationLet=='e'
          theta=288;
      end



      if orientationNum==1;
          betaY=0;
          betaZ=0;
      elseif orientationNum==2
          betaY=(180-(180*dihedral/pi));
          betaZ=36;
```

```
      elseif orientationNum==3
          betaY=(180-(180*dihedral/pi));
          betaZ=36+72;
      elseif orientationNum==4
          betaY=(180-(180*dihedral/pi));
          betaZ=36+(72*2);
      elseif orientationNum==5
          betaY=(180-(180*dihedral/pi)) - 0.12258;
          betaZ=36+(72*3);
      elseif orientationNum==6
          betaY=(180-(180*dihedral/pi));
          betaZ=36+(72*4);
      elseif orientationNum==7
          betaY=180-(180-(180*dihedral/pi));
          betaZ=0;
          theta=theta-180;
      elseif orientationNum==8
          betaY=(180-(180-(180*dihedral/pi))) - 0.12258;
          betaZ=72;
          theta=theta-180;
      elseif orientationNum==9
          betaY=180-(180-(180*dihedral/pi));
          betaZ=2*72;
          theta=theta-180;
      elseif orientationNum==10
          betaY=180-(180-(180*dihedral/pi));
          betaZ=3*72;
          theta=theta-180;
      elseif orientationNum==11
          betaY=180-(180-(180*dihedral/pi));
          betaZ=4*72;
          theta=theta-180;
      elseif orientationNum==12

          betaY=180;
          betaZ=0;
      end




%       for theta=[0 72 144 216 288]
%       if orientationNum==7;
%           theta=theta-180;
%       end

        radCentre=[cosd(theta) -sind(theta) 0; sind(theta) cosd(theta) 0; 0↙
0 1]*Spot01;

    %%%%%%%%%%%%%%%%%%%%%%%%%%%%%%%%%%%%%%%%%%%%%%%%%%%%%%%%%%%%%%%%%%%
 %%%%%%%%%%%%%%%%%%%%% Apply orientation corrections on top plane then
 %%%%%%%%%%%%%%%%%%%%% rotate
      if orientationLet=='a'

      elseif orientationLet=='b'
```

```
          %radCentre=[radCentre(1,1)-0.068; radCentre(2,1)+0.037; radCentre↙
(3,1)]
      elseif orientationLet=='c'

      elseif orientationLet=='d'



      elseif orientationLet=='e'

      end
 %%%%%%%%%%%%%%%%%%%%%%%%%%%%%%%%%%%%%%%%%%%%%%%%%%%%%%%%%%%%

        ux=0;
        uy=1;
        uz=0;


        RotY=[ux^2+(1+ux^2)*cosd(betaY) ux*uy*(1-cosd(betaY))-uz*sind(betaY)↙
ux*uz*(1-cosd(betaY))+uy*sind(betaY);.....
            ux*uy*(1-cosd(betaY))+uz*sind(betaY) uy^2+(1-uy^2)*cosd(betaY)↙
uy*uz*(1-cosd(betaY))-ux*sind(betaY);....
            ux*uz*(1-cosd(betaY))-uy*sind(betaY) uy*uz*(1-cosd(betaY))↙
+ux*sind(betaY) uz^2+(1-uz^2)*cosd(betaY)];

        radCentre=RotY*radCentre;

        ux=0;
        uy=0;
        uz=1;


        RotZ=[ux^2+(1+ux^2)*cosd(betaZ) ux*uy*(1-cosd(betaZ))-uz*sind(betaZ)↙
ux*uz*(1-cosd(betaZ))+uy*sind(betaZ);.....
            ux*uy*(1-cosd(betaZ))+uz*sind(betaZ) uy^2+(1-uy^2)*cosd(betaZ)↙
uy*uz*(1-cosd(betaZ))-ux*sind(betaZ);....
            ux*uz*(1-cosd(betaZ))-uy*sind(betaZ) uy*uz*(1-cosd(betaZ))↙
+ux*sind(betaZ) uz^2+(1-uz^2)*cosd(betaZ)];

        radCentre=RotZ*radCentre;



        xData=radCentre(1,1);
        yData=radCentre(2,1);
        zData=radCentre(3,1);


        %%% return the film spots in global (dode) coordinates
        globCoord=[xData yData zData;globCoord];


end
```

```
%%%% Plot Film onto dode
%%% Patch film onto dode point 13

film_vertex13=[vertex_matrix(13,1)+filmshift_x vertex_matrix(13,2)-↵
filmshift_y vertex_matrix(13,3);....
    vertex_matrix(13,1)+filmshift_x+filmheight vertex_matrix(13,2)-↵
filmshift_y vertex_matrix(13,3);....
    vertex_matrix(13,1)+filmshift_x+filmheight vertex_matrix(13,2)-↵
filmshift_y-filmwidth vertex_matrix(13,3);....
    vertex_matrix(13,1)+filmshift_x vertex_matrix(13,2)-filmshift_y-↵
filmwidth vertex_matrix(13,3)];


  film_vertex13=[cosd(theta) -sind(theta) 0; sind(theta) cosd(theta) 0; 0 0↵
1]*transpose(film_vertex13);
  film_vertex13=RotY*film_vertex13;
  film_vertex13=RotZ*film_vertex13;
  film_vertex13=transpose(film_vertex13);

film_faces=[1 2 3 4];

patch('Vertices',film_vertex13,'Faces',film_faces,...
    'FaceVertexCData',hsv(1),'FaceColor','g');
alpha(0.1);
```

References

Arjomandy, B., & Altschuler, M., (2000). A quality assurance device for the accuracy of the isocentres of teletherapy and simulation machines. *Phys. Med. Biol.,* 45, 2207–2217.

Benedict, S. & Bova, F., (2008). Anniversary Paper: The role of medical physicists in developing stereotactic radiosurgery. *Medical Physics*, 35(9), 4263-4277.

D'Souza, H., & Joshi, RC., (1999). Variation in the isocentre of a Philips Linear Accelerator (SL–20) used for stereotactic radiosurgery/stereotactic radiotherapy. *Australasian Radiology,* 43, 342–345.

Devic, S., & Seuntjens, J., (2005). Precise radiochromic film dosimetry using a flat-bed document scanner. *Medical Physics*, 32(7), 2245 - 2253.

Fitzgibbon, A., & Pilu, M., (1999). Direct Least Square Fitting of Ellipses. *IEEE Transactions on Pattern Analysis and Machine Intelligence*, 21(5), 476 – 480.

Greenberg, M., (2010). *Handbook of Neurosurgery*. New York, NY: Published by Thieme Publishers.

International Specialty Products (2007). *GAFCHROMIC® EBT Self-Developing Film for Radiotherapy Dosimetry*. Retrieved May 27, 2009, from http://online1.ispcorp.com/_layouts/ Gafchromic/ index.html

Karger, C., & Hartmann, G., (2001). A method for determining the alignment accuracy of the treatment table axis at an isocentric irradiation facility. *Physics in Medicine and Biology,* 46, N19-N26.

Keller, B., & Beachey, D., (2007). Experimental measurement of radiological penumbra associated with intermediate energy x-rays (1 MV) and small radiosurgery field sizes. *Medical Physics*, 34(10), 3996 – 4002.

Lutz, W., & Winston, K., & Maleki, N., (1988). A System for Stereotactic Radiosurgery with a Linear Accelerator. *Int. J. Radiation Oncol. Biol. Phys*., 14, 373-381.

Pike, G., & Podgorsak, E., (1989). Dose Distribution in Radiosurgery. *Medical Physics*, 17(2), 296 – 304.

Podgorsak, E. & Pike, B., (1990). Radiosurgery with photon beams" physical aspects and adequacy of linear accelerators. *Radiotherapy and Oncology*, 17, 349-358.

Podgorsak, E. & Poffenbarger, B., (1998). Viability of an isocentric cobalt-60 teletherapy unit for stereotactic radiosurgery. *Medical Physics*, 25(10), 1935-1943.

Podgorsak, E. (2003). *Review of Radiation Oncology Physics: A Handbook for Teachers and Students.* Educational Reports Series, May 1, 2003.

Robar, J., & Clark, B., (1999). The use of radiographic film for linear accelerator stereotactic radiosurgical dosimetry. *Medical Physics*, 26(10), 2144 - 2150.

Schell, M., & Bova, F., (1995). *AAPM Report No. 54. Stereotactic Radiosurgery Report of Task Group 42 Radiation Therapy Committee*. Woodbury, NY: Published by the American Institute of Physics, Inc.

Solberg, T., & Antonio, A., (1998). Technical Aspects of LINAC Radiosurgery for the Treatment of Small Functional Targets. *Journal of Radiosurgery*, 1(2), 115 – 127.

Tomé, W., & Sanford, L., (2000). A high-precision system for conformal intracranial radiotherapy. *Int. J. Radiation Oncology Biol. Phys*., 47(4), 1137–1143.

Tsai, J., & Buck, B., (1991). Quality assurance in Stereotactic Radiosurgery using a standard linear accelerator. *Int. J. Radiation Oncology Biol. Phys*., 21, 737-748.

Winkler, P., & Bergmann, H., (2003). Introducing a system for automated control of rotation axes, collimator and laser adjustment for a medical linear accelerator. *Phys. Med. Biol*., 48, 1123–1132.

Glossary

AAPM – American Association of Physicist in Medicine

Accelerator – A device which accelerates charged particles to very high energies.

CT – Imaging modality : Computed Tomography

CyberKnife – A radiosurgery treatment unit consisting of a miniature Linac mounted on a robotic arm.

Cyclotron – A machine which accelerates charged particles in a circular path through an alternating electric field and static magnetic field.

Dose – energy absorbed in a medium through ionizing radiation.

EPID – Electron Portal Imaging Display

Fractionation – The division of radiation therapy treatments into multiple treatments or regimens.

GammaKnife – A stereotactic treatment unit which uses stationary radioactive cobalt sources focused at a common point.

Gy – Unit of dose equivalent to Joules/Kg.

Ionization Chamber – A device used to measure the ionization intensity of the gas within the chamber during irradiation.

IMRT – Intensity Modulated Radiation Therapy

iPET – Intermediate Photon Energy Therapy

Isocentre – the location in space at which the radiation beams intersect by rotation of the treatment couch, gantry, and collimator.

Isodose – a line connecting all doses of the same value.

KeV – unit of energy for particles in kilo-electron-volts.

Linear Accelerator – A device which accelerates charged particles to high energies in a straight path.

MeV – unit of energy for particles in mega-electron-volts.

MLC - multi-leaf collimator. A device with moveable collimating leafs used to conform the radiation to the target.

mMLC – micro multi-leaf collimator. A device with thin moveable collimating leafs (thinner than typical MLCs) used to conform the radiation to the target.

Monitor Unit (MU) – A numerical value input to a medical Linac that defines the total dose of radiation to be delivered. Commonly calibrated to 1cGy/MU.

MRI – Imaging Modality: Magnetic Resonance Imaging

Penumbra – The distance over which the radiation dose falls from 80% to 20% relative to the central axis dose.

PDD – Percent Depth Dose, the relative dose of a radiation beam at a certain depth in a material to its maximum level.

PET – Imaging modality: Positron Emission Tomography

PTV – Planning Target Volume

QA – Quality Assurance

Radiosurgery – A non-invasive brain surgery procedure which uses focused ionizing radiation to treat cancerous tumours and other lesions in a single treatment.

Radiotherapy – A medical procedure used to treat cancer using ionizing doses of radiation delivered to the target.

Stereotactic Radiosurgery (SRS) – A special technique of external beam radiation therapy (EBRT) that uses a device to immobilize the patient and highly focused radiation beams to treat the patient.

Index